Forecasting Research

Met O 11 Scientific Note No. 17

The dynamical structure of some North Atlantic depressions simulated by the fine-mesh model

by

G.J. Shutts

January 1990

Meteorological Office (Met O 11)
London Road, Bracknell, Berkshire RG12 2SZ, England

MET O 11 Scientific Note No. 17

THE DYNAMICAL STRUCTURE OF SOME NORTH ATLANTIC DEPRESSIONS SIMULATED BY THE FINE-MESH MODEL

by

G. J. Shutts

January 1990

LONDON, METEOROLOGICAL OFFICE.
Met.O.11 Scientific Note No.17

The dynamical structure of some North Atlantic depressions simulated by the fine-mesh model.

05750390 551.515.11

Met O 11 (Forecasting Research)
Meteorological Office
London Road
Bracknell
Berkshire RG12 2SZ
ENGLAND

Abstract

The baroclinic structure and symmetric stability of eight cases of Atlantic cyclogenesis simulated in the Fine-Mesh model are briefly portrayed. Certain combinations (and modes of presentation) of diagnostics are shown to provide a vivid picture of baroclinic development eg. potential vorticity maps on the 330 K isentropic surface (plotted with three tone shading) together with the potential temperature at 900 mb. Inspection of the model's 850 mb wet-bulb potential temperature fields suggests the need for some modification of the textbook Norwegian model of frontal analysis as has been noted by others (eg. Shapiro, 1989). In most cases of rapid cyclogenesis in the model, a low-level warm-cored depression forms by what appears to be an advective process.

Vertical cross-sections through rapidly developing systems frequently reveal grid-scale temperature contrasts of ≃ 10 K in association with fronts extending up to 700 mb. The baroclinicity is often concentrated into two zones associated with upper and lower tropospheric fronts that do not align. This happens when the primary jet lies over the position of the main surface front and probably accounts for the double structure of cloud head systems seen in satellite imagery. The primary jet axis tends to be displaced much further towards the cold air in the early stages of non-explosive cyclogenesis implying a weaker coupling between upper potential vorticity and lower tropospheric thermal anomalies than for the explosively deepening cases.

A method for calculating the *slantwise convective available potential energy* (SCAPE) of boundary layer air parcels is outlined and SCAPE maps are shown for each case. Regions of large SCAPE (> 1000 JKg^{-1}) are often, though not exclusively, found in rapid cyclogenesis events.

1. Introduction

This study evolved from the Meteorological Office's investigation of the October Storm (eg. Shutts, 1989) and the realization that many aspects of the structure and evolution of depressions simulated in the Fine-Mesh model would be of general interest to the research community. A set of Fine-Mesh model forecasts for explosive cyclogenesis events following on from the October Storm were subjected to detailed diagnostic analysis with particular interest centring on the degree of slantwise stability in the pre-storm environment. These cases were contrasted with four other cyclogenesis events which one might consider to be run-of-the-mill. For the purposes of this paper, no attempt will be made to assess the quality of these operational forecasts. Most of the forecasts were in fact very good and did not suffer from the observational data inadequacies that caused the poor operational forecast of the October Storm.

The purpose of this paper is threefold:

1) to introduce forecasters to potential vorticity diagnostics as an aid to visualising cyclogenesis

2) to give research workers (particularly those outside The Meteorological Office) some idea of the dynamical structure of depressions in Fine-Mesh model forecasts

3) to discuss SCAPE maps and their potential use to the forecaster

using eight Fine-Mesh model forecasts as illustration.

The intention is to let the pictures speak for themselves, with a few comments for guidance, rather than to attempt a detailed verbal description of each synoptic event. Before discussing the individual cases, a short review of the potential vorticity and SCAPE concepts is appropriate.

2. 'New' diagnostics

(a) Isentropic potential vorticity maps

The value of isentropic potential vorticity (PV) maps stems principally from the following two facts

1) a fluid parcel conserves PV following its motion in adiabatic and inviscid flow

2) given some kind of filtering (or balance) approximation which eliminates high frequency gravity and sound waves, the wind, temperature and pressure can be determined from a knowledge of the full three-dimensional distribution of PV coupled with appropriate boundary conditions (ie. the 'invertibility principle' as defined by Hoskins et al, 1985).

Lateral boundary conditions do not concern us here if we consider the global domain, and the upper boundary condition can, for purposes of this discussion, be taken as the requirement that potential temperature be constant at a given height or pressure in the stratosphere. The specification of potential temperature on the lower boundary of the domain on the other hand is an important input to the mathematical solution of the invertibility problem in meteorological applications and is a key element in the PV description of cyclogenesis. Hoskins el (1985), to whom we owe the practical PV view of cyclogenesis and Rossby wave propagation, follow Bretherton (1966) in regarding the surface potential temperature distribution as an infinitesimal sheet of infinite PV (by imagining an isentropic layer running just beneath the actual surface). This mathematical device has some conceptual advantages and enables one to specify the whole problem (interior and boundary) in terms of PV rather than interior PV plus boundary potential temperature. Nevertheless, we shall adhere to the latter view since it probably fits in better with the forecaster's interest in low-level thermal advection in the description of development.

Although the potential vorticity field exhibits a wide range of variation within the troposphere and stratosphere, its form is dominated by the contrast between high PV in the stratosphere and low PV in the troposphere. Mathematical solutions to the invertibility principle which assume uniform PV in the troposphere and stratosphere separately are surprisingly complete in their description of real flow structures (eg. Hoskins el al, 1985). The height of the tropopause and the surface potential temperature are then key ingredients in providing a broad-brush description of the entire three-dimensional flow. At a somewhat finer scale, one must account for the high PV associated with lower tropospheric frontal zones and the tropopause folding effect in upper fronts.

A tropopause sloping from ≈ 16 km in the tropics to 7 km near the poles

can be shown to imply a cyclonic circumpolar vortex with maximum wind strength near the tropopause. The 330 K isentropic surface passes from the troposphere in middle and low latitudes into the stratosphere in high latitudes. As a consequence, PV plotted on this surface shows an abrupt increase where the isentropic surface intersects the tropopause and the jetstream lies just to the low PV side of this. Short wave upper level troughs are readily identifiable as waves in this PV boundary and, in the model at least, are frequently accompanied by a local maximum in PV.

As explained by Hoskins et al (1985), baroclinic instability can be viewed as the mutual interaction and enhancement of upper level PV 'anomalies' and near-surface thermal anomalies. To portray this interaction it is convenient to combine PV on the 330 K isentropic surface with the potential temperature at 900 mb. In a developing depression the thermal ridge in the lower troposphere precedes an upper level PV anomaly. Air is forced to ascend just ahead of a PV anomaly so that the ascent of warm air in the thermal ridge provides the necessary energy conversion for development. The static stability can be shown to be weak beneath a PV anomaly so that - as can be inferred from satellite imagery - organised convection in cold air over the oceans is often enhanced in their proximity.

Potential vorticity is not conserved following the motion of an air parcel in the presence of diabatic heating or mixing processes but this does little to detract from its value as a diagnostic. Diabatic processes have rather long time scales compared to advective processes in the upper troposphere so that PV is approximately conserved. The invertibility principle is unaffected by non-conservative effects provided that they do not seriously disrupt the balance assumption. Isentropic PV maps are therefore a natural way of following the evolution of an upper level disturbance. By picking an isentropic surface which passes through the mean position of the polar front jet, a more sharply focussed picture of short wave/jetstreak features is obtained and at a level where their amplitude is a maximum. 250 or 500 mb height charts are not quite as forceful in emphasising these aspects of the flow and, of course, geopotential height does not have the tracer property of PV.

(b) SCAPE maps

A measure of the kinetic energy realizable in cumulonimbus convection may be obtained by assuming conservation of equivalent potential temperature during

the saturated state (potential temperature if dry) of an air parcel lifted pseudo-adiabatically to its neutral buoyancy level, and computing the work done by the buoyancy force. This quantity is known as the Convective Available Potential Energy or CAPE and corresponds to the positive area on the tephigram between environment and parcel curves. No account is taken of the horizontal momentum of the air parcel, either with regard to vertical mixing or the effect that the environment might have upon it.

Parcel theory can also be applied to arbitrary quasi-two dimensional displacements in a frontal environment but in this case it is appropriate to consider the horizontal momentum of parcels also. For an infinite tube of air oriented along a two-dimensional front the absolute momentum M (=fx+v) is conserved where f is the Coriolis parameter, x is the distance normal to the front and v is the along front wind component. Conservation of equivalent potential temperature (θ_E) and absolute momentum in arbitrary cross-frontal displacements leads not only to a vertical buoyancy force but also a horizontal inertia force in the positive x direction given by $f(M_P-M_E)$ where M_P is the absolute momentum of the parcel and M_E is the absolute momentum of the ambient environment. This is just the excess Coriolis force the parcel has over its environment resulting from the conservation of absolute momentum. The parcel may be stable to displacements in any direction or it may have another equilibrium point where its potential temperature is equal to that of the environment on the absolute momentum surface M_P. The total work done by the buoyancy and excess Coriolis force in reaching this point is called the Slantwise Convective Available Potential Energy or SCAPE (Emanuel, 1983) : its value can be shown to be independent of the path taken (Shutts, 1990).

The case of neutral stability to slantwise motion (SCAPE=0) is of considerable interest. If the frontal environment is characterised by coincident M and θ_E surfaces, then an infinitesimal saturated air parcel displaced along these surfaces would never generate any buoyancy or excess Coriolis force and at each position would be in geostrophic and hydrostatic balance with its surroundings. Regions of frontal zones satisfying this condition are very responsive to frontogenetic forcing. Emanuel et al (1987) have shown, using a two-dimensional semi-geostrophic model, that baroclinic development in such an environment would lead to the ascending air being concentrated in a thin sheet oriented along the M surfaces with weak descent elsewhere. They also showed that the growth rate of instability is 2.5 times as fast as that in the

corresponding 'dry' problem and that the scale of the cyclonic region is reduced by 60%. Little is known about baroclinic instability in a moist slantwise *unstable* environment.

Since SCAPE can be calculated without reference to any particular path between the initial parcel position and its final equilibrium point we are at liberty to choose one. If we consider the parcel to move along the M surface on which it sat initially then the excess Coriolis force is zero and only the work done by the buoyancy force need be considered (Emanuel, 1983). *But this is the same as evaluating CAPE using an environment profile taken from the M surface.* Of course to make any sense of SCAPE in the real world we must not have to depend too heavily on the two-dimensionality assumption. From a practical point of view, a procedure for calculating SCAPE at any model point needs to be established : such a method is discussed in Shutts (1990) and is briefly outlined here.

Define two components of the absolute momentum $M=fx+v$ and $N=\int f dy-u$ where x and y are distances, and u and v are velocity components, measured in the eastward and northward directions respectively. If M_P and N_P are the geostrophic absolute momentum components of the parcel at its initial position, then SCAPE is defined to be equal to the CAPE measured along the line of intersection of the M_P and N_P surfaces. As discussed in Shutts (1990), M and N are used in place of M_g and N_g. For a two-dimensional front with arbitrary orientation the definition above leads to the same value of SCAPE as would be obtained by defining x to be the cross-frontal coordinate. In the Fine-Mesh model, M and N are identified for gridpoints in the lowest model level. A search is then carried out on all the model levels for the gridbox containing the intersection point of these absolute momentum surfaces : temperature, pressure and relative humidity are then bilinearly interpolated to the point of intersection at each level and a thermodynamic profile is obtained. This profile is then used as input to an operational program for calculating CAPE and the maps thereby obtained give SCAPE.

Given the current state of knowledge concerning the role of SCAPE in cyclonic and frontal development the following two potential uses of SCAPE maps should be considered:

1) as an indication of the likihood of rapid cyclogenesis characterised by tight inner cores and hurricane-force winds

2) as an indicator of potentially heavy frontal rain accompanying slantwise convection.

The October Storm is the archtype of 1) with a powerful upper PV anomaly engaging an intense baroclinic zone with abundant SCAPE in the warm air (Shutts, 1989). Of course SCAPE maps can only be as good as the analysis from which they were derived. At frontal scales, model analyses are largely a model creation and are influenced by resolution limitations. Indeed the model is unlikely to be able to describe slantwise convection explicitly and so the appearance of large values of SCAPE in the model may reflect the model's inability to neutralize itself to slantwise instabilities.

3. The case studies

(a) January 30 1988

This explosive cyclogenesis case in the central Atlantic was notable for its impressive split cloud head structure (Met. Mag., May 1988 - satellite photograph) and was simulated well by the Fine-Mesh model. Figs. 1 a-d show the mean sea-level pressure, potential vorticity on the 330 K isentropic surface + 900 mb. θ contours, 850 mb. θ_ω and 700 mb. vertical velocity respectively at the analysis time 12Z. The system was already deepening rapidly at this stage with a central pressure of 995 mb. and a distinct upper PV anomaly engaging a thermal ridge in an intense baroclinic zone. The 850 mb. θ_ω field is suggestive of the T-bone frontal structure discussed by Shapiro (1989) with a warm front extending toward the rear of the system, a region of weak gradient near the low centre and a cold front to the south. The 700 mb. vertical velocity field reveals concentrated ascent to the north of the low centre and extending along the warm front; a region of descent immediately to the south of the depression and, even further south, a strip of ascent associated with the cold front.

By 00Z on the 31st the depression has deepened to 980 mb (implying a deepening rate of 30 mb./day) and lies beneath the high PV values at the apex of the thermal ridge (Fig. 2b). An intense warm front is again separated from

the cold front by a relatively warm intermediate zone near the depression centre. A narrow band of high θ_w exists ahead of the cold front and behind the eastern portion of the warm front (shaded in Fig. 2c). Ascent at 700 mb. is organised into three distinct bands; the warm front extending to the depression centre where the core of rapid ascent lies, a narrow cold frontal band disjointed from the depression centre and warm front, and a cold air band to the rear of the system.

A vertical cross-section of normal wind component, potential temperature and wind vectors along the line indicated in Fig. 2c is shown in Fig. 3a. The upper jet axis is situated slightly equatorward of the position of the surface low with the normal component exceeding 83 ms^{-1}. An intense frontal zone extending from the surface up to 600 mb. is characterised by a zone of marked potential temperature gradient (Fig. 3b) and horizontal/vertical wind shear. An upper cold frontal zone and tropopause fold associated with the primary jet extends down to 700 mb on the warm side of the surface front splitting the baroclinicity into two distinct zones (Fig. 3b). The dashed lined in Fig. 3b shows the outline of the model's cloud boundary. A pronounced dry slot extends downwards from the tropopause fold region to the top of the warm sector boundary just ahead of the cold front. This split cloud structure corresponds well with that evident in satellite imagery. Unfortunately, it is one of the few cases we have studied which does have a realistic cloud structure in the early stages of cyclogenesis.

The absolute momentum /θ_w cross-section (Fig. 3c) shows that the main frontal zone is characterized by (potentially) neutral or unstable slantwise stability. The SCAPE map at the analysis time (Fig. 4) reveals an extensive area of potential slantwise instability in the warm sector with SCAPE values as high as 1700 JKg^{-1}.

(b) February 8 1988

Operational Fine-Mesh model forecasts for this day were indicating that an intense depression would bring winds as least as strong as those of the October Storm to Southern England at 12Z on the following day. News of this was passed to the media and the next morning the *Daily Mail* carried the frontpage headline 'Hurricane High Noon'. The actual event turned out to be not quite as spectacular for England as suggested by the model but was still a good forecast. The sea-level pressure field for the forecast from 00Z 8/2/88 already

shows a well developed depression near 48 N 40 W with central pressure 989 mb (Fig. 5a). Fig. 5b shows an extremely intense thermal ridge at 900 mb. with two tongues of high PV at upper levels - one extending to the apex of the ridge and the other well to the rear of the system over the cold air. The θ_w field (Fig. 5c) follows the 900 mb. θ field in emphasising the remarkable frontal contrast. The vertical motion field at 700 mb. is dominated by a vigorous core of rising motion with peak ascent rate of over 90 mb./hr. (Fig. 5d). Warm and cold frontal ascent bands are also clearly in evidence.

At 00Z on the 9th the depression has deepened to 949 mb. west of Ireland with a very strong pressure gradient on its south-west flank (Fig. 6a). The potential vorticity anomaly appears much stronger at this stage and lies over and just upstream of a closed centre of warm air (at 900 mb.) which in turn is embedded in an extrusion of warm sector air (Fig. 6b). This apparent non-conservation of PV on the 330 K surface is noted from time to time : its source is not known though it could simply be due to truncation error in the model and/or the diagnostic calculation of PV itself. The *seclusion* of warm sector air is readily identifiable in the θ_w field with a local maximum located on the inside of a bent back warm front which curls around the western flank of the low (Fig. 6c). The most intense vertical velocities occurred much earlier in the forecast : at 00Z on the 9th the strongest ascent (50 mb./hr.) is near the apex of the classical warm sector (Fig. 6d).

Vertical cross-sections were obtained along the line indicated in Fig. 5c for the analysis time. Fig. 7a shows a primary jetstream with axis more or less above the position of the surface front and with a normal wind component of 81 ms^{-1}. A quite remarkable low-level jet with peak speed of $\simeq$ 52 ms^{-1} exists in the warm air near 850 mb. The baroclinicity does not exhibit as clearly a defined split structure as the previous case (Fig. 7b); neither is there as much potential slantwise instability in the frontal zone judging from the relative orientation of the M and θ_w surfaces in Fig. 7c. This is confirmed by the SCAPE map at the analysis time which shows values < 600 JKg^{-1} in the warm air (Fig. 8).

(c) September 30 1988

The depression featured in this case study developed explosively from the remnants of hurricane Helene and is structurally quite different from the previous two cases. At the analysis time 00Z 30/09/88, it is at the height of

its rapid deepening phase with a central pressure of 983 mb near 48 N 40 W (Fig. 9a). Fig. 9b shows a rather circular PV anomaly well to the west of a similar sized low-level thermal anomaly with closed contours. The high values of θ_w at 850 mb. confirm the tropical origin of the airmass (Fig. 9c). The strongest ascent at 700 mb. occurs in the warm front on the northern side of the depression (Fig. 9d).

At 18Z on the same day, the depression has moved northeastward and deepened to 956 mb. (Fig. 10a). Its centre lies within warm air at low levels just ahead of an isolated upper level PV anomaly (Fig. 10b). The warm front is again bent back around the western and southern flanks of the low with a cold front failing to extend to the depression centre (Fig. 10c). Ascent at 700 mb. is concentrated in the warm front to the north and east of the depression centre (Fig. 10d).

Cross-sections were obtained at 06Z 30/9/88 (ie. T+6 hrs) along the line indicated in the 850 mb. potential temperature map at the same time (Fig. 11). Fig. 12a reveals a broad and deep region in the warm air with no appreciable horizontal or vertical wind shear and with a normal wind component of about 35 ms^{-1}. The upper jet is also very broad with a normal wind component of $\simeq$ 45 ms^{-1}. No split baroclinic structure is evident in the potential temperature cross-section (Fig. 12b). A curious feature of the tropical airmass is the apparent alternation of layers with high stability and nearly neutral stability. The relative humidity (not shown) in this region is extremely dry above the boundary layer with values typically of 10 %.

The M/θ_w cross-section reveals an unusual level of stability to slantwise displacements in the frontal zone due to a local maximum of θ_w at 850 mb. (Fig. 12c) : consistent with this, no significant SCAPE for boundary layer air parcels was found in the vicinity of the old hurricane at the analysis time (Fig. 13).

(d) January 12 1989

This forecast features a spectacular explosive development with central pressure falling by 73 mb. in 30 hours. At the analysis time 00Z 12/1/89, the model had a broad low pressure region with central pressure 1008 mb. centred near 43 N 48 W (Fig. 14 a). An upper PV anomaly extends southwards into the low pressure region even at this stage with further anomalies upstream (Fig. 14 b). The 900 mb. θ contours indicate a broad baroclinic zone to the west of the low

and a more concentrated frontal region to the east (Figs. 14 b and c). Weak ascent occurs in an extensive region to the north and east of the low with descent near 60 W. (Fig. 14d).

At 06Z on January 13 (T+30 hrs.) the depression (central pressure 935 mb) exhibits a distinct inner core where the pressure gradient is substantially greater than at larger radii (Fig. 15a). This coincides with a cut-off warm anomaly at 900 mb. and high potential vorticity upstream (Fig. 15b). The seclusion process is graphically portrayed by the 850 mb. θ_ω field (Fig. 15c) with a pronounced local maximum at the depression centre, a bent back warm front curling around the western flank of the low and a long cold front whose intensity diminishes within 1000 km of the low centre. As found in the previous cases, the strongest ascent at 700 mb. takes place in the warm front close to the low centre (Fig. 15d). A curved band of strong descent extends around the southern and western flanks of the low.

Cross-sections were obtained at 06Z on the 12th (T+6 hrs.) along the line indicated in the 850 mb. potential temperature map (Fig. 16). The normal wind component shows the axis of the primary jetstream to be located slightly to the warm side of the surface low with a speed of 60 ms^{-1} (Fig. 17a). A small secondary jet can be found above another intense baroclinic zone SE of Newfoundland (see Fig. 16). The air behind this front is extremely cold and stable : at the northwestern end of the cross-section the temperature is more or less isothermal at -27°C from the ground to 600 mb. The wind vectors in the plane of the cross-section show only weak ascent under the primary jet at this stage. A split baroclinic structure is apparent in the potential temperature field (Fig. 17b).

The M/θ_ω cross-section at 06Z 12/1/89 reveals a considerable level of potential slantwise instability in the main frontal zone with θ_ω surfaces sloping much more steeply than M surfaces (Fig. 17c). The warm boundary layer air is potentially unstable in the usual convective sense. The SCAPE map at the analysis time shows a high degree of instability in the warm air ahead of the cold front (Fig. 18).

(e) January 18 1988

In this 36 hour Fine-Mesh forecast initialised at 12Z 17/1/88, a depression develops by 27 mb. in the last 24 hours putting it into the explosive deepening category according to the criterion of Sanders and Bosart (1980) though

Meteorological Office forecasters would probably regard this deepening rate as 'normal'. Because little happens in the first 12 hours, it is appropriate to consider the maps at 00Z on the 18th (T+12) rather than the analysis time. The incipient depression then lies near 45 N 20 W with a central pressure of 1013 mb. (Fig. 19a). An elongated PV anomaly approaches about 15° west of this, ahead of a 900 mb. thermal ridge which is coincident with the low centre (Fig. 19b). A weak PV anomaly already appears to exist near and to the east of the surface low. To the west of the developing surface system the θ_w gradient is split into two intense frontal zones with a strong ridge in phase with the low (Fig. 19c). At this stage most of the ascent at 700 mb. is taking place well to the south-west of the low (Fig. 19d).

At 00Z 19/1/88 the low has deepened to 986 mb. just south of Ireland (Fig. 20a) and is accompanied by a weak thermal ridge at 900 mb. and strong upper PV anomaly to the south (Fig. 20 b). There is little sign of an intense bent back warm front in this case with rather weak θ_w gradients until Biscay and Portugal where the cold front lies (Fig. 20c). The vertical velocity at 700 mb. shows no intense updraught phase ($\omega < -50$ mb./hr.) throughout the development and at 00Z on the 19th only a weak area of ascent occurs north of the low centre across Ireland and Scotland and also further south ahead of the cold front (Fig. 20 d).

Cross-sections were obtained along the line indicated in Fig. 19c for the same time. Two surface frontal zones can be found, each with a local normal wind component maximum and ascent. The depression forms in the more southerly of the two frontal zones to the south of the upper jet axis (Fig. 21a). These two surface fronts are clearly identifiable in the potential temperature cross-section (Fig. 21b) : the thermal contrast across the main front is about one half of that found in cases (a) and (b).

The M/θ_w cross-section shows considerable potential slantwise instability in the main frontal zone below 700 mb. (Fig. 21c). The SCAPE map at 00Z 18/1/88 shows quite extensive though small slantwise convective instability (Fig. 22).

(f) August 22 1988

To span the whole range of depression types it was decided to include this case which had virtually no intensification. At the data time of 00Z 22/8/88, a low complex was situated near 44 N 55 W with a primary centre of 1003 mb. near 45 N 53 W (Fig. 23 a). The main upper potential vorticity anomaly lay a

considerable distance to the west at about 46 N 70 W with little coupling to the thermal ridge associated with the primary low (Figs. 23 b and c). The vertical velocity map at 700 mb. for the analysis time shows a long chain of upward motion maxima associated with the frontal zone (Fig. 23 d).

At 00Z on the 23rd the primary low has deepened by only one millibar and has moved to 55 N 35 W (Fig. 24 a). The principal PV anomaly on the 330 K surface is still located well away from the surface low towards the cold air (Fig. 24 b) suggesting little coupling with the low level thermal anomaly. The θ_w field at 850 mb does not indicate any strong fronts near the low centre - only a broad tongue of high values directed towards the depression centre (Fig. 24c). Ascent at 700 mb. now takes place in an elongated zone ahead of the advancing tongue of warm air (Fig. 24 d).

Cross-sections along the line indicated in Fig. 24c at 00Z 23/8/88 show a primary upper-level jetstream lying on the cold side of the surface front with a suggestion of a low-level jet in the warm air (Fig. 25a).The θ cross-section (Fig. 25c) shows a broad and unremarkable baroclinic zone. The M/θ_w section indicates an extensive region of mid-level potential symmetric instability though a strongly symmetrically stable boundary layer on the warm side of the surface front (Fig. 25 b). Little SCAPE for boundary layer air parcels can be found anywhere near the depression (Fig. 26).

(g) **March 11 1989**

This late winter case is good example of a non-explosive cyclogenesis event, deepening by only 12 mb. in 24 hours . At the analysis time 00Z 11/3/89 the depression has a double centre located near 45 N 45 W with central pressures of 1006 and 1010 mb. (Fig. 27a). An intense baroclinic extends northeastwards into this region with rather weak PV anomalies aloft (Fig. 27 b). The 850 mb. θ_w map shows a very strong airmass contrast near and upstream of the low centre (Fig. 27 c) with quite strong ascent at 700 mb. indicated on the forward side of the thermal ridge (Fig. 26 d).

At 00Z 12/3/89 the depression still has a double centre with corresponding central pressures of 997 and 998 mb. (Fig. 28a). The PV anomaly at upper levels is still rather weak with no values greater than 10 PV units near the low (Fig. 28b). No warm core seclusion process has taken place during the development : only a long tongue of high θ_w can be found at 850 mb. (Fig. 28c). The 700 mb. vertical velocity is characterised by two ascent regions located near local

intensifications of the θ_w gradient (Fig. 28d).

Vertical cross-sections were taken along the line indicated in Fig. 27c at the analysis time. In contrast to the explosive deepening cases, this one has all the attributes of a classical ana-cold front with the main jet axis positioned well to the cold air side of the surface front (Fig. 29a). The low-level thermal contrast is as great as that occurring in the explosive cases though no split baroclinicity field is evident (Fig. 29b).

The M/θ_w field shows that frontal zone is approximately moist slantwise neutral below 600 mb. and stable above (Fig. 29c). Only weak SCAPE values can be found in the warm air - typically less than 400 JKg^{-1} to the southeast of the low complex (Fig. 30).

(h) December 3 1988

This cyclogenesis case is also a fine example of a non-explosively deepening system. The main development took place from T+12 hrs to the end of the 36 hour forecast starting from 12Z December 2 1988. At 00Z 3/12/88 the low in question was centred near 44 N 50 W with a central pressure of 995 mb. (Fig. 31a) and lay in a long, very intense frontal zone (Fig. 31 b and c). A broad upper level PV anomaly lay well back in the cold air; some negative PV is evident above the low on the warm side of the surface front. Upward motion is concentrated close to the centre of the low and embedded in the frontal ascent (Fig. 31d).

At 00Z 4/12/88 the central pressure of the low is 977 mb. implying a 24 hour deepening of 18 mb. (Fig. 32a). The PV boundary between tropospheric and stratospheric air is only slightly perturbed by the development with a PV maimum of 9 PV units near the apex of the thermal ridge (Fig. 32b). The 850 mb. θ_w field shows warm air seclusion with the development of a bent back warm front (Fig. 32c). Notice the different impression one gets of the strength and extent of the cold front from the 900 mb. θ and 850 mb. θ_w maps (Fig. 32c). The sharp cold frontal θ gradient is well to the southwest of the system. Fig. 32d shows a rather weak vertical velocity pattern with far more symmetry between the strength of the upward and downward motion than in any of the explosively deepening systems.

Cross-sections were taken along the line indicated in Fig. 31c for 00Z 3/12/88. The normal wind component plot shows the 79 ms^{-1} jet maximum to be positioned well to the cold air side of the surface front as in the previous

case (Fig. 33a). Two strong horizontal shear zones associated with the upper and low-levels front are particularly noticeable. Their relative disposition causes a small region of strong anticyclonic vorticity just to the rear of the lower tropospheric front and extending up to 600 mb. The absolute momentum surfaces (Fig. 33c) flatten out in this region and some buckling is found - consistent with existence of a zone of negative potential vorticity. There is no split in the baroclinicity and the intense horizontal gradients associated with the upper and lower fronts are aligned (Fig. 33b). The M/θ_w cross-section (Fig. 33c) does not reveal much potential slantwise instability except, of course, in the zone of negative potential vorticity to the rear of the lower tropospheric front which is unconditionally dry symmetrically unstable. The SCAPE chart (Fig. 34) actually shows that to the south-west of the low centre there is a region of substantial SCAPE though it is not known if this influenced the development.

4. Discussion and conclusions

It is very difficult to summarize the time evolution of a low pressure system with a few pictures and even more difficult to try to draw general conclusions based on eight case studies. There is great variety of ways in which cyclogenesis can take place. The author subscribes to the Hoskins and McIntyre thesis that, with the proper use of colour or grey tone shading, isentropic potential vorticity maps provide a powerful means of visualising the dynamically important features of the upper level flow and their interaction with lower tropospheric frontal zones. Unfortunately, considerable exposure to quasi-geostrophic and semi-geostrophic theory is necessary before the full significance of potential vorticity maps can be appreciated. Until good three-dimensional inversion routine become available for solving the invertibility problem in a practical context, even the experienced dynamicist will have a rather qualitative understanding of the interaction of PV anomalies. The existence of regions of moist slantwise neutrality or instability causes qualitatively different flow responses which are not well understood. The forecaster needs to see PV charts in the same optimized graphical format for a long period of time before he or she will feel at home with them.
Combining PV with other diagnostic quantities such low-level potential temperature or wind vectors plus isotachs is likely to give new insights and help bridge the gap between 500 mb height and isentropic PV maps.

There is no consensus of opinion as to which isentropic surface is best to

use. Although some account must be taken of the seasonal variation of the tropopause with respect to isentropic surfaces, a selection of isentropic levels between 300 K and 330 K would probably cover most situations in middle latitudes. An additional worry concerns the lack of compatibility between horizontal and vertical resolution in the Fine-Mesh model near the tropopause. The crudest Rossby height argument would imply that the vertical layer separation should be $\simeq f/N$ times the horizontal gridlength where f is the Coriolis parameter and N is the buoyancy frequency : this would be about 400 m just above the tropopause and 1.5 km below. The level separation in the Fine-Mesh model is currently about 60 mb. near the tropopause which is $\simeq$ 2 km. Potential vorticity is commonly computed by forming the product of the absolute vorticity measured on a θ surface with the stability $\partial\theta/\partial p$. This means that the isentropic absolute vorticity at a gridpoint is a mean over an area $\simeq$ 150 km wide whereas the stability is a mean over a 4 km layer near the tropopause - a rather serious mismatch which must distort the analysis of PV structures making them look more like absolute vorticity features. These comments are in line with the current ground swell of opinion that the vertical resolution in current operational forecast models is incompatible with their horizontal resolution (Lindzen and Fox-Rabinovitz, 1989).

It is not clear how useful SCAPE maps might be to the practising forecaster but they are certainly of considerable scientific interest. Although areas of large and positive SCAPE appear in two of the explosive cyclogenesis cases considered here, as well as the October 1987 Storm, they are not a prerequisite for explosive development. It may be that depressions which develop in an environment of considerable slantwise instability differ in structure and intensity from the common-or-garden variety. A speculation that has been uppermost in the author's mind since the October Storm event is that depressions which have tight, sub-synoptic scale cores with hurricane force winds are those which develop in an environment of great moist slantwise instability. Case studies of explosive cyclogenesis carried out by Bosart (1988) and Reed and Albright (1986) were also concerned with this possibility. A related speculation considers the cloud head phenomenon (known to accompany such systems, Bottger et al, 1975), to be a visual manifestation of vigorous slantwise convective ascent forced by an upper level PV anomaly. Only a carefully designed numerical modelling study, using very high hoizontal and vertical resolution, will be able to answer these questions.

Apart from presenting these new diagnostics, some interesting tentative findings have emerged from the study of the October Storm (Shutts, 1989) and these eight cyclogenesis events .

(1) there is a case for deviating from standard frontal analysis practice so as to take full account of the disjointed frontal structures indicated by the model eg. bent back warm fronts and cold fronts which do not join with the warm front.

(2) in the early stages of baroclinic development, the relative disposition of the primary jet axis and near surface front are different for explosive and non-explosive deepening events. In the former the upper jet is almost coincident with the position of the surface depression and main frontal zone : non-explosive cases have jetstream axes well behind the surface front over the cold air.

(3) as a consequence of (2), the positions of the upper and lower tropospheric fronts in explosively deepening systems cause the overall baroclinicity to be split (particularly striking in case (a)). In the non-explosively deepening events studied here, there was a tendency for the horizontal θ gradients associated with upper and lower tropospheric fronts to align in a classical ana-cold frontal structure.

(4) it is proposed on the basis of (3) that the split cloud head structure known to precede explosive deepening (Monk and Bader (1988)) is a visual manifestation of the split baroclinicity and associated moisture distribution. Fig. 35 is schematic picture comparing a vertical cross-section through the baroclinic environment of an incipient explosive development with that of a non-explosive system. The axis of the primary jet approximately marks the edge a pre-existing upper level cirrus shield at the tropopause fold. Rapid frontogenesis aided by slantwise convective ascent leads to the formation of a distinct sheet of stratiform cloud

extending well over the cold air.

The greater meridional extent of the overall cloud system in explosive deepening events is consistent with the different relative disposition of upper and lower fronts. In the non-explosive case, the upper cirrus shield overlaps, or merges with, the lower tropospheric frontal cloud. The absence of much overlap between the edge of the jetstream cirrus and the position of the surface front in explosively deepening systems increases the total area of cloud cover.

Finally, one might well ask the question, ' Why should cyclonic development be explosive if the upper jet is located over the surface front?' The probable answer is that with this flow configuration the potential vorticity anomaly is more nearly overhead the primary surface front implying a stronger degree of coupling between upper and lower level disturbances. There is considerable scope for numerical experimentation to examine the growth of baroclinic disturbances with different idealised initial flow states. These would do much to answer some of the questions posed in this paper concerning the dynamical factors favouring explosive cyclogenesis.

5. Acknowledgments

I would like to thank G. Monk, M. Young, A. Waters and Drs M. Bader and T. Davies for many helpful conversations concerning satellite imagery and Fine-Mesh model interpretation. The programing involved in this work was carried out by Mr. J. Wyatt.

6. References

Bottger, H., M. Eckardt and U. Katergiannakis (1975) ' Forecasting extratropical storms with hurricane intensity using satellite information', J. Appl. Met., 14, 1259-1265.

Bretherton, F.P. (1966) ' Critical layer instability in baroclinic flows', Quart. J. Roy. Met. Soc., 92, 325-334.

Emanuel, K. (1983) ' On assessing local conditional symmetric instability from atmospheric soundings', Mon. Wea. Rev., 111, 2016-2033.

Emanuel, K., M. Fantini and A.J. Thorpe (1987) ' Baroclinic instability in an environment of small stability to moist slantwise convection. Part I : Two-dimensional models', J. Atmos. Sci., 44, 1559-1573.

Hoskins, B.J., M.E. McIntyre (1985) ' On the use and significance of isentropic potential vorticity maps', Quart. J. Roy. Met. Soc., 111, 877-916.

Lindzen, R.S. and Fox-Rabinovitz (1989) ' Consistent vertical and horizontal resolution', Mon. Wea. Rev., 117, 2575-2583.

Monk, G.A. and M. Bader (1988) ' Satellite images showing the development of the Storm of 15-16 October 1987', Weather, 43, 130-134.

Shapiro, M. A. (1989) ' The mesoscale structure of extratropical marine cyclones', IAMAP 89 Conference preprint volume, MP-24, Univ. Reading, England.

Shutts, G.J. (1989) ' Dynamical aspects of the October Storm 1987' : a study of a successful Fine-Mesh model simulation', MetO(11) Sci. Note No. 15, Met. Office, Bracknell, England.

Shutts, G.J. (1990) ' SCAPE charts from numerical weather prediction model fields', (in preparation)

7. Figure Legends

Fig. 1 Maps at 12Z 30/1/88:

(a) Sea-level pressure (mb.). Cont. Int. 4 mb.

(b) Potential vorticity on the 330 K isentropic surface (shaded) with potential temperature at 900 mb. (Cont. Int. 2 K). PV is shaded at 4 levels : dark, > 10 PVU; medium, 6-10 PVU; light, 2-6 PVU; very faint, negative PV.

(c) Wet-bulb potential temperature at 850 mb. (Cont. Int. 2 K). Shaded if θ_w > 12 °C.

(d) Vertical velocity (Dp/Dt) at 700 mb. (Cont. Int. 10 mb./hr.). Upward motion shaded.

Fig. 2 as for Fig. 1 at 00Z 31/1/88

Fig. 3 Vertical cross-sections along the line indicated in Fig. 2 (c) at 00Z 31/1/88:

(a) normal component (solid lines, Cont. Int. 5 ms^{-1}), potential temperature (dashed lines, Cont. Int. 5 K) and wind vectors in plane of cross-section

(b) potential temperature (Cont. Int. 1 K)

(c) absolute momentum (solid lines, Cont. Int. 5 ms^{-1}) and wet-bulb potential temperature (dot-dash, Cont. Int. 1 K)

Fig. 4 SCAPE map at 12Z 30/1/88. Numbers are in $J.Kg^{-1}$ X 100 and the solid contour is 1000 $J.Kg^{-1}$.

Fig. 5 as for Fig. 1 except at 00Z 8/2/88

Fig. 6 as for Fig. 1 except at 00Z 9/2/88

Figs. 7 as for Figs. 3 except at 00Z 8/2/88

Fig. 8 as for Fig. 4 except at 06Z 8/2/88.

Fig. 9 as for Fig. 1 except at 00Z 30/9/88.

Fig. 10 as for Fig. 1 except at 18Z 30/9/88

Fig. 11 Potential temperature map at 850 mb. 06Z 30/9/88 with line of cross-sections.

Fig. 12 as for Fig. 3 except at 06Z 30/9/88.

Fig. 13 as for Fig. 4 except at 00Z 30/9/88.

Fig. 14 as for Fig. 1 except at 00Z 12/1/89.

Fig. 15 as for Fig. 1 except at 06Z 13/1/89.

Fig. 16 Potential temperature at 850 mb. for 06Z 12/1/89 with line of cross-sections.

Fig. 17 as for Fig. 3 except for 06Z 12/1/89.

Fig. 18 as for Fig. 4 except at 12Z 12/1/89.

Fig. 19 as for Fig. 1 except at 00Z 18/1/88.

Fig. 20 as for Fig. 1 except at 00Z 19/1/88.

Fig. 21 as for Fig. 3 except at 00Z 18/1/88.

Fig. 22 as for Fig. 4 except at 00Z 18/1/88.

Fig. 23 as for Fig. 1 except at 00Z 22/8/88.

Fig. 24 as for Fig. 1 except at 00Z 23/8/88.

Fig. 25 as for Fig. 3 except at 00Z 23/8/88.

Fig. 26 as for Fig. 4 except at 00Z 23/8/88.

Fig. 27 as for Fig. 1 except at 00Z 11/3/89.

Fig. 28 as for Fig. 1 except at 00Z 12/3/89.

Fig. 29 as for Fig. 3 except at 00Z 11/3/89.

Fig. 30 as for Fig. 4 except at 00Z 11/3/89.

Fig. 31 as for Fig. 1 except at 00Z 3/12/88.

Fig. 32 as for Fig. 1 except at 00Z 4/12/88.

Fig. 33 as for Fig. 3 except at 00Z 3/12/88.

Fig. 34 as for Fig. 4 except at 00Z 3/12/88.

Fig. 35 Schematic pictures showing the relative disposition of upper and lower fronts in a cross-section normal to the flow in (a) explosively deepening systems and (b) non-explosively deepening systems.

FIG. 1

PSTAR
VALID AT 12Z ON 30/1/1988 DAY 30 DATA TIME 12Z ON 30/1/1988 DAY 30
SURFACE

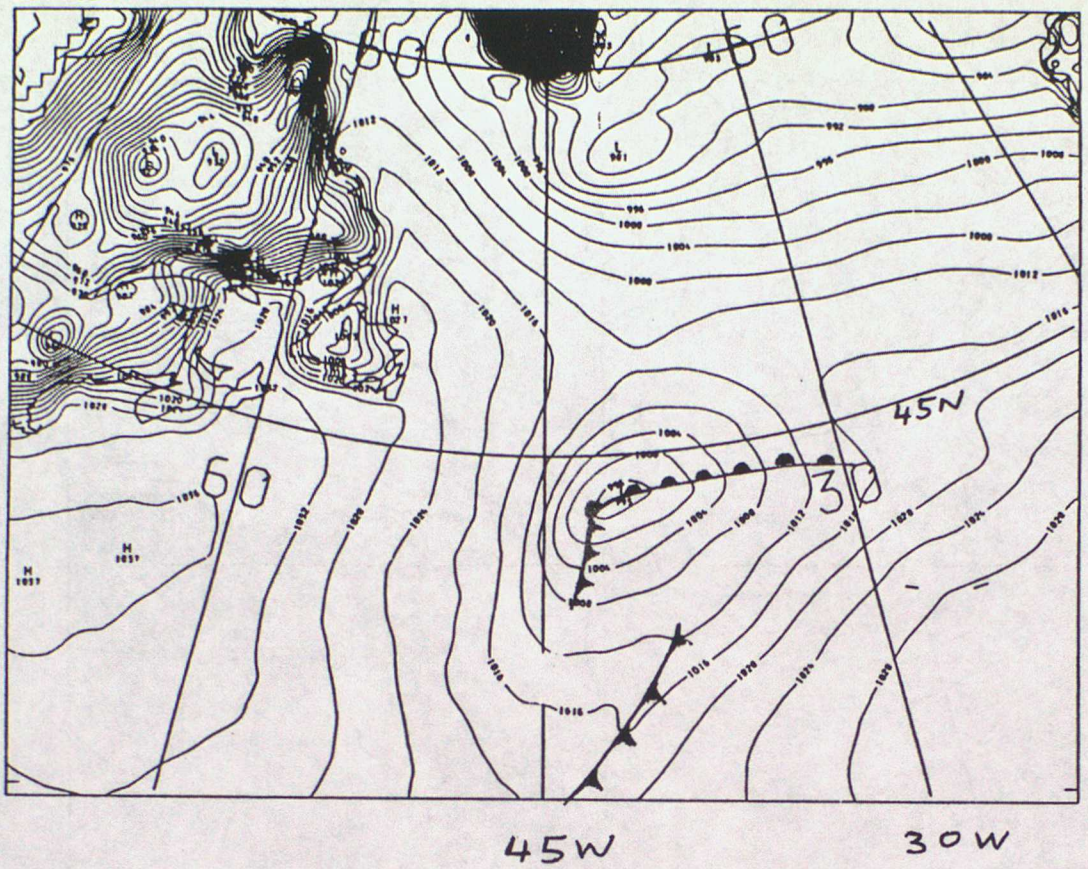

(a)

PV CHART THETA=330.0
900MB POTENTIAL TEMPERATURE
VALID AT 12Z ON 30/1/1988 DAY 30 DATA TIME 12Z ON 30/1/1988 DAY 30
LEVEL: 50 MB

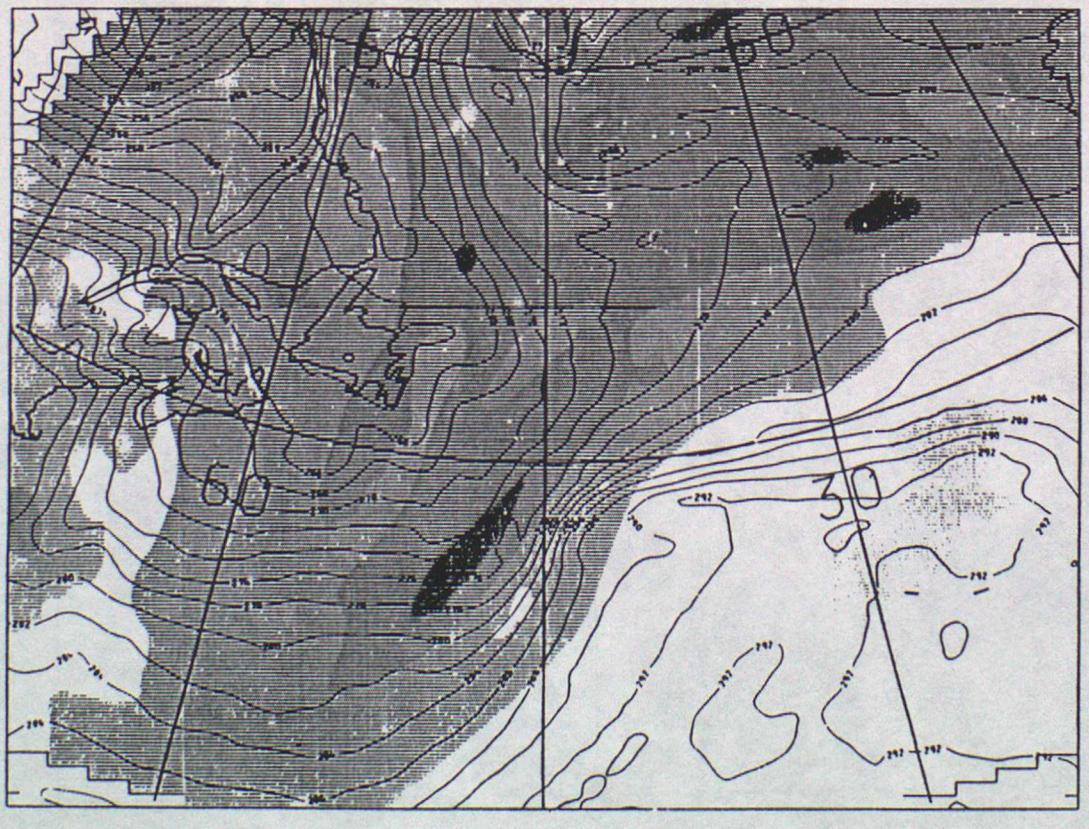

(b)

FIG. 1

WET BULB POT TEMP
VALID AT 12Z ON 30/1/1988 DAY 30 DATA TIME 12Z ON 30/1/1988 DAY 30
LEVEL: 850 MB

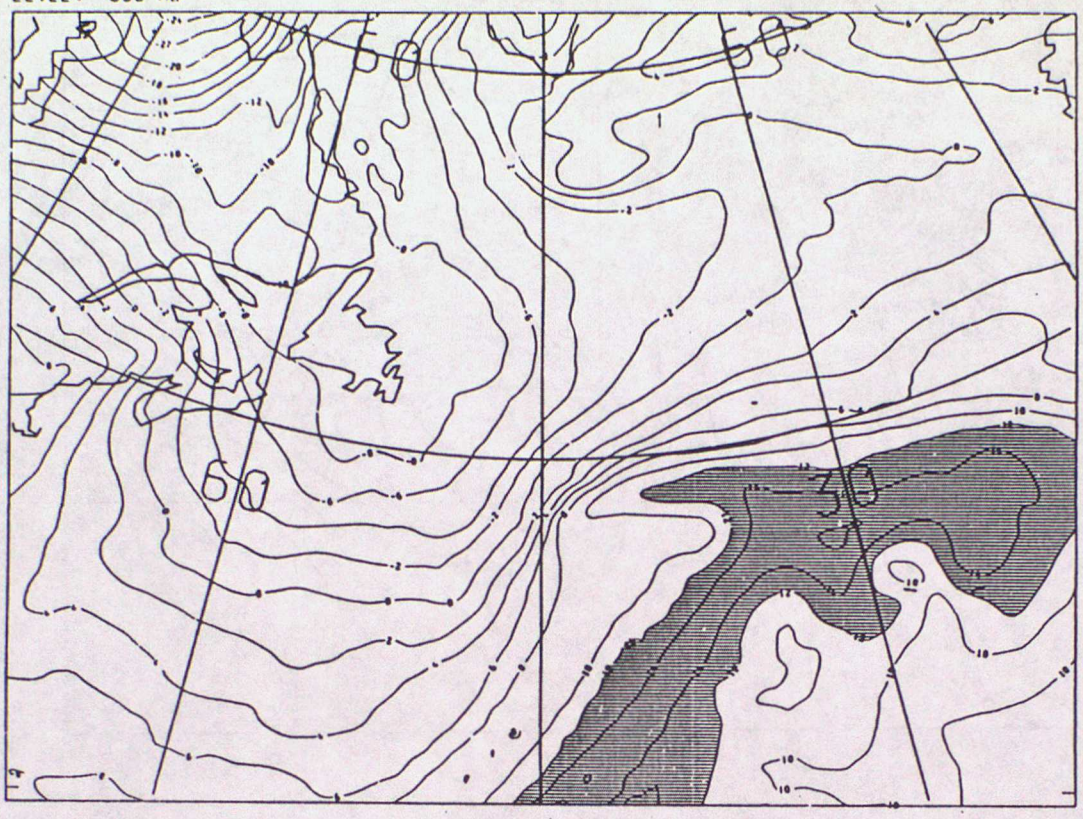

(c)

VERTICAL VELOCITY
VALID AT 12Z ON 30/1/1988 DAY 30 DATA TIME 12Z ON 30/1/1988 DAY 30
LEVEL: 700 MB

(d)

FIG. 2

PSTAR
VALID AT 0Z ON 31/1/1988 DAY 31 DATA TIME 12Z ON 30/1/1988 DAY 30
SURFACE

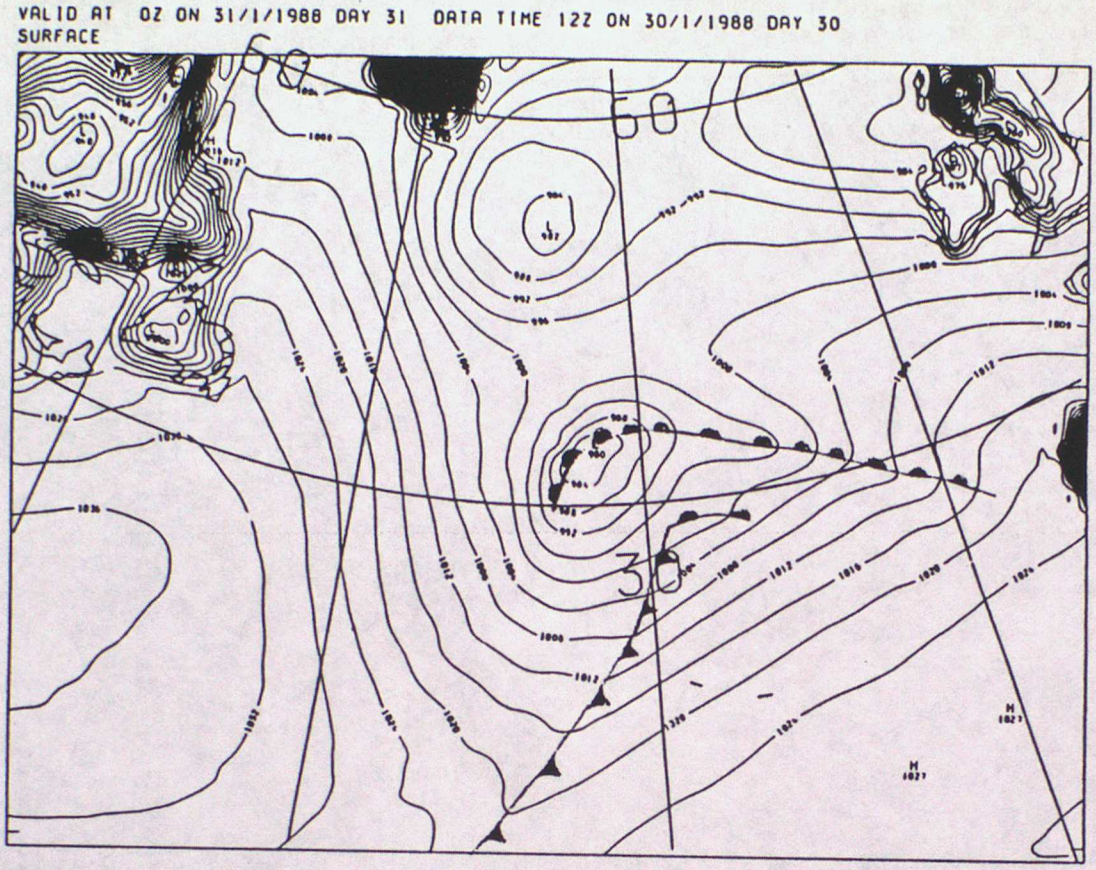

(a)

PV CHART THETA=330.0
900MB POTENTIAL TEMPERATURE
VALID AT 0Z ON 31/1/1988 DAY 31 DATA TIME 12Z ON 30/1/1988 DAY 30
LEVEL: 50 MB

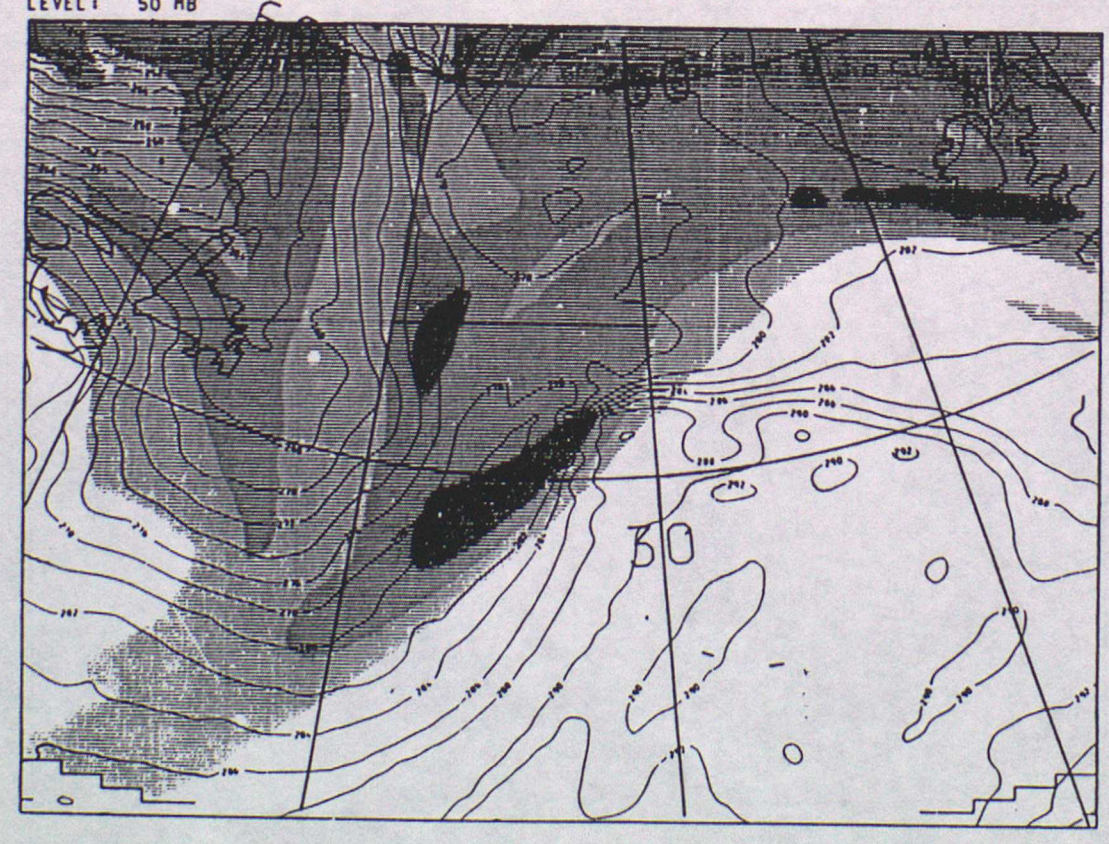

(b)

Fig. 2

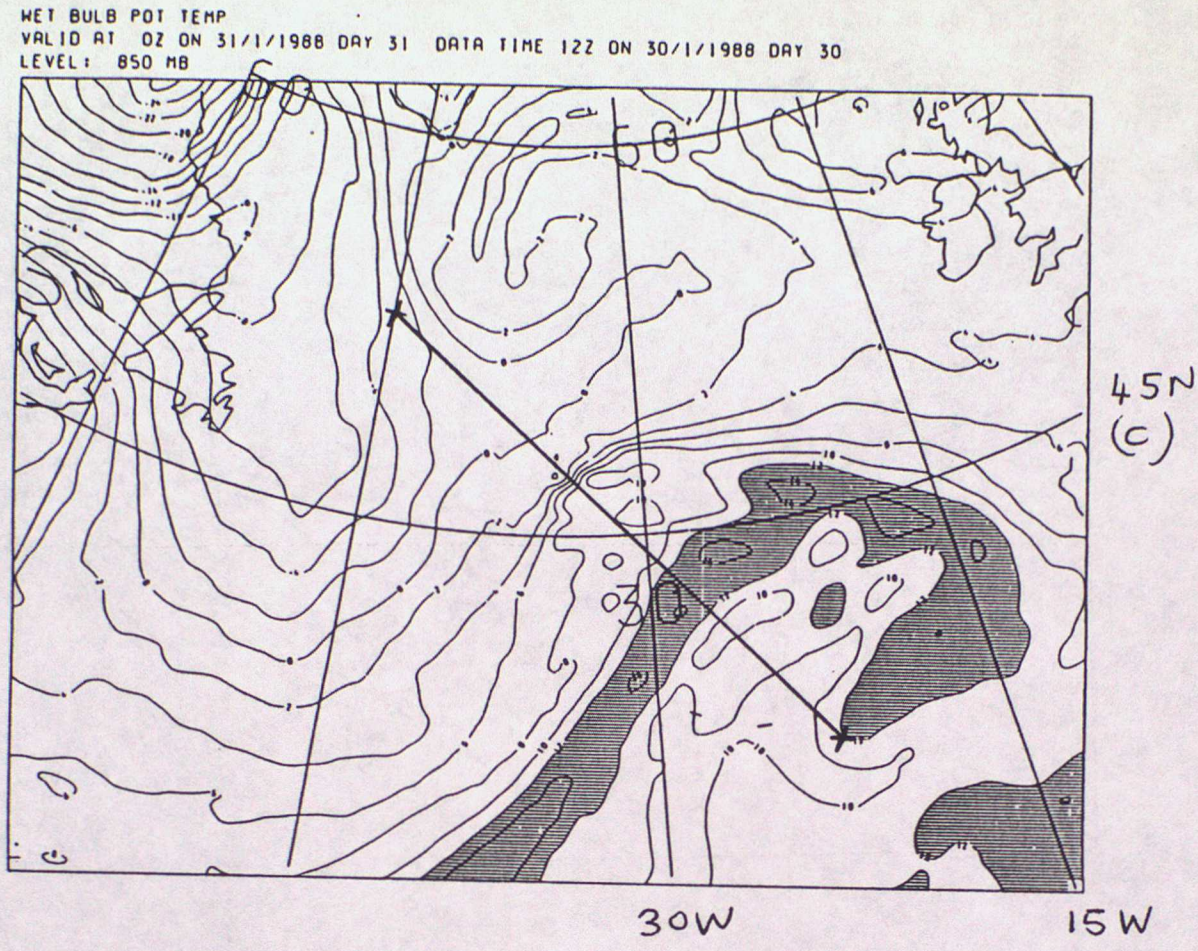
WET BULB POT TEMP
VALID AT 0Z ON 31/1/1988 DAY 31 DATA TIME 12Z ON 30/1/1988 DAY 30
LEVEL: 850 MB
45N
(c)
30W
15W


VERTICAL VELOCITY
VALID AT 0Z ON 31/1/1988 DAY 31 DATA TIME 12Z ON 30/1/1988 DAY 30
LEVEL: 700 MB
(d)

FIG. 3

GC. X-SECTION. V=SOLID CONTOURS -VE SHADED. U&W ARROWS. POT.TEMP=PECKED CONTOURS
VALID AT 0Z ON 31/1/1988 DAY 31 DATA TIME 12Z ON 30/1/1988 DAY 30

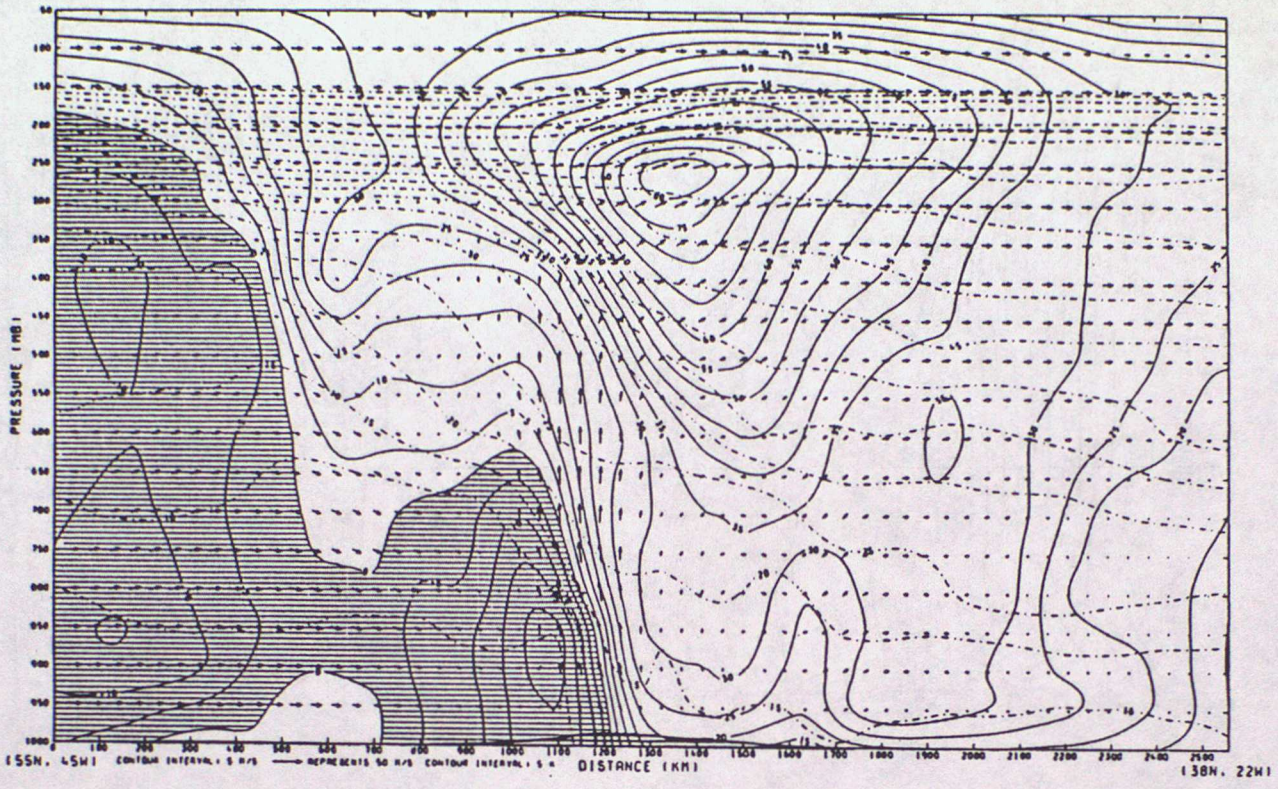

(a)

POTENTIAL TEMPERATURE
VALID AT 0Z ON 31/1/1988 DAY 31 DATA TIME 12Z ON 30/1/1988 DAY 30

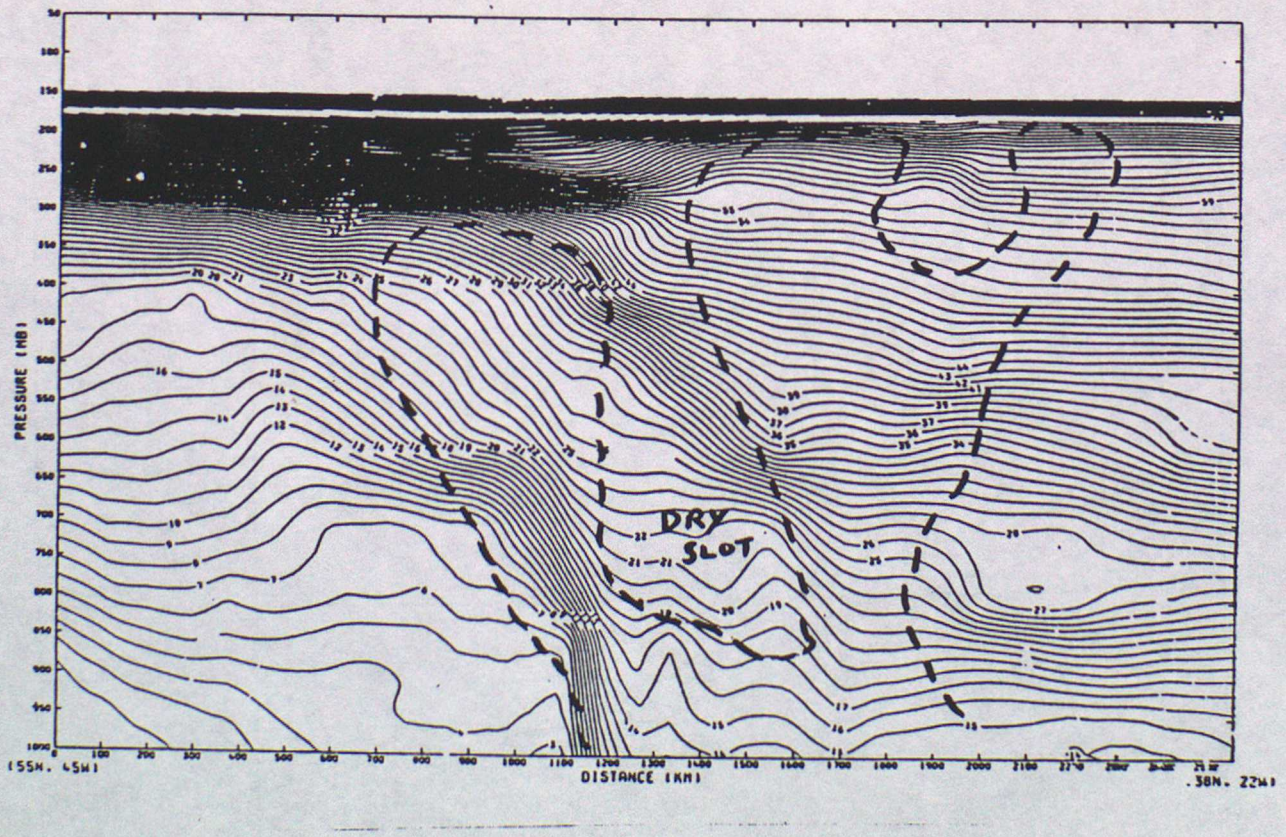

(b)

FIG. 3 (c)

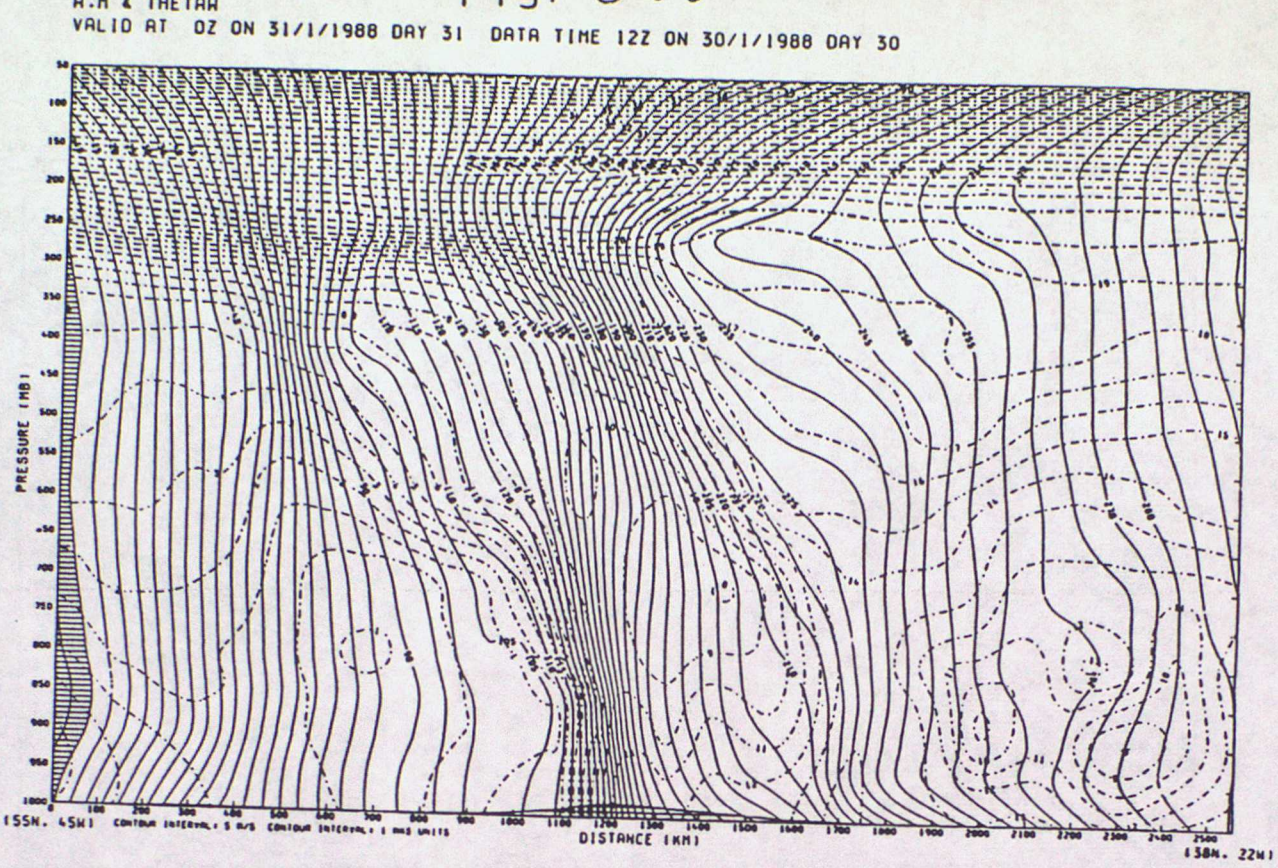

FIG. 4

SCAPE (J/KG X .01) PLOTTED WHERE SCAPE > 100 J/KG

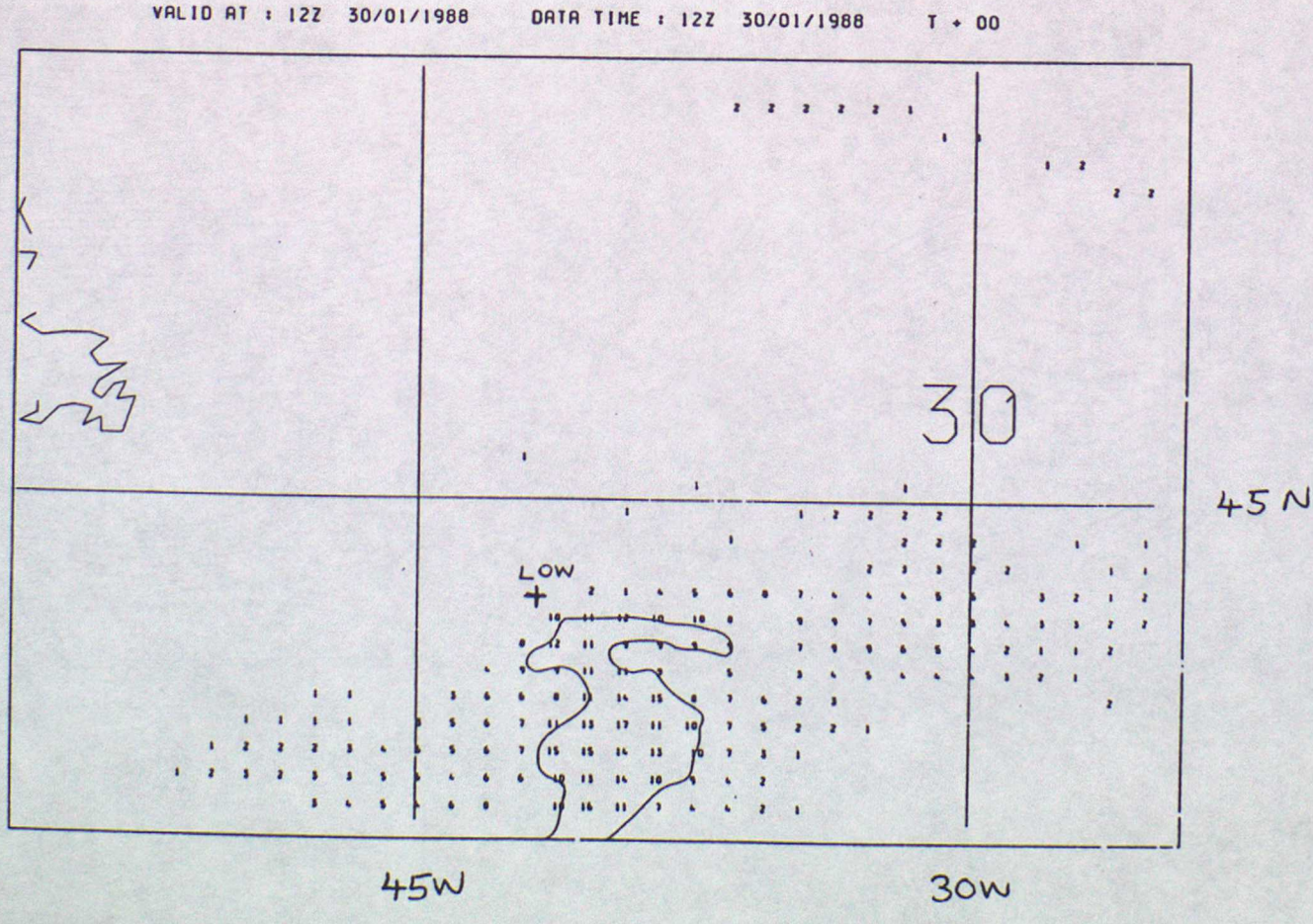

FIG. 5

PSTAR
VALID AT 0Z ON 8/2/1988 DAY 39 DATA TIME 0Z ON 8/2/1988 DAY 39
SURFACE

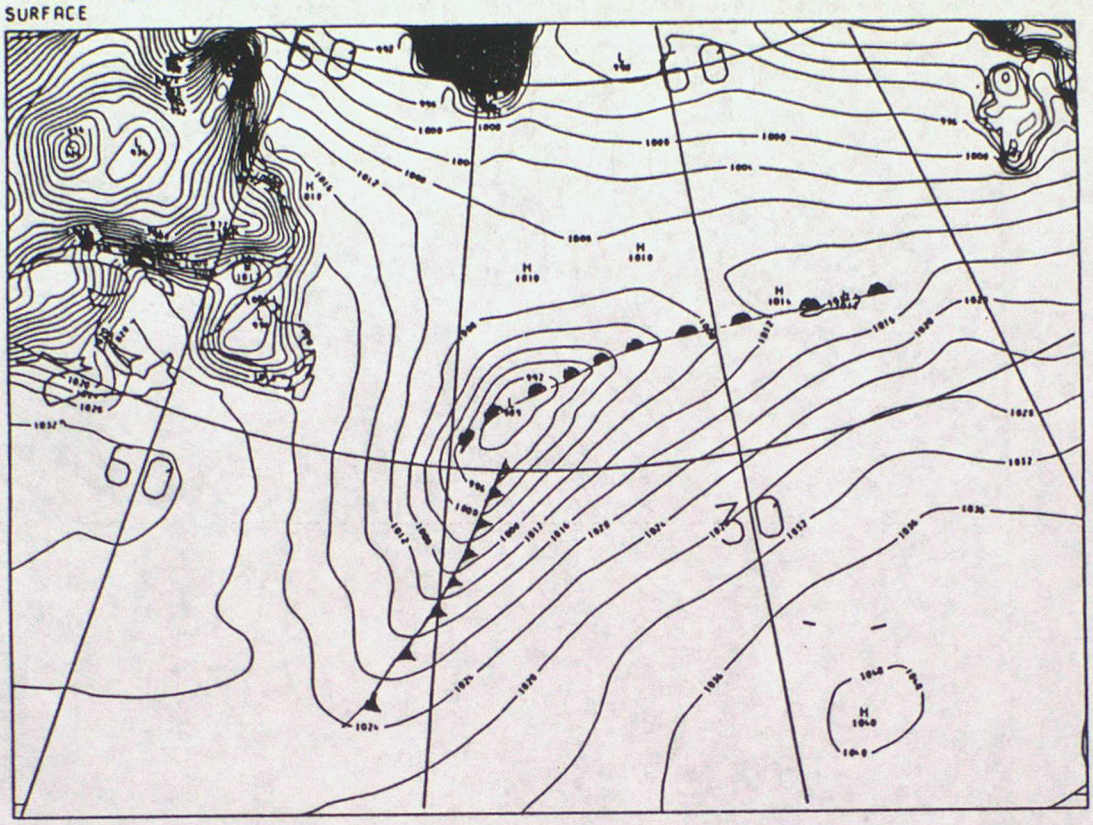

45N
(a)

PV CHART THETA=330.0
900MB POTENTIAL TEMPERATURE
VALID AT 0Z ON 8/2/1988 DAY 39 DATA TIME 0Z ON 8/2/1988 DAY 39
LEVEL: 50 MB

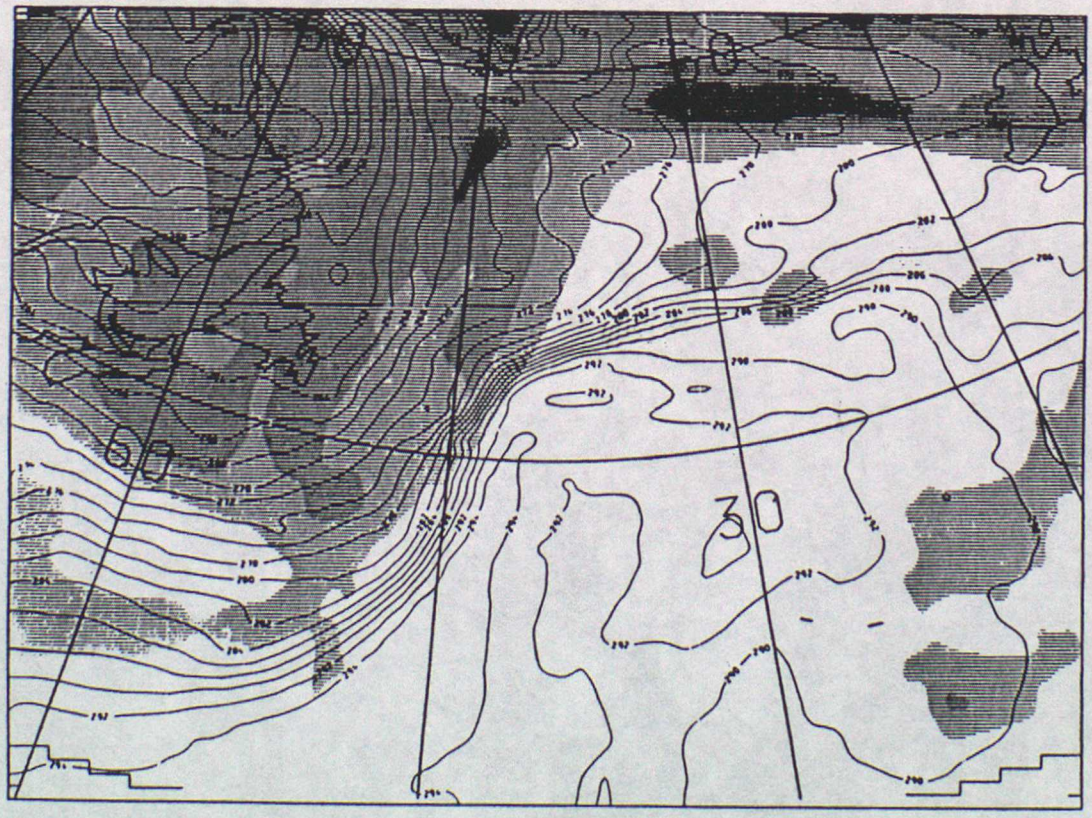

(b)

Fig. 5

WET BULB POT TEMP
VALID AT 0Z ON 8/2/1988 DAY 39 DATA TIME 0Z ON 8/2/1988 DAY 39
LEVEL: 850 MB

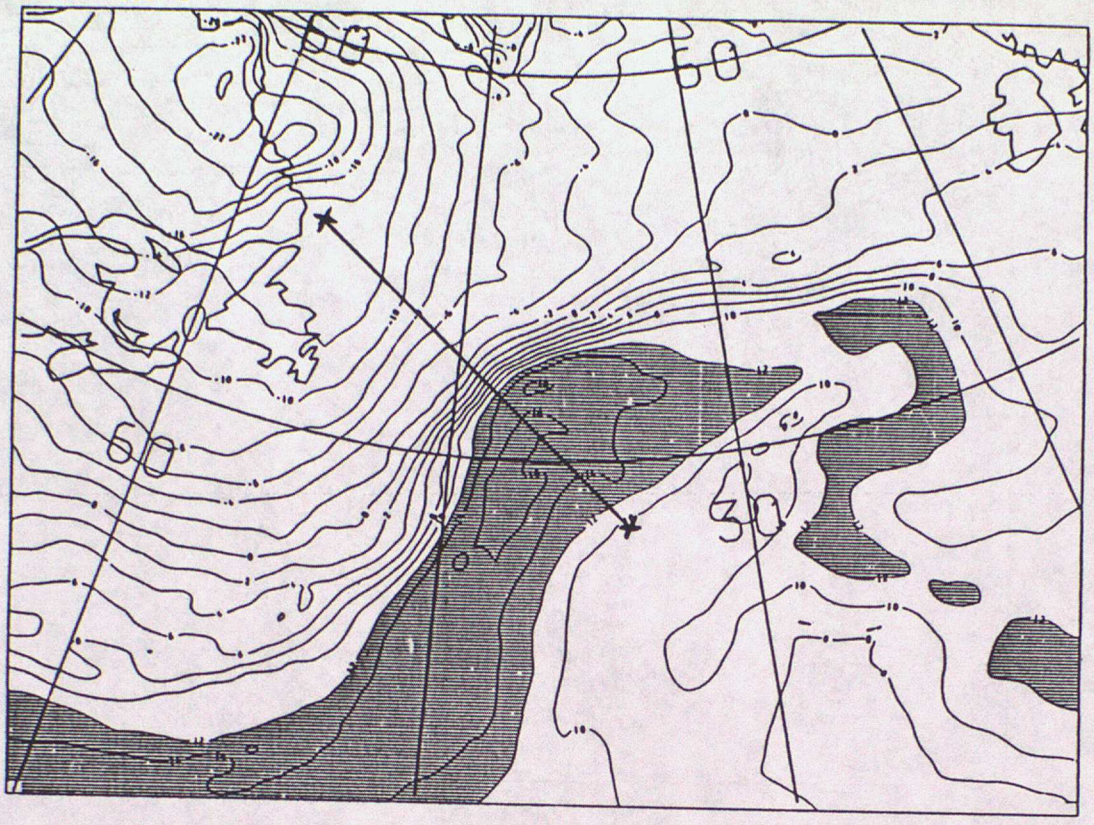

(c)

VERTICAL VELOCITY
VALID AT 0Z ON 8/2/1988 DAY 39 DATA TIME 0Z ON 8/2/1988 DAY 39
LEVEL: 700 MB

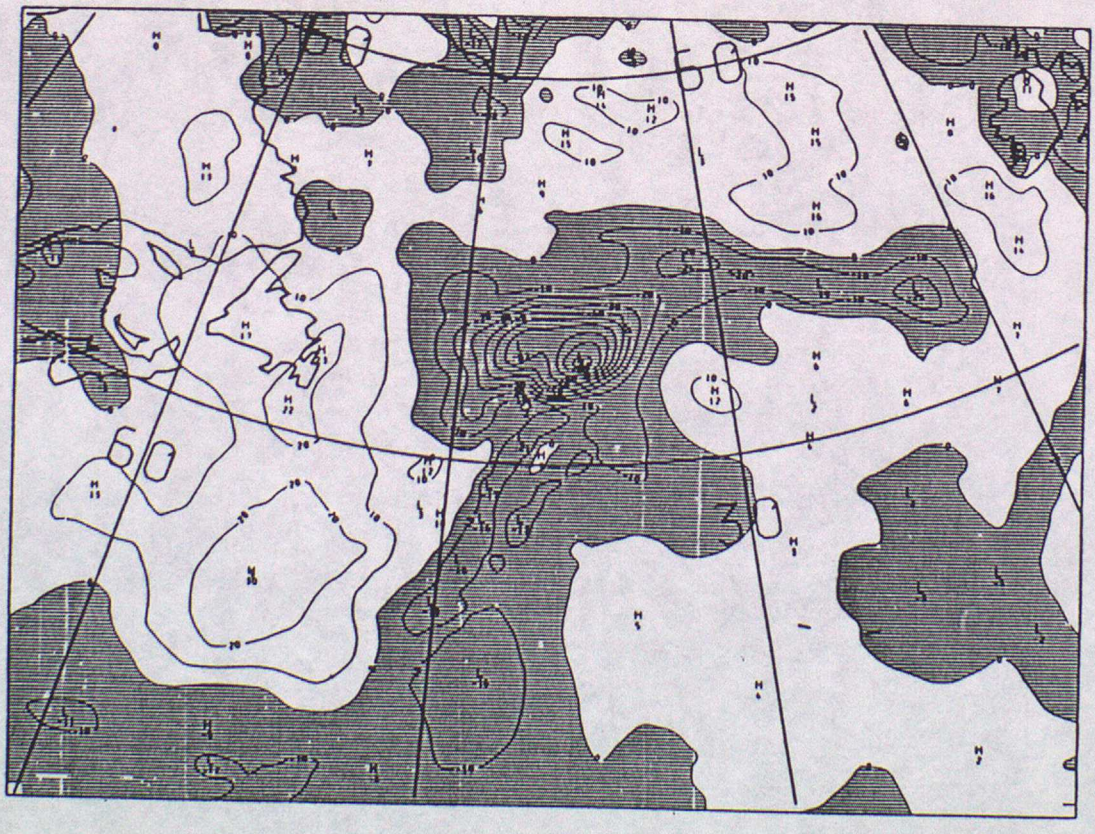

(d)

Fig. 6

PMSL
VALID AT 0Z ON 9/2/1988 DAY 40 DATA TIME 0Z ON 8/2/1988 DAY 39
SEA LEVEL

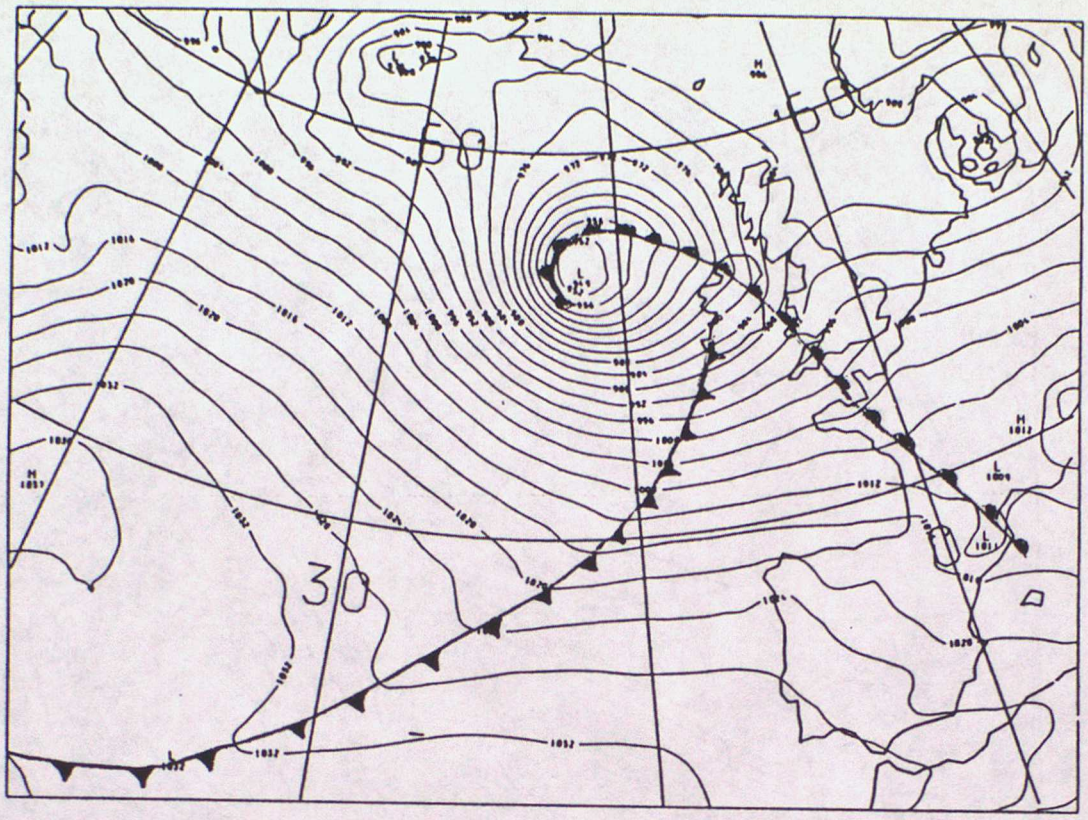

(a)

45N

PV CHART THETA=330.0
900MB POTENTIAL TEMPERATURE
VALID AT 0Z ON 9/2/1988 DAY 40 DATA TIME 0Z ON 8/2/1988 DAY 39
LEVEL: 50 MB

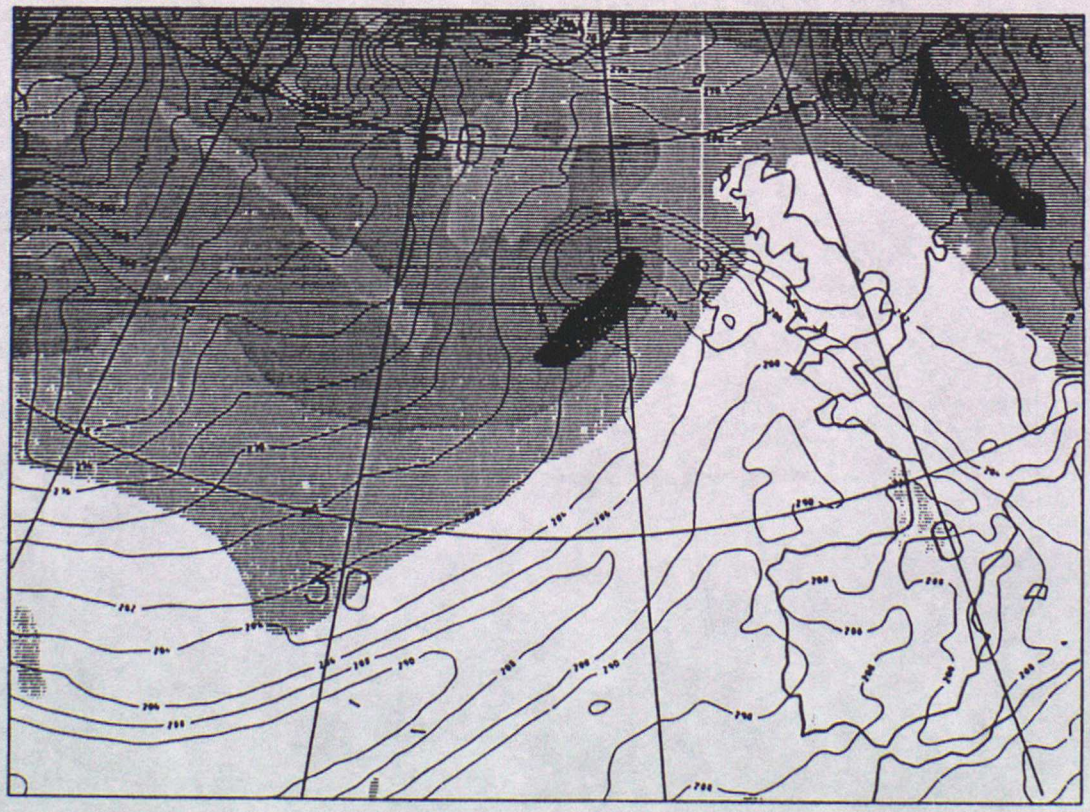

(b)

FIG. 6

WET BULB POT TEMP
VALID AT 0Z ON 9/2/1988 DAY 40 DATA TIME 0Z ON 8/2/1988 DAY 39
LEVEL: 850 MB

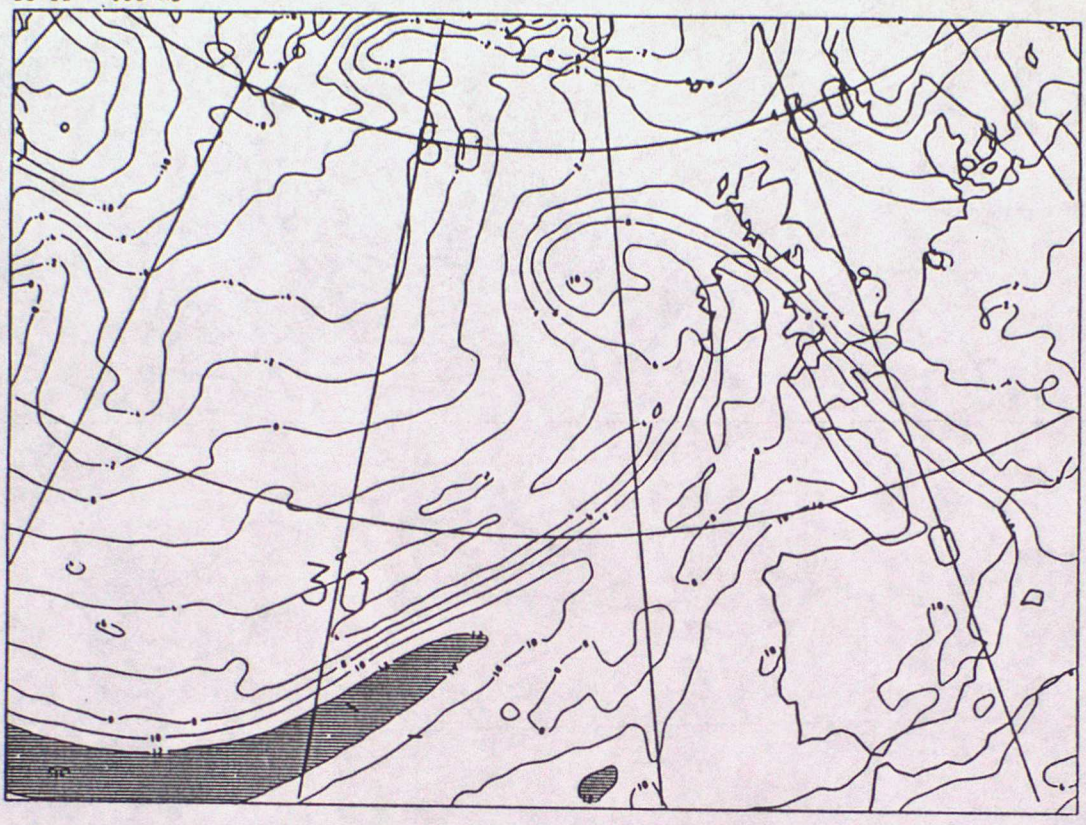

(c)

VERTICAL VELOCITY
VALID AT 0Z ON 9/2/1988 DAY 40 DATA TIME 0Z ON 8/2/1988 DAY 39
LEVEL: 700 MB

(d)

Fig. 7

GC. X-SECTION. V=SOLID CONTOURS -VE SHADED. U&W ARROWS. POT.TEMP=PECKED CONTOURS
VALID AT 0Z ON 8/2/1988 DAY 39 DATA TIME 0Z ON 8/2/1988 DAY 39

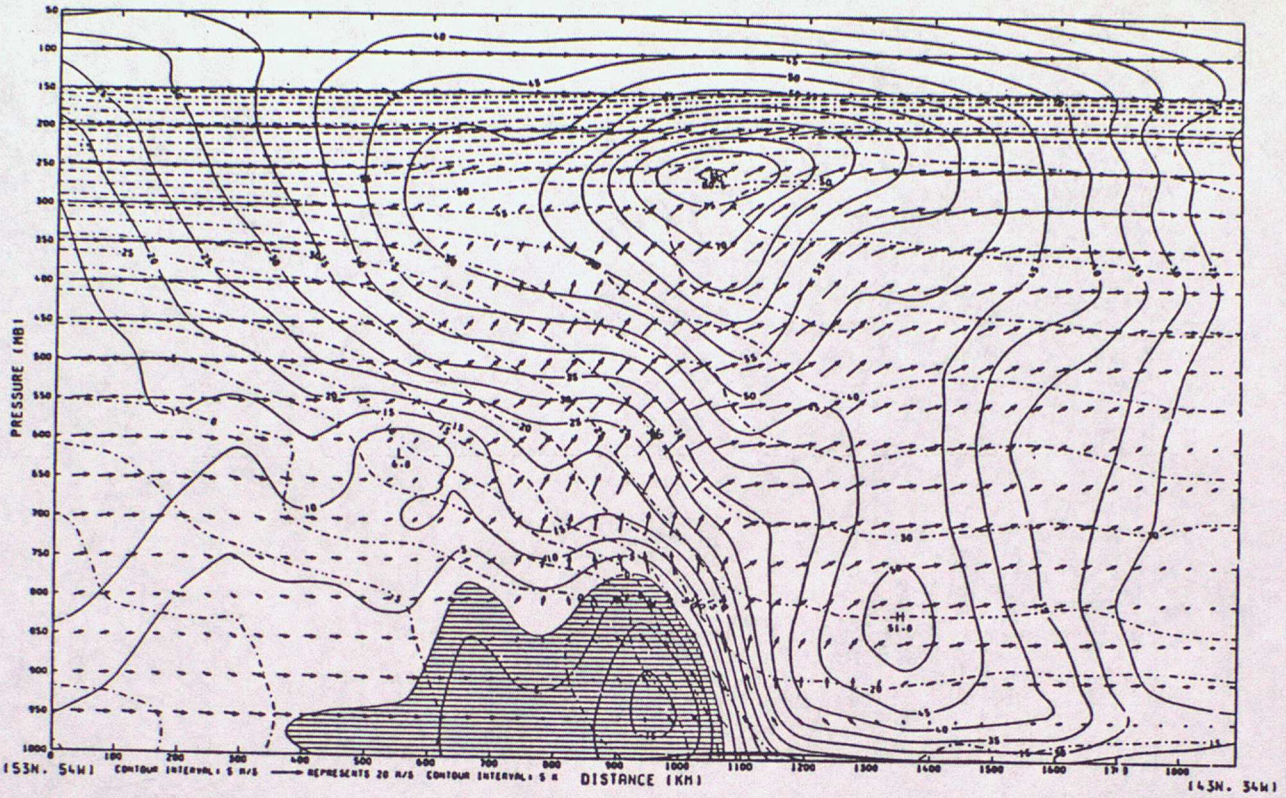

(a)

THETA
VALID AT 0Z ON 8/2/1988 DAY 39 DATA TIME 0Z ON 8/2/1988 DAY 39

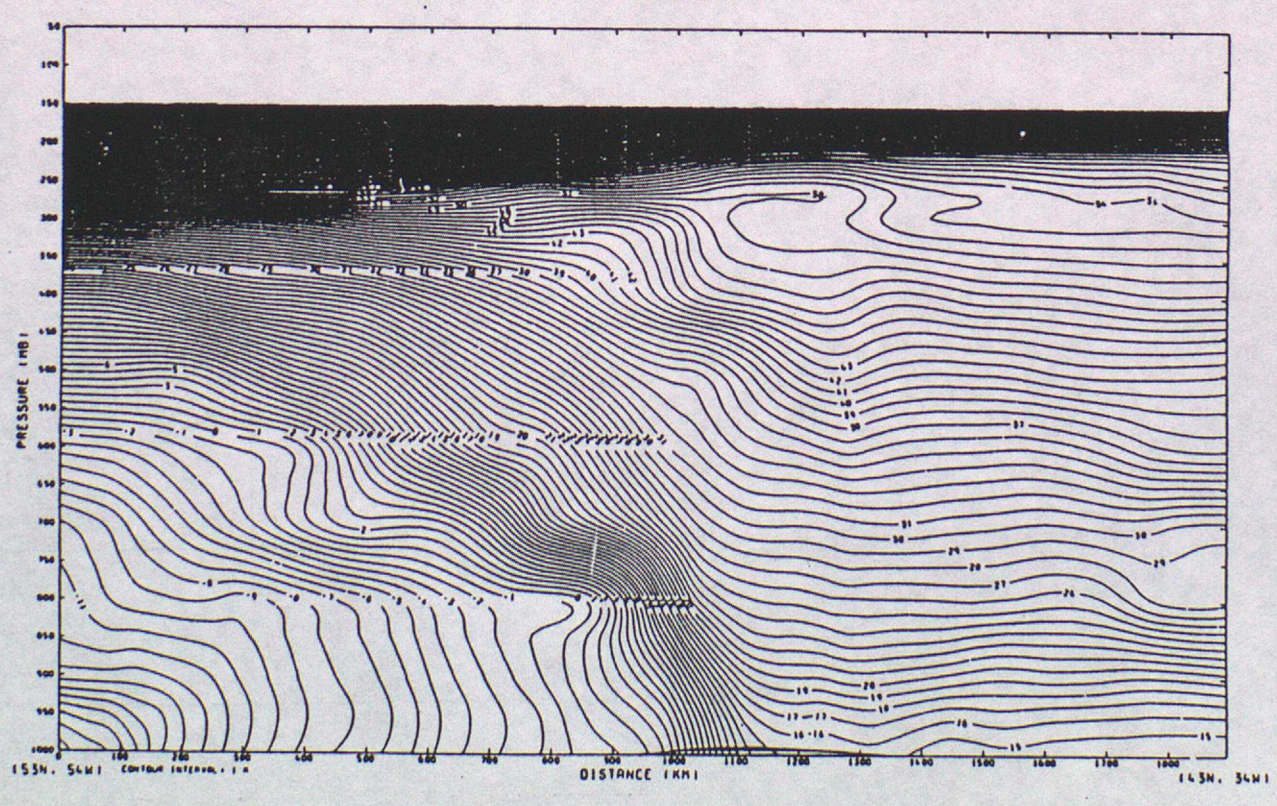

(b)

FIG. 7c

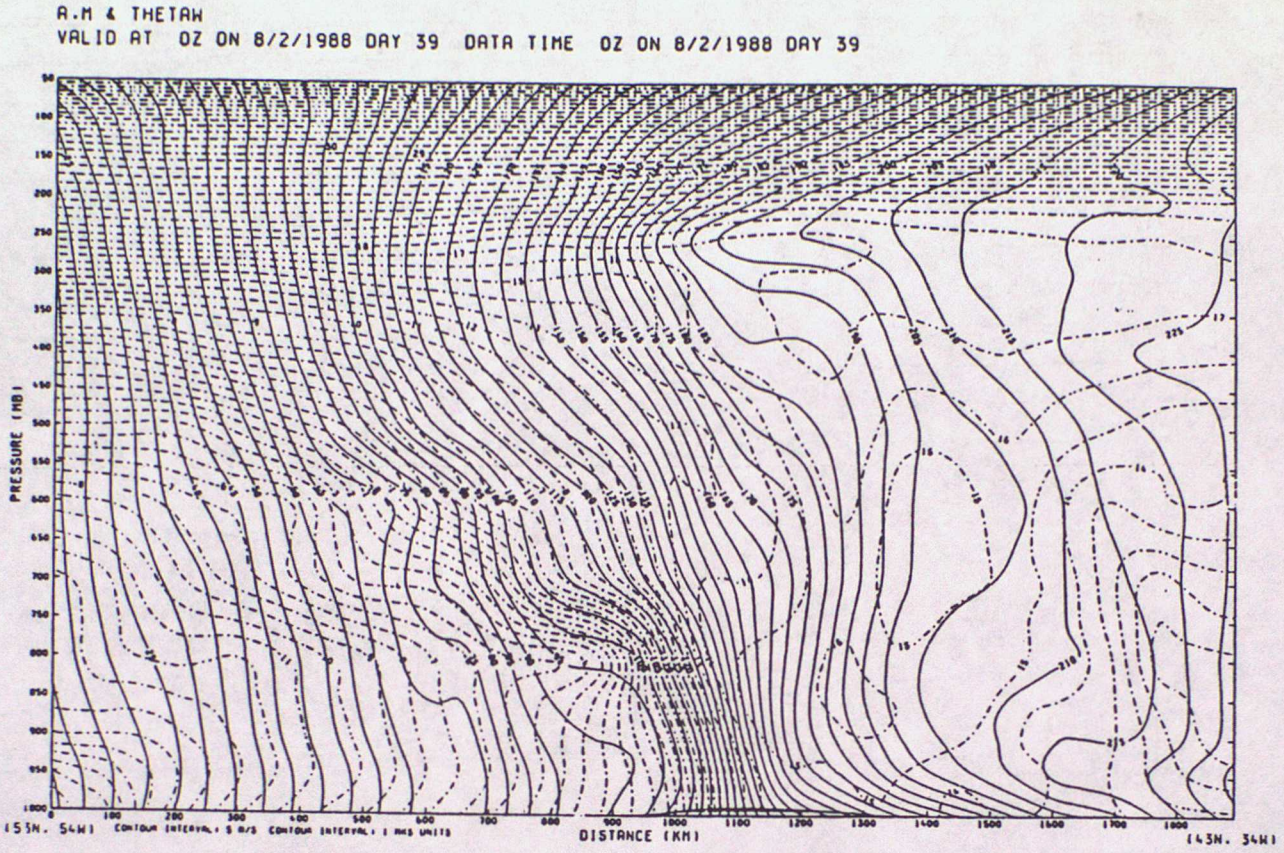

FIG. 8

SCAPE (J/KG X .01) PLOTTED WHERE SCAPE > 100 J/KG

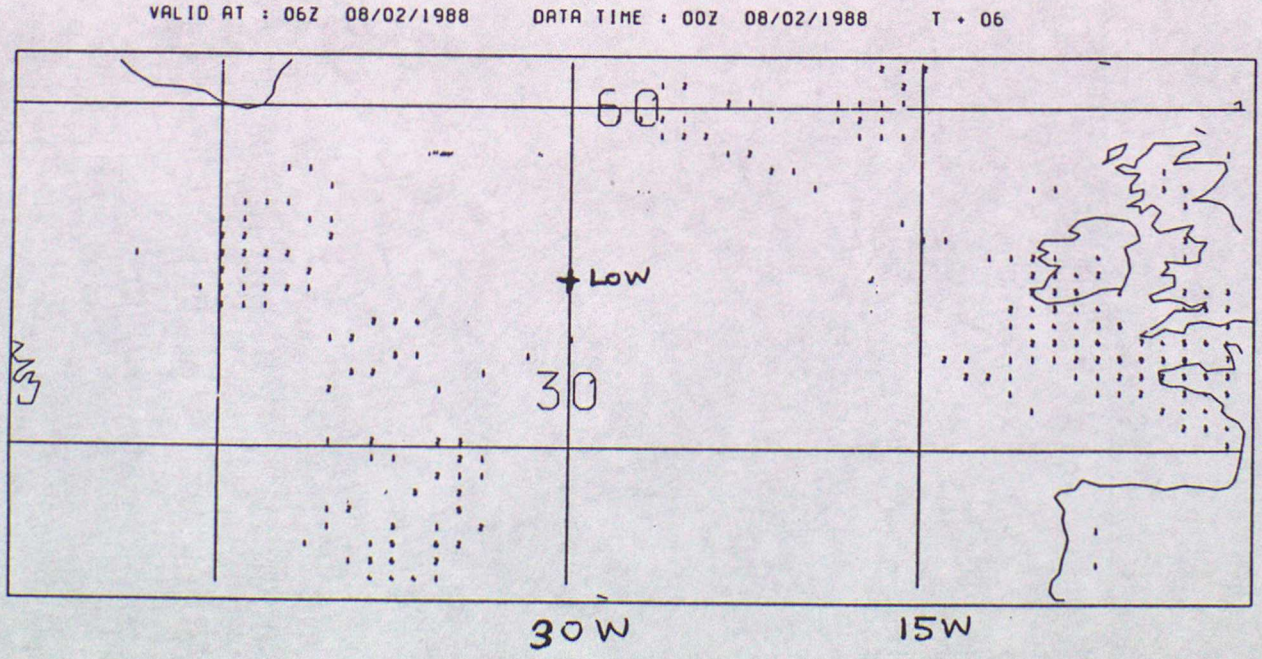

Fig. 9

PMSL
VALID AT 0Z ON 30/9/1988 DAY 274 DATA TIME 0Z ON 30/9/1988 DAY 274
SEA LEVEL

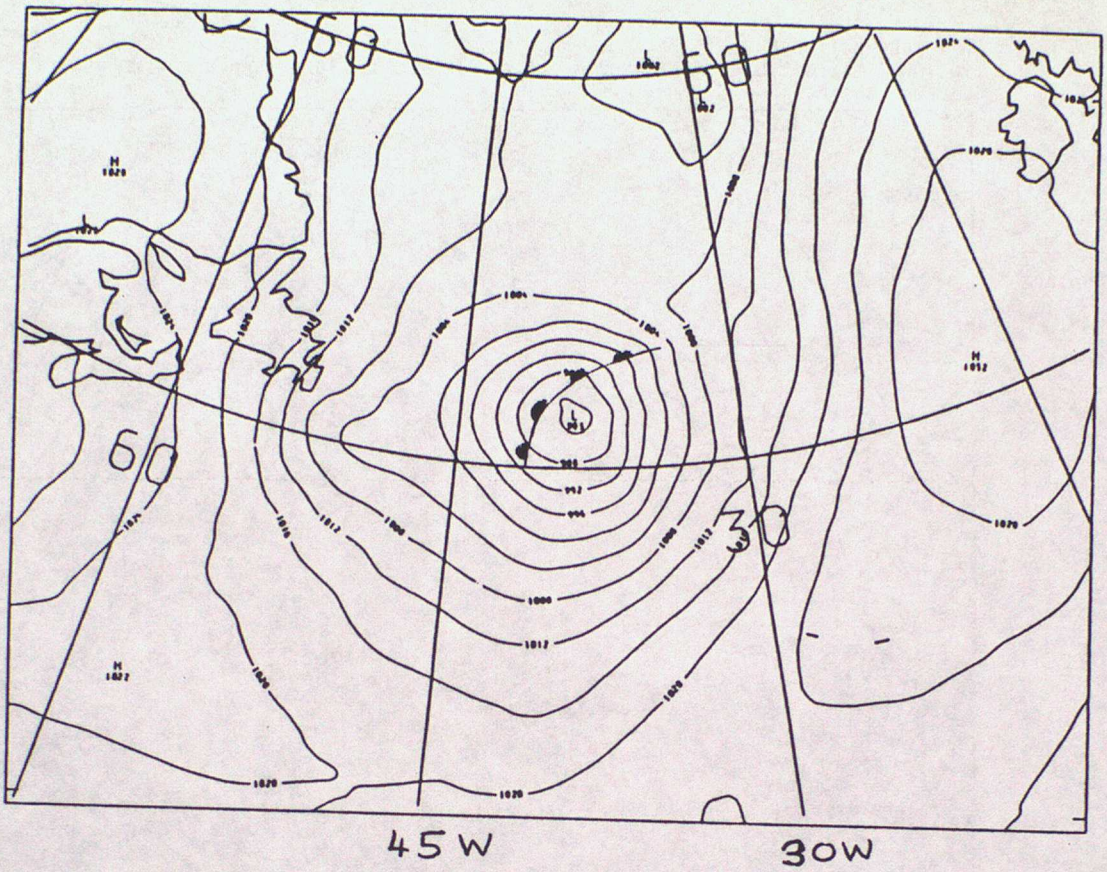

(a)

PV CHART THETA=330.0
900MB POTENTIAL TEMPERATURE
VALID AT 0Z ON 30/9/1988 DAY 274 DATA TIME 0Z ON 30/9/1988 DAY 274
LEVEL: 50 MB

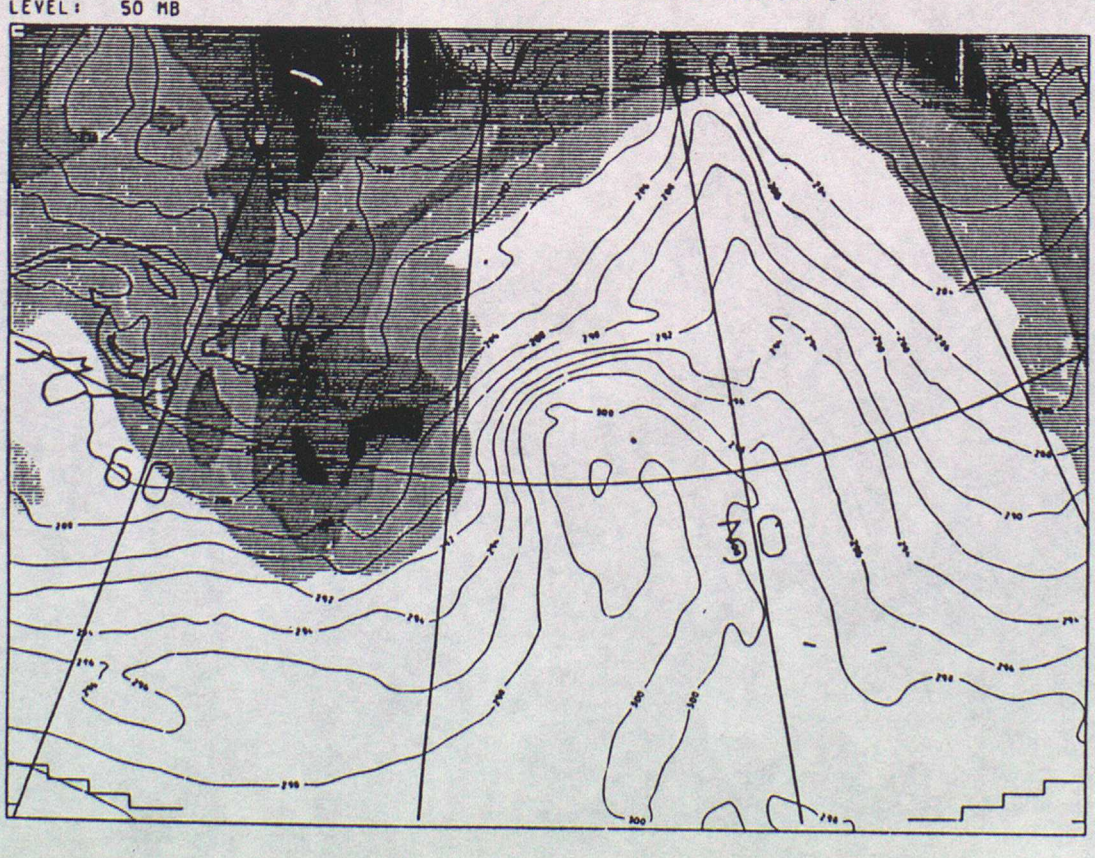

(b)

FIG. 9

WET BULB POT TEMP
VALID AT 0Z ON 30/9/1988 DAY 274 DATA TIME 0Z ON 30/9/1988 DAY 274
LEVEL: 850 MB

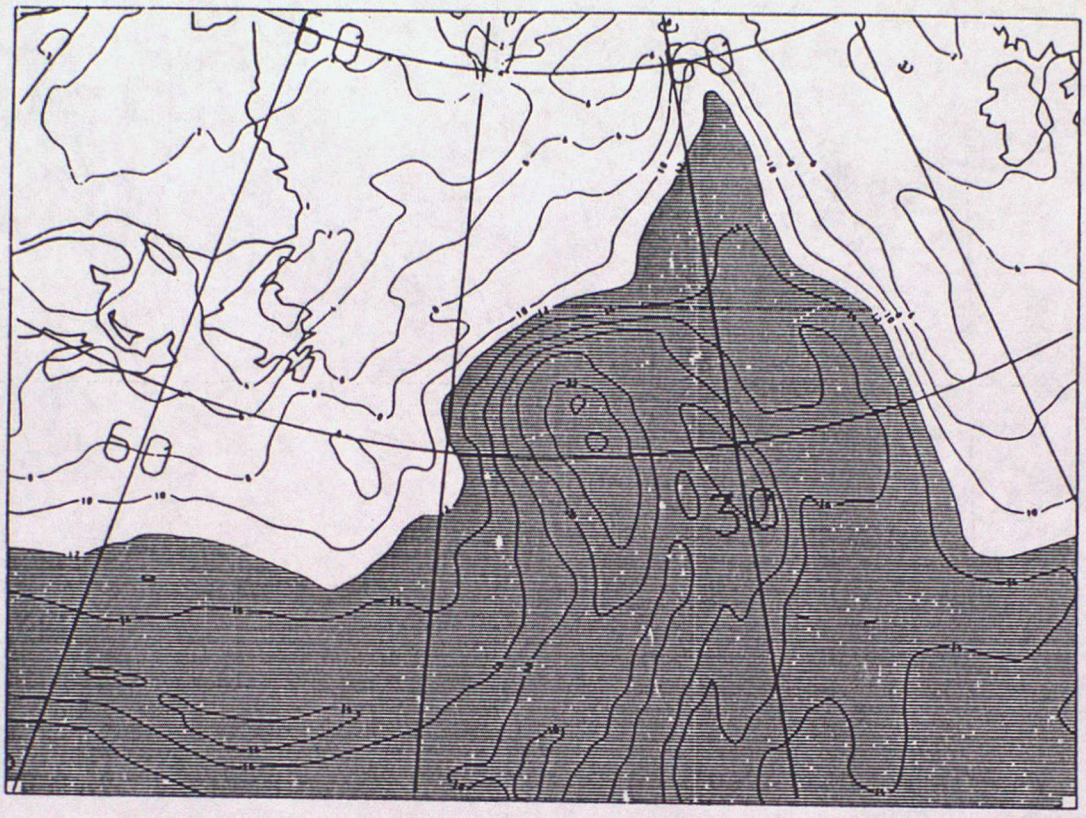

(c)

VERTICAL VELOCITY
VALID AT 0Z ON 30/9/1988 DAY 274 DATA TIME 0Z ON 30/9/1988 DAY 274
LEVEL: 700 MB

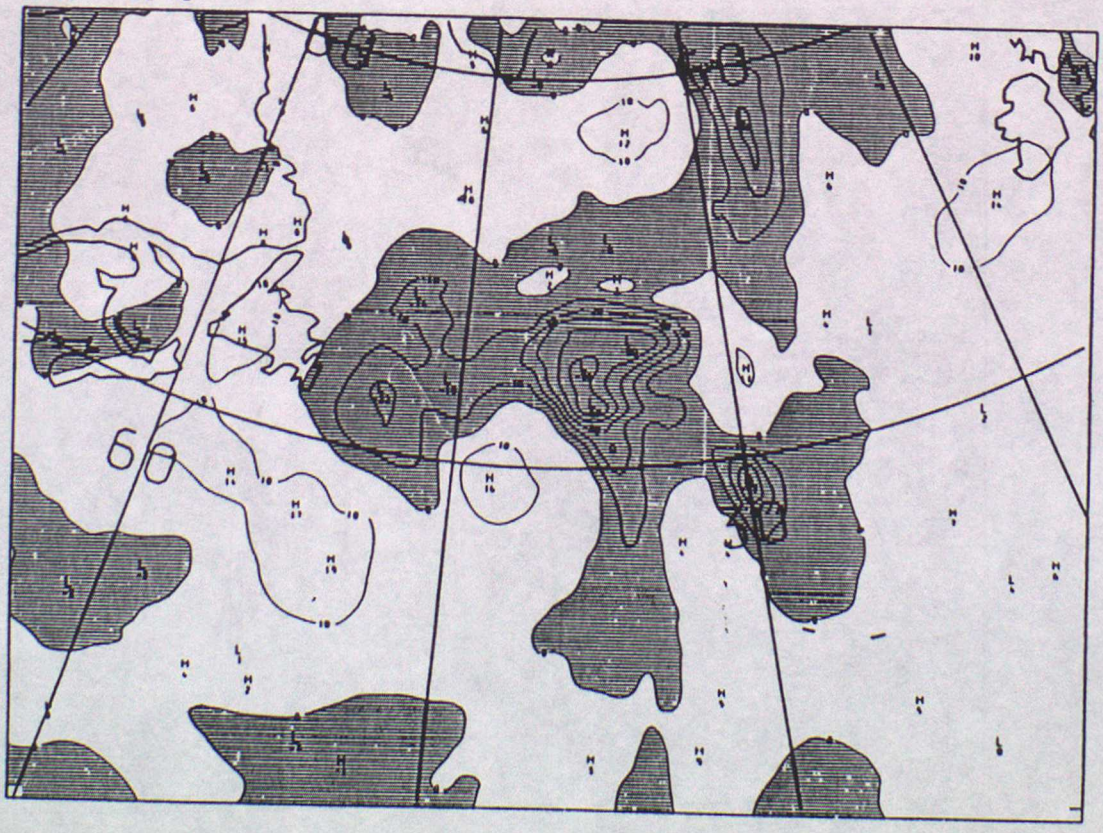

(d)

FIG. 10

PMSL
VALID AT 18Z ON 30/9/1988 DAY 274 DATA TIME 0Z ON 30/9/1988 DAY 274
SEA LEVEL

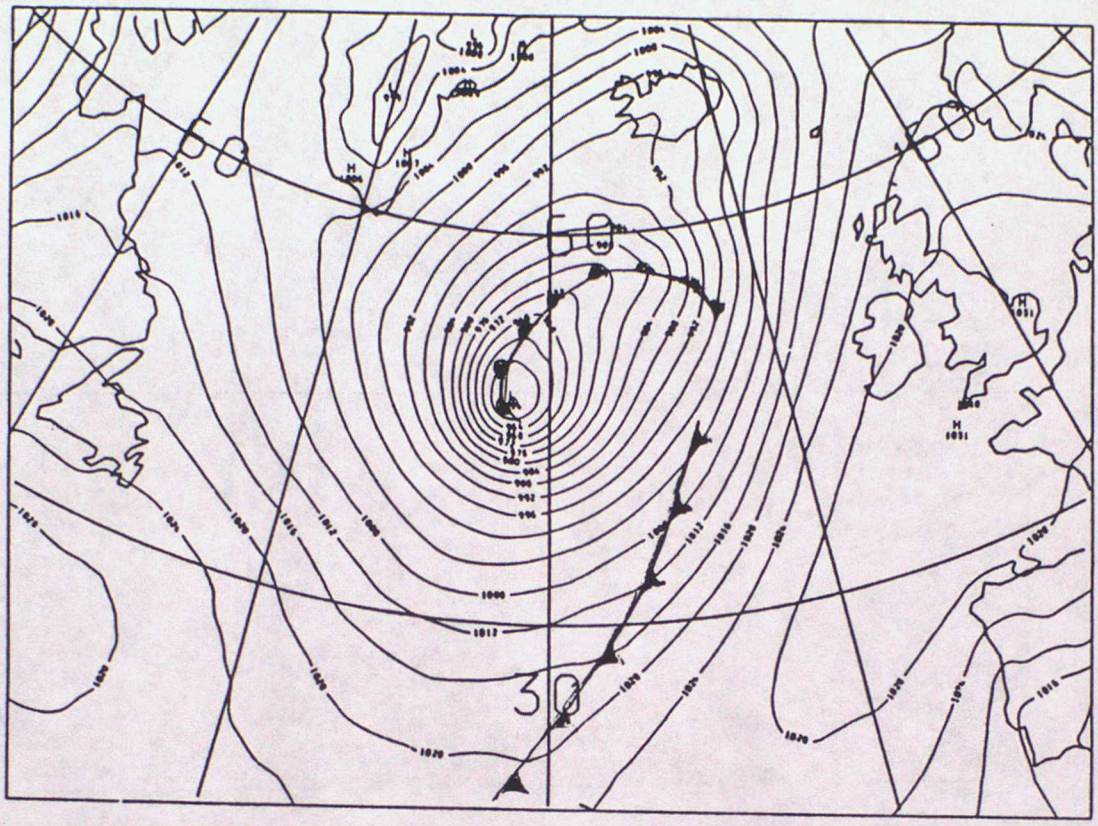

(a)

PV CHART THETA=330.0
900MB POTENTIAL TEMPERATURE
VALID AT 18Z ON 30/9/1988 DAY 274 DATA TIME 0Z ON 30/9/1988 DAY 274
LEVEL: 50 MB

(b)

FIG. 10

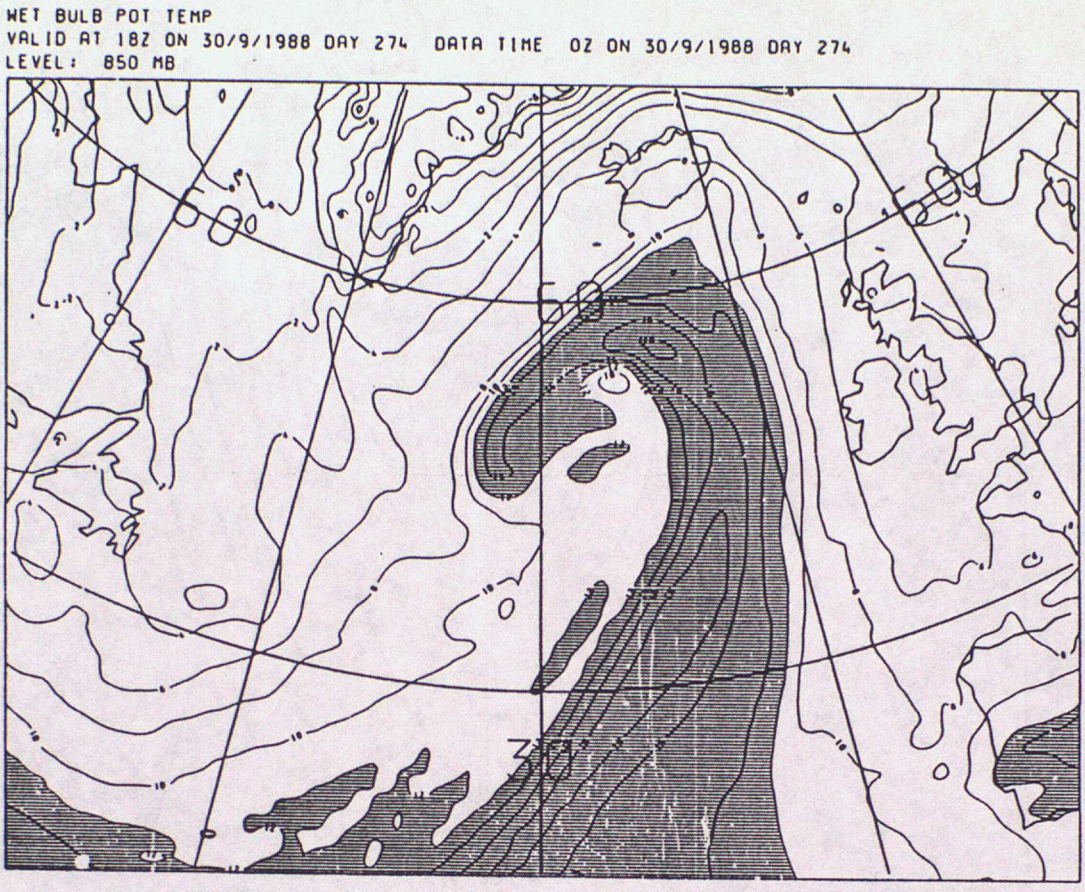
WET BULB POT TEMP
VALID AT 18Z ON 30/9/1988 DAY 274 DATA TIME 0Z ON 30/9/1988 DAY 274
LEVEL: 850 MB

(c)

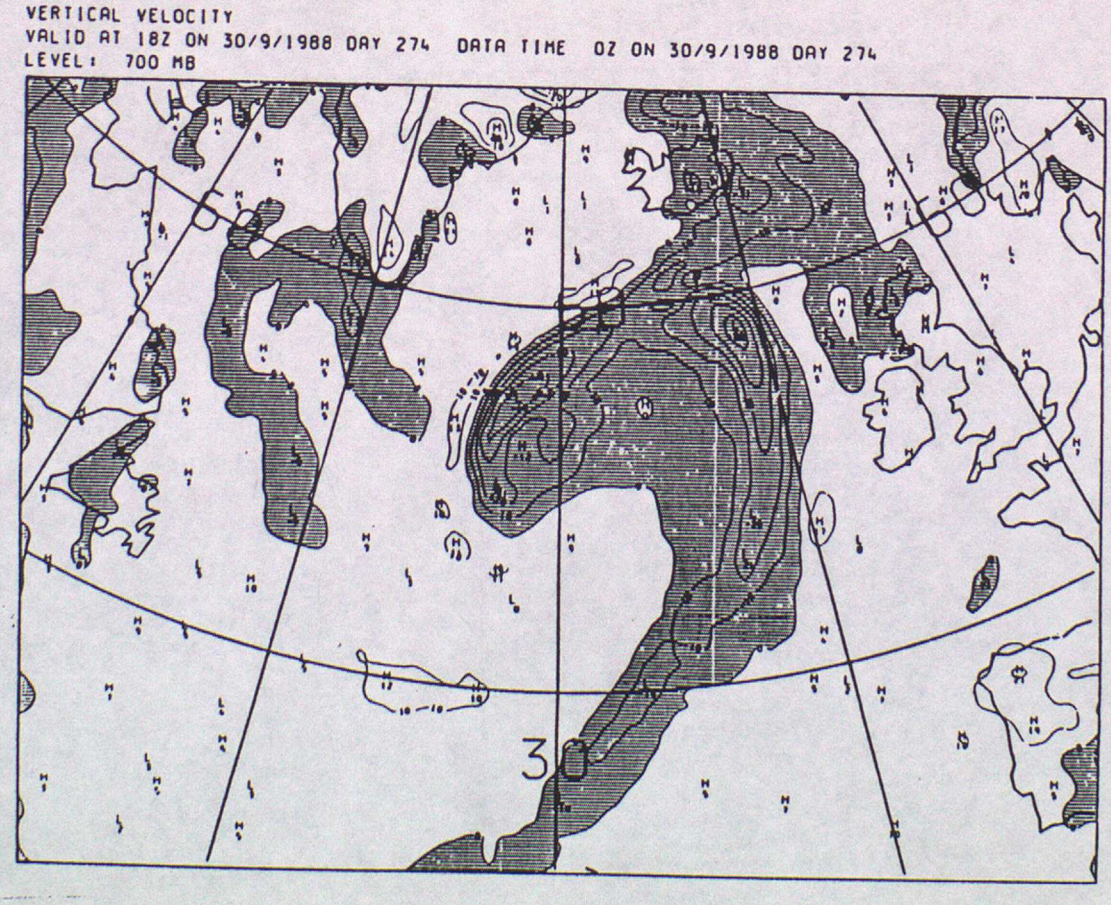
VERTICAL VELOCITY
VALID AT 18Z ON 30/9/1988 DAY 274 DATA TIME 0Z ON 30/9/1988 DAY 274
LEVEL: 700 MB

(d)

FIG. 11

POTENTIAL TEMPERATURE

VALID AT 6Z ON 30/9/1988 DAY 274 DATA TIME 0Z ON 30/9/1988 DAY 274
LEVEL: 850 MB

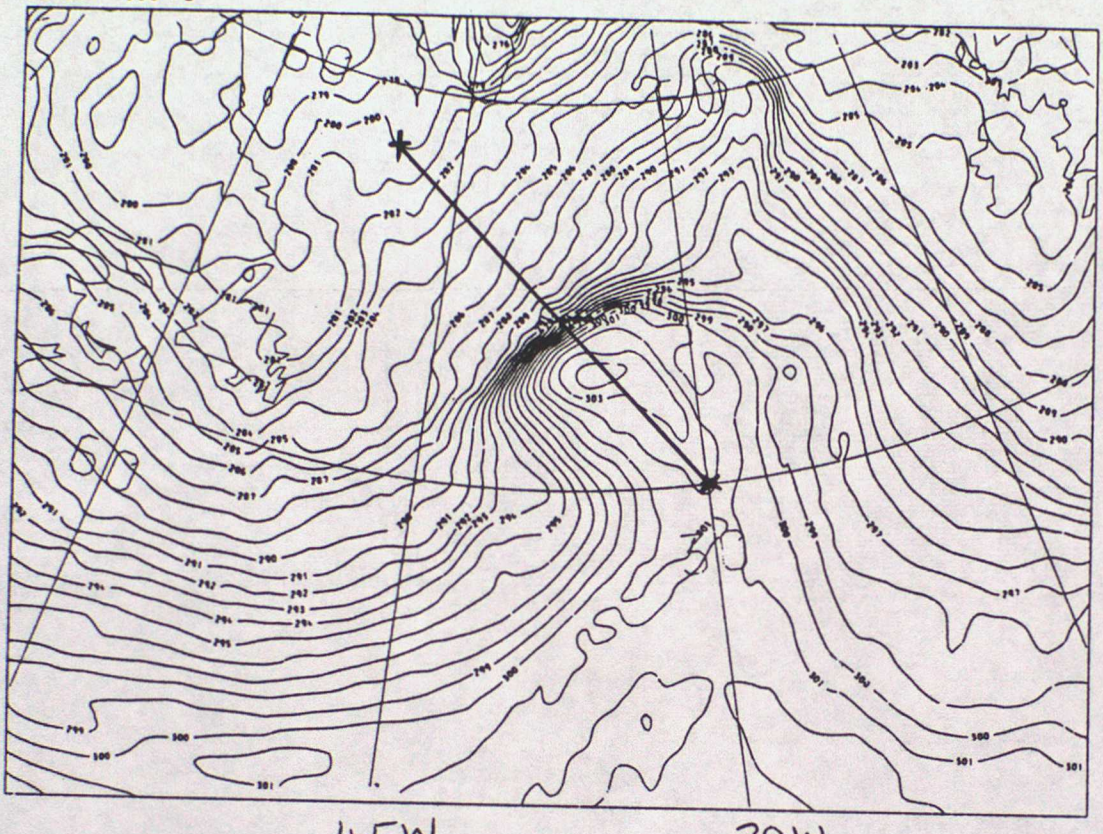

FIG. 12

GC. X-SECTION. V=SOLID CONTOURS -VE SHADED. U&W ARROWS. POT.TEMP=PECKED CONTOURS
VALID AT 6Z ON 30/9/1988 DAY 274 DATA TIME 0Z ON 30/9/1988 DAY 274

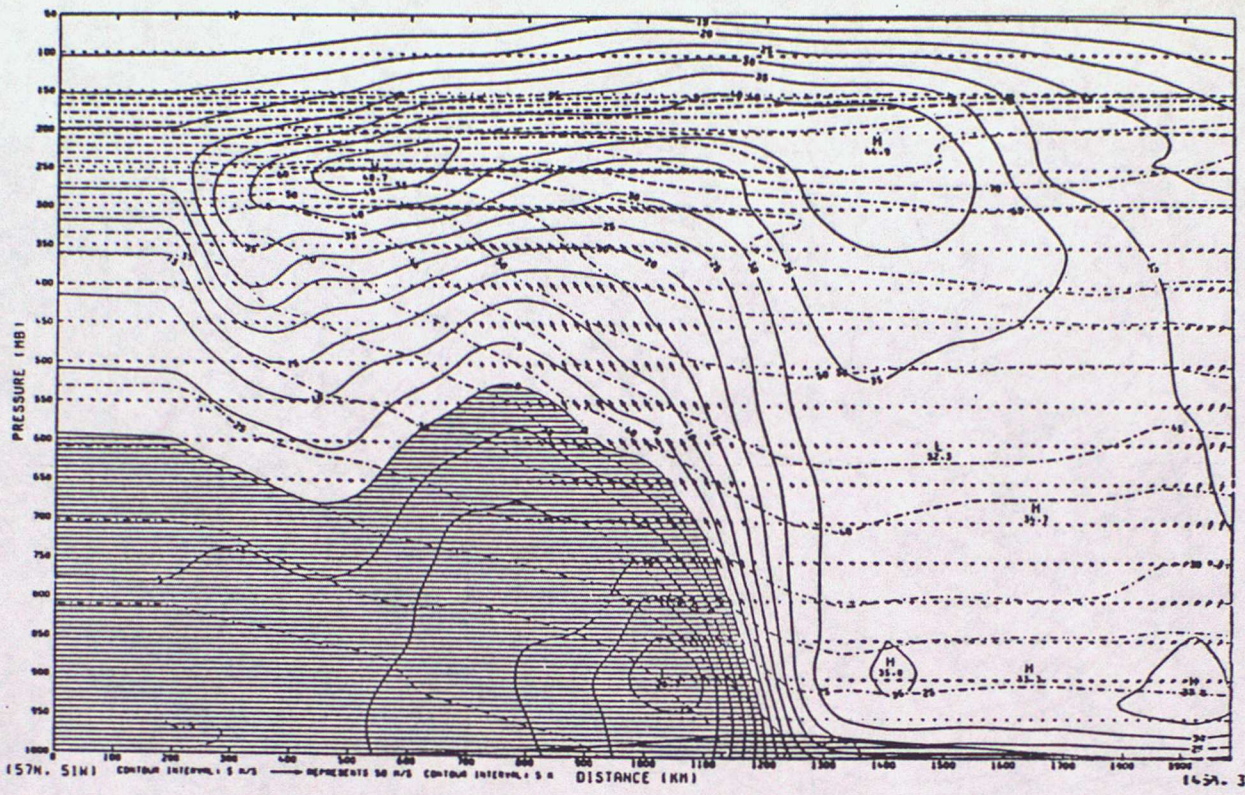

(a)

POTENTIAL TEMPERATURE
VALID AT 6Z ON 30/9/1988 DAY 274 DATA TIME 0Z ON 30/9/1988 DAY 274

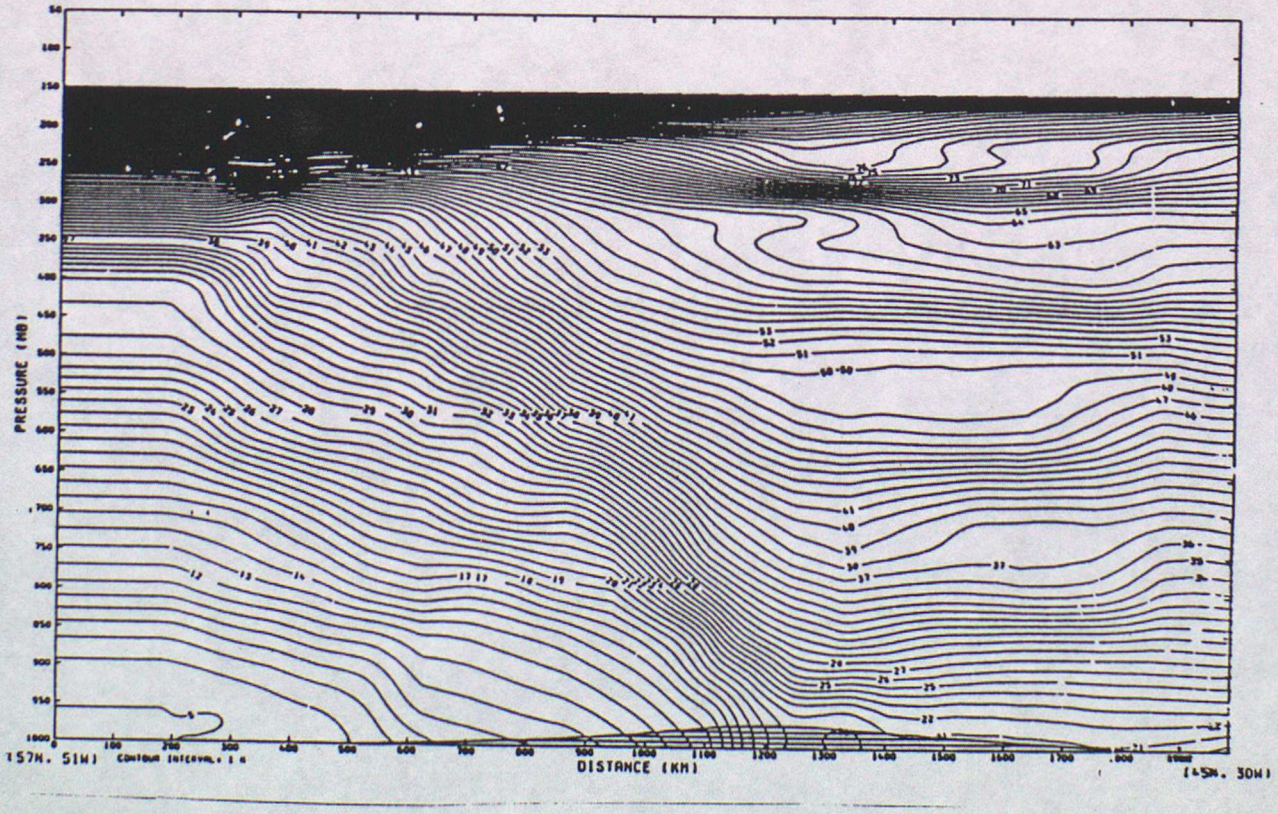

(b)

FIG. 12(c)

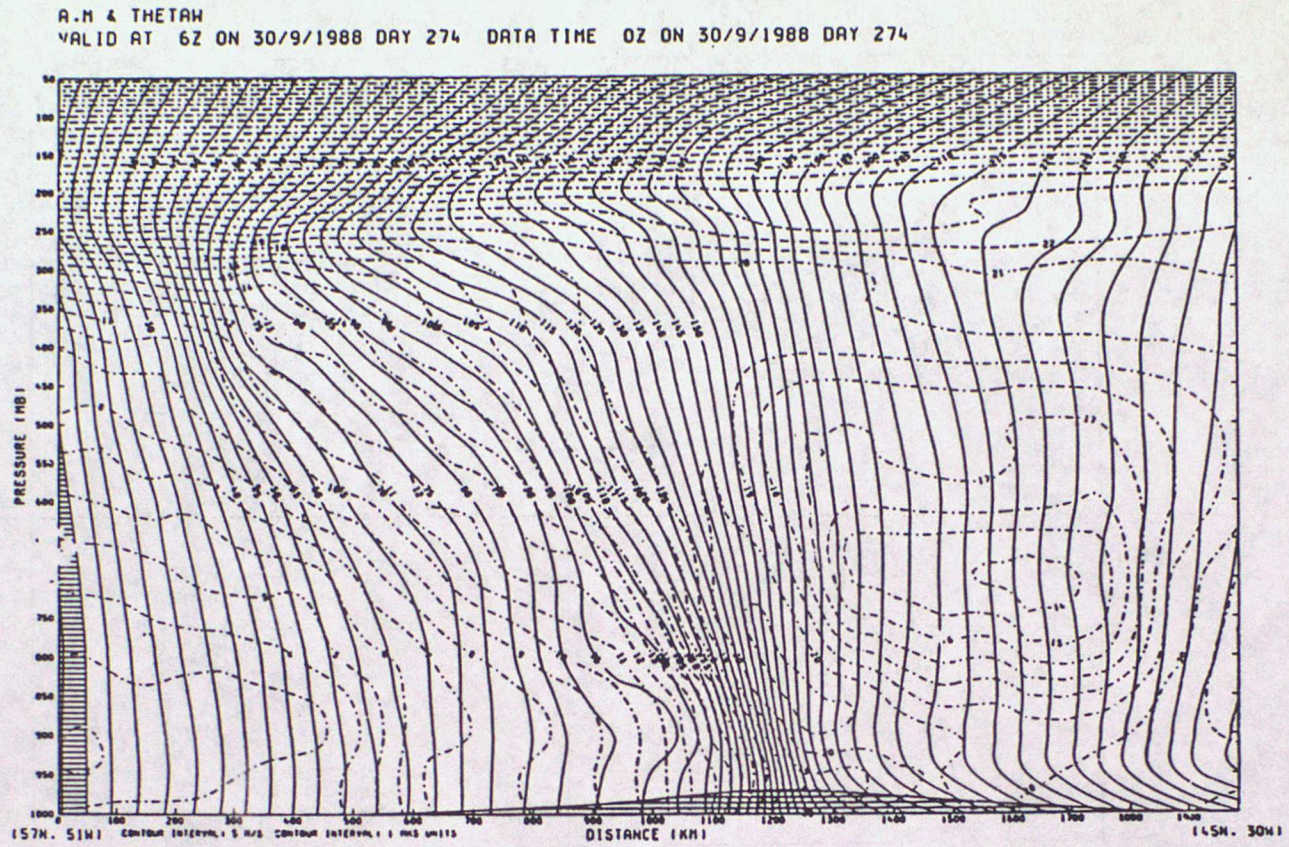

FIG. 13

SCAPE (J/KG X .01) PLOTTED WHERE SCAPE > 100 J/KG

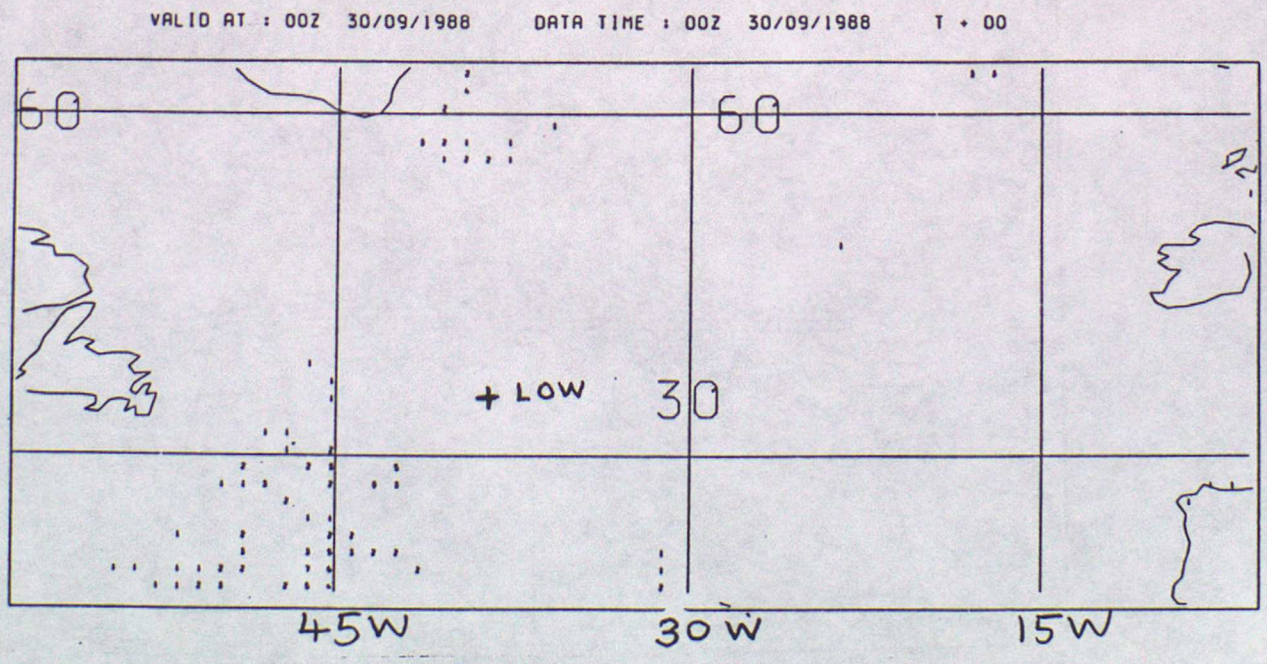

FIG. 14

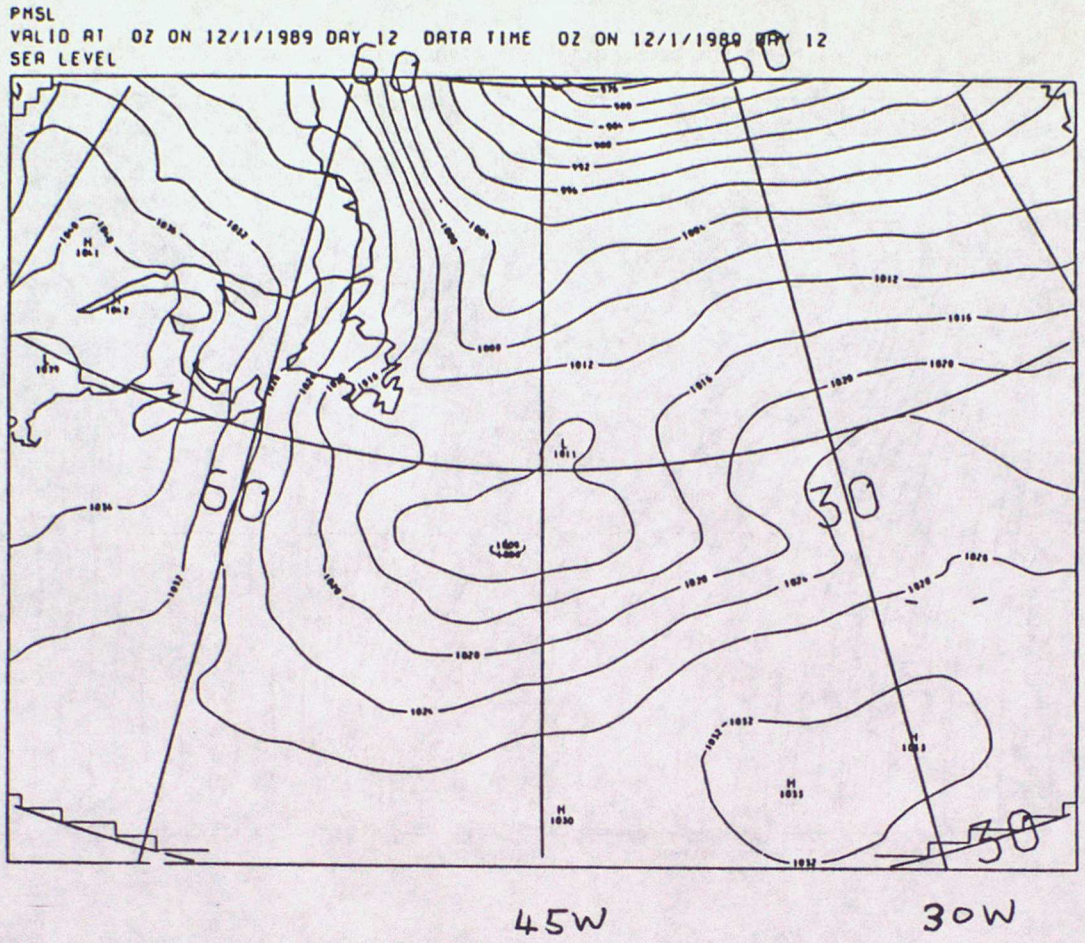
PMSL
VALID AT 0Z ON 12/1/1989 DAY 12 DATA TIME 0Z ON 12/1/1989 DAY 12
SEA LEVEL
60
60
45N
30
30
45W
30W

(a)

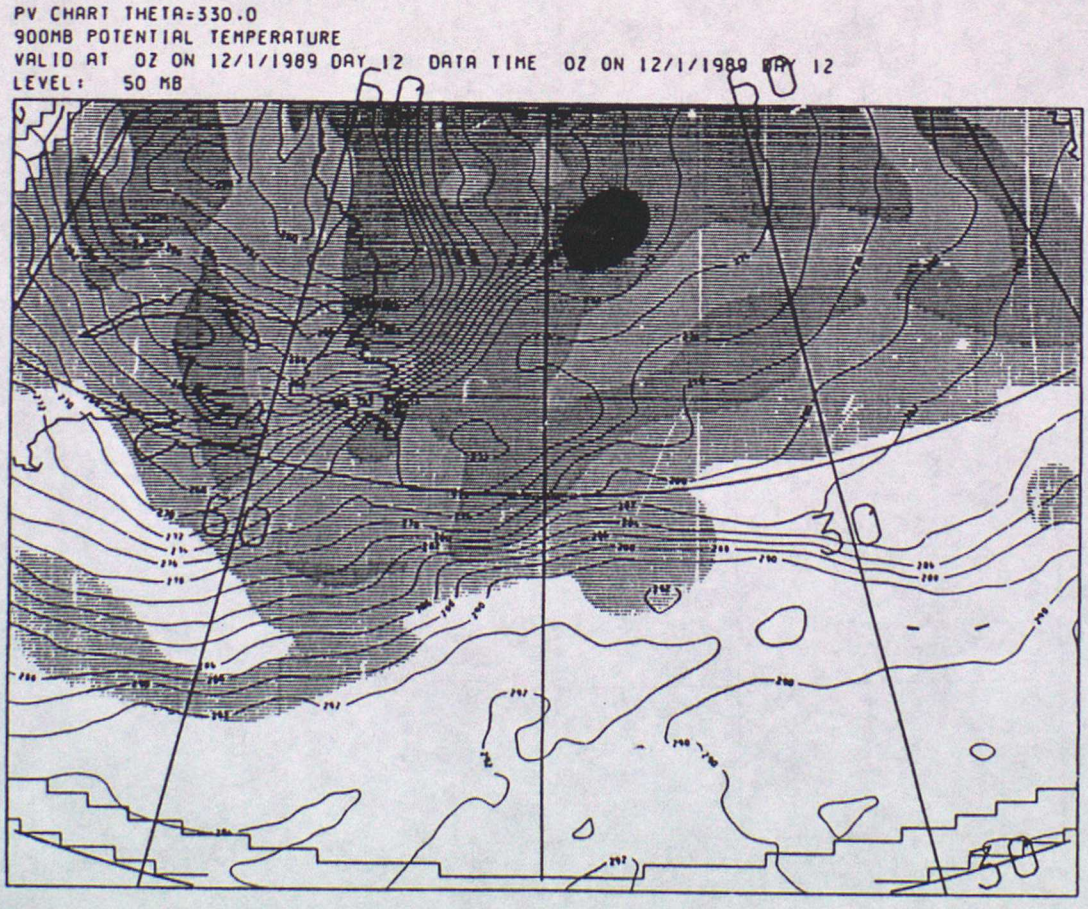
PV CHART THETA=330.0
900MB POTENTIAL TEMPERATURE
VALID AT 0Z ON 12/1/1989 DAY 12 DATA TIME 0Z ON 12/1/1989 DAY 12
LEVEL: 50 MB
60
60
60
30
30

(b)

FIG. 14

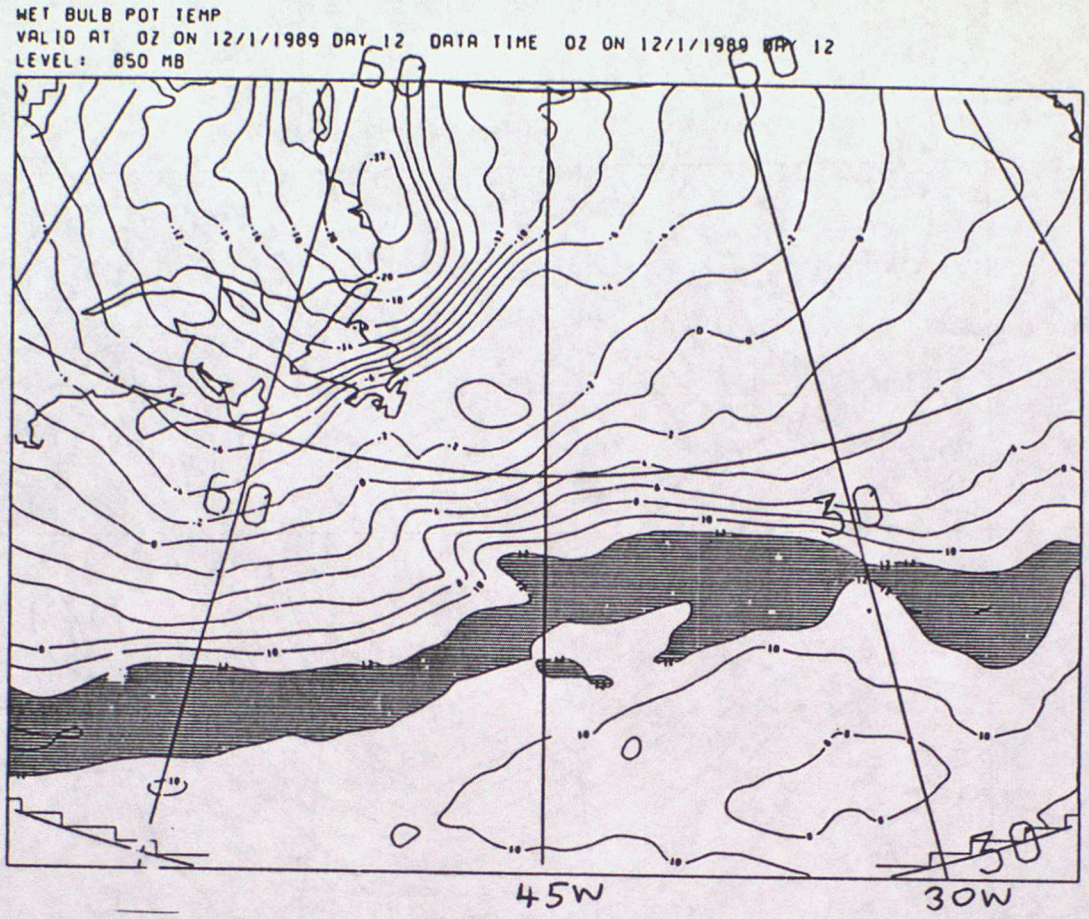
WET BULB POT TEMP
VALID AT 0Z ON 12/1/1989 DAY 12 DATA TIME 0Z ON 12/1/1989 DAY 12
LEVEL: 850 MB
60
60
60
30
45W
30W
45N

(c)

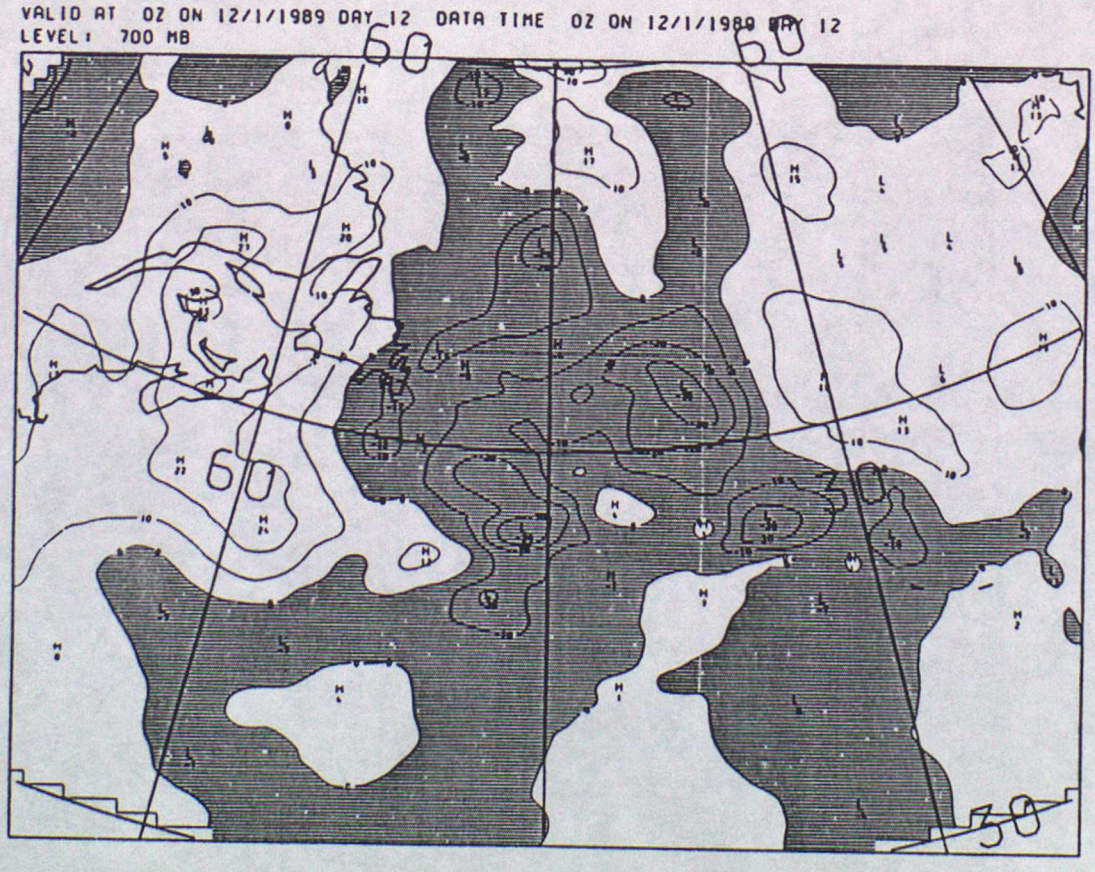
VERTICAL VELOCITY
VALID AT 0Z ON 12/1/1989 DAY 12 DATA TIME 0Z ON 12/1/1989 DAY 12
LEVEL: 700 MB
60
60
60
30

(d)

FIG. 15

PMSL
VALID AT 6Z ON 13/1/1989 DAY 13 DATA TIME 0Z ON 12/1/1989 DAY 12
SEA LEVEL

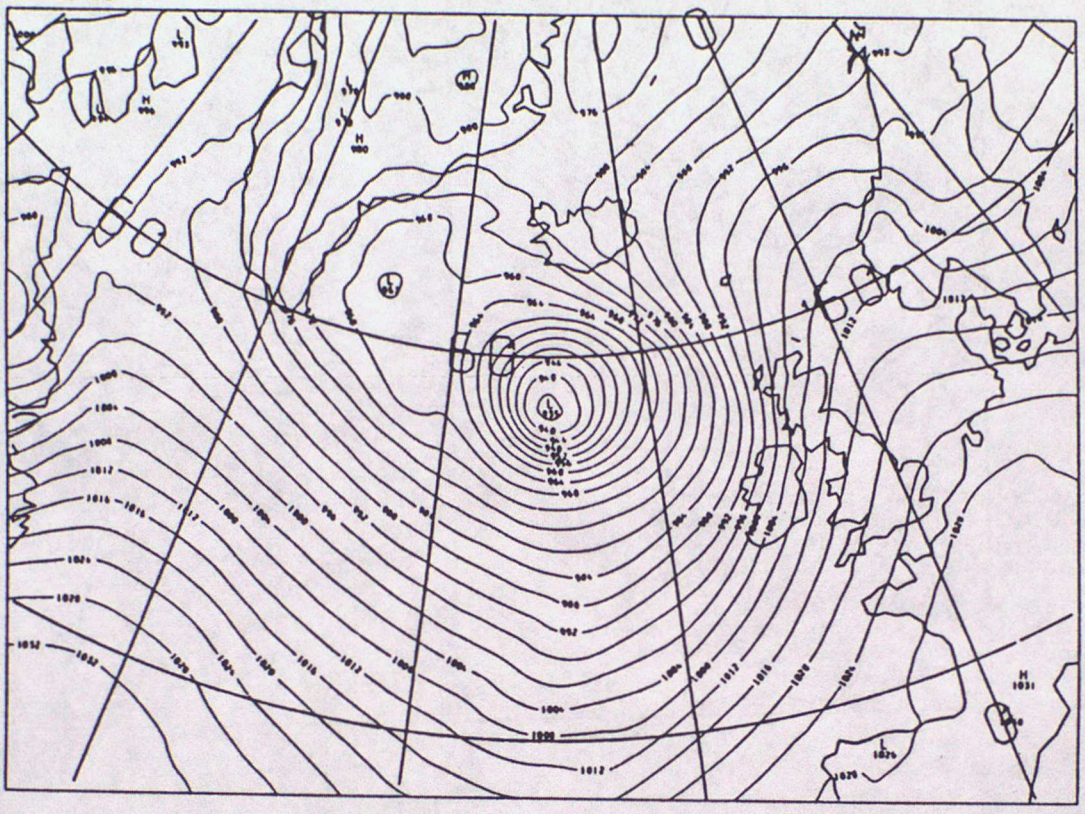

(a)

45 N

30W 15W

PV CHART THETA=330.0
900MB POTENTIAL TEMPERATURE
VALID AT 6Z ON 13/1/1989 DAY 13 DATA TIME 0Z ON 12/1/1989 DAY 12
LEVEL: 50 MB

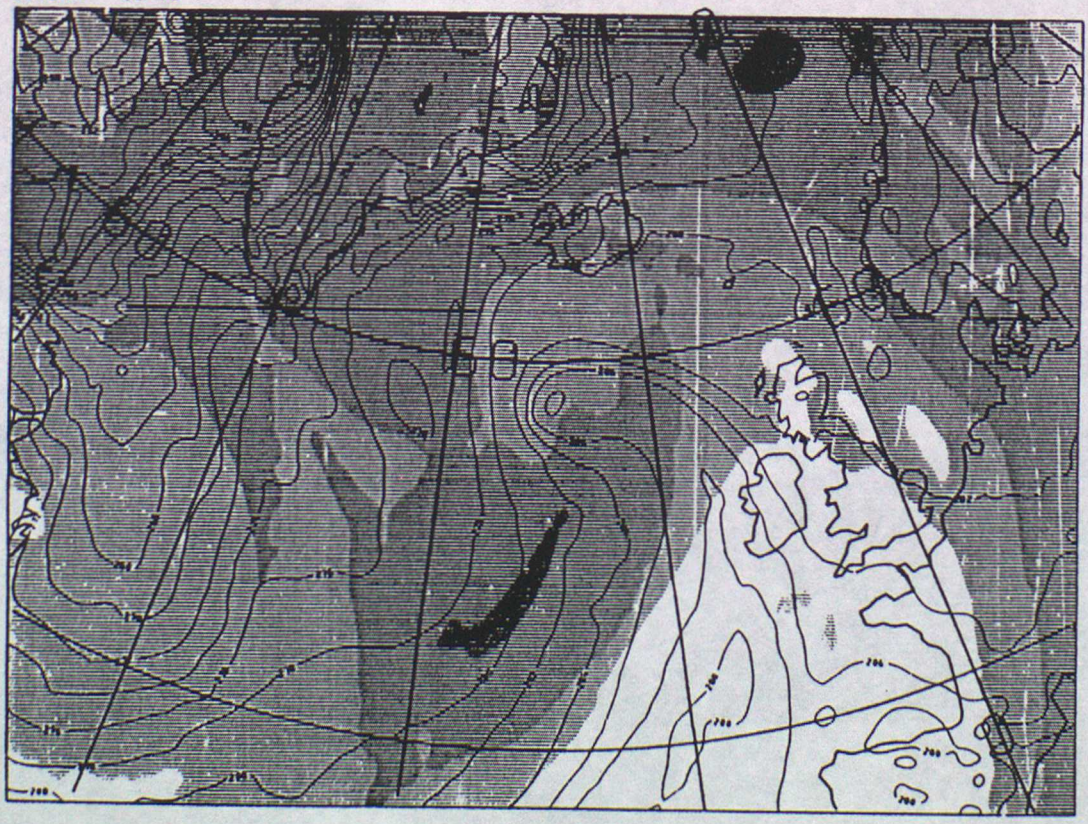

(b)

FIG. 15

WET BULB POT TEMP
VALID AT 6Z ON 13/1/1989 DAY 13 DATA TIME 0Z ON 12/1/1989 DAY 12
LEVEL: 850 MB

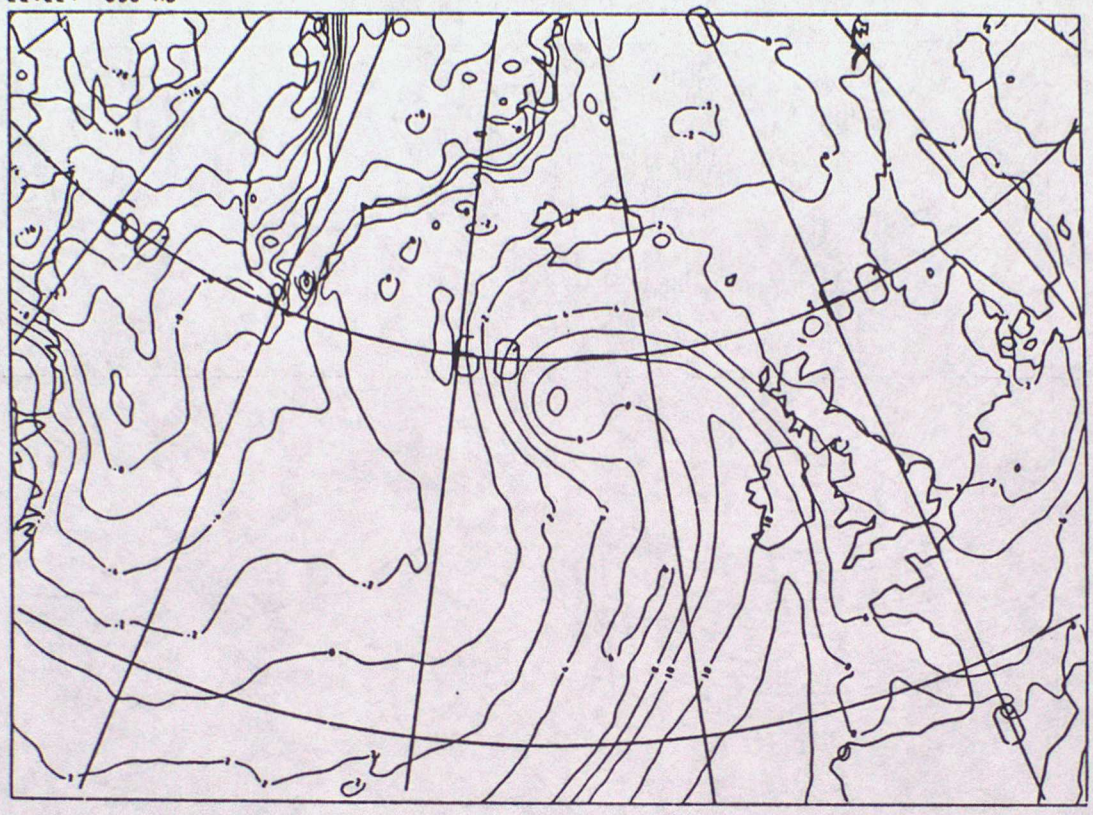

(c)

VERTICAL VELOCITY
VALID AT 6Z ON 13/1/1989 DAY 13 DATA TIME 0Z ON 12/1/1989 DAY 12
LEVEL: 700 MB

(d)

FIG. 16

POTENTIAL TEMPERATURE

VALID AT 6Z ON 12/1/1989 DAY 12 DATA TIME 0Z ON 12/1/1989 DAY 12
LEVEL: 850 MB

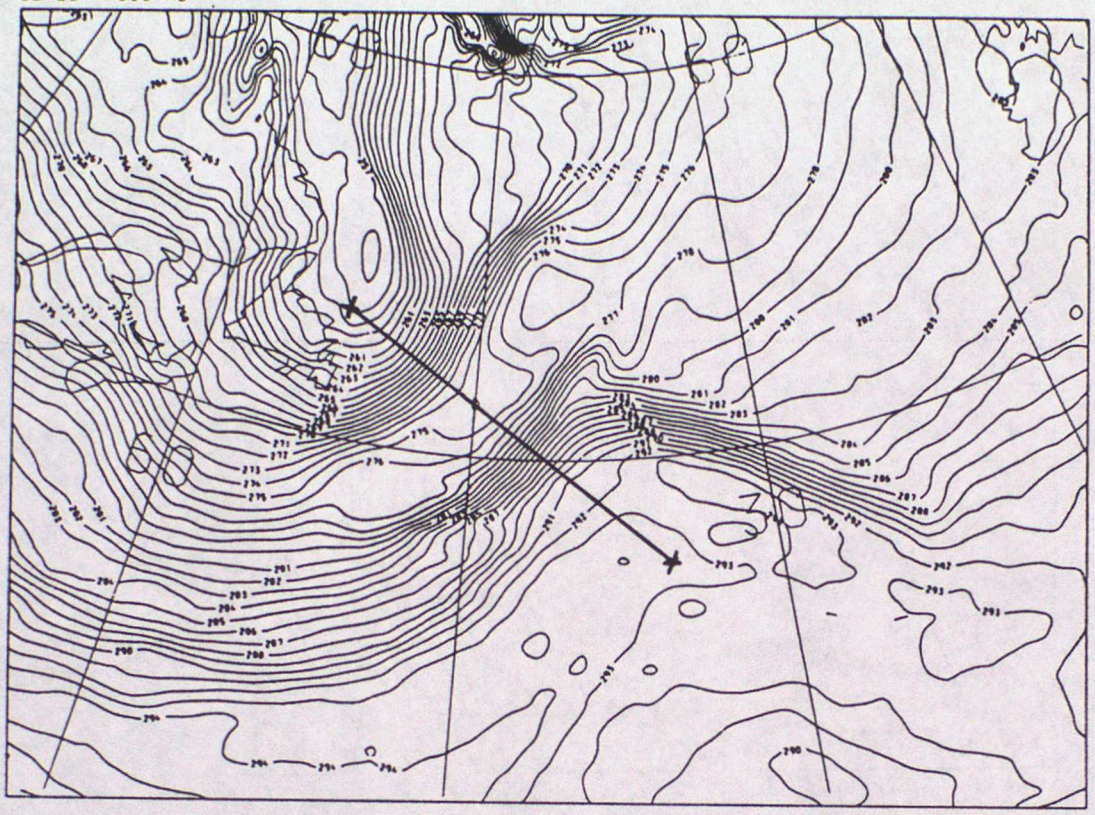

Fig. 17

GC. X-SECTION. V=SOLID CONTOURS -VE SHADED. U&W ARROWS. POT.TEMP=PECKED CONTOURS
VALID AT 6Z ON 12/1/1989 DAY 12 DATA TIME 0Z ON 12/1/1989 DAY 12

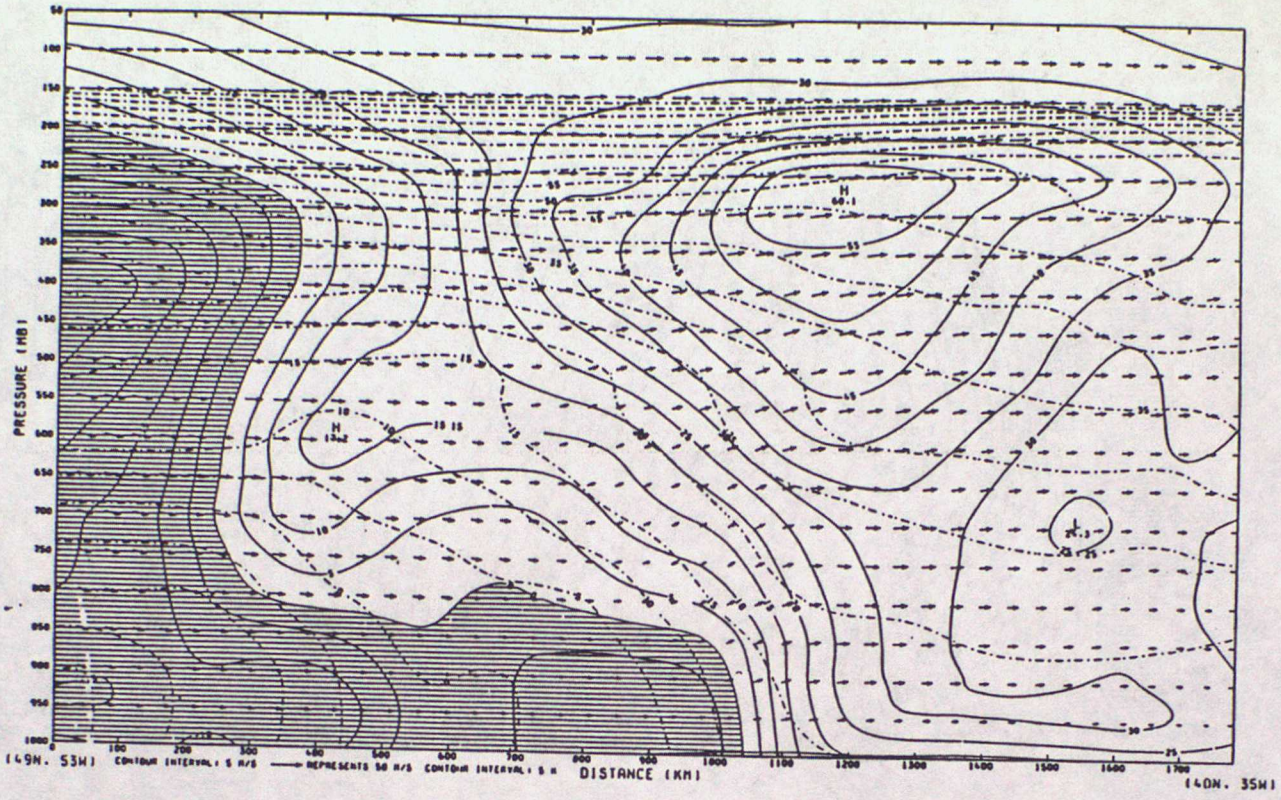

(a)

THETA
VALID AT 6Z ON 12/1/1989 DAY 12 DATA TIME 0Z ON 12/1/1989 DAY 12

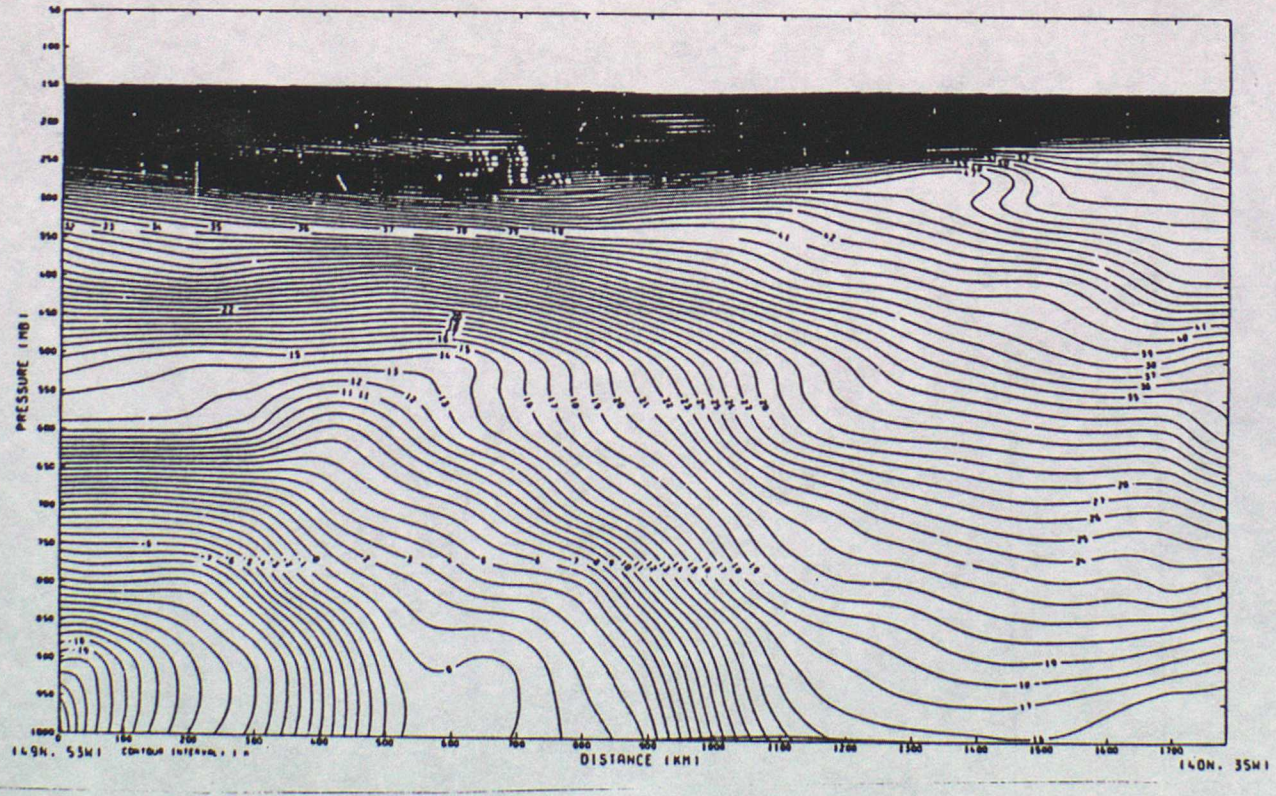

(b)

FIG. 17(c)

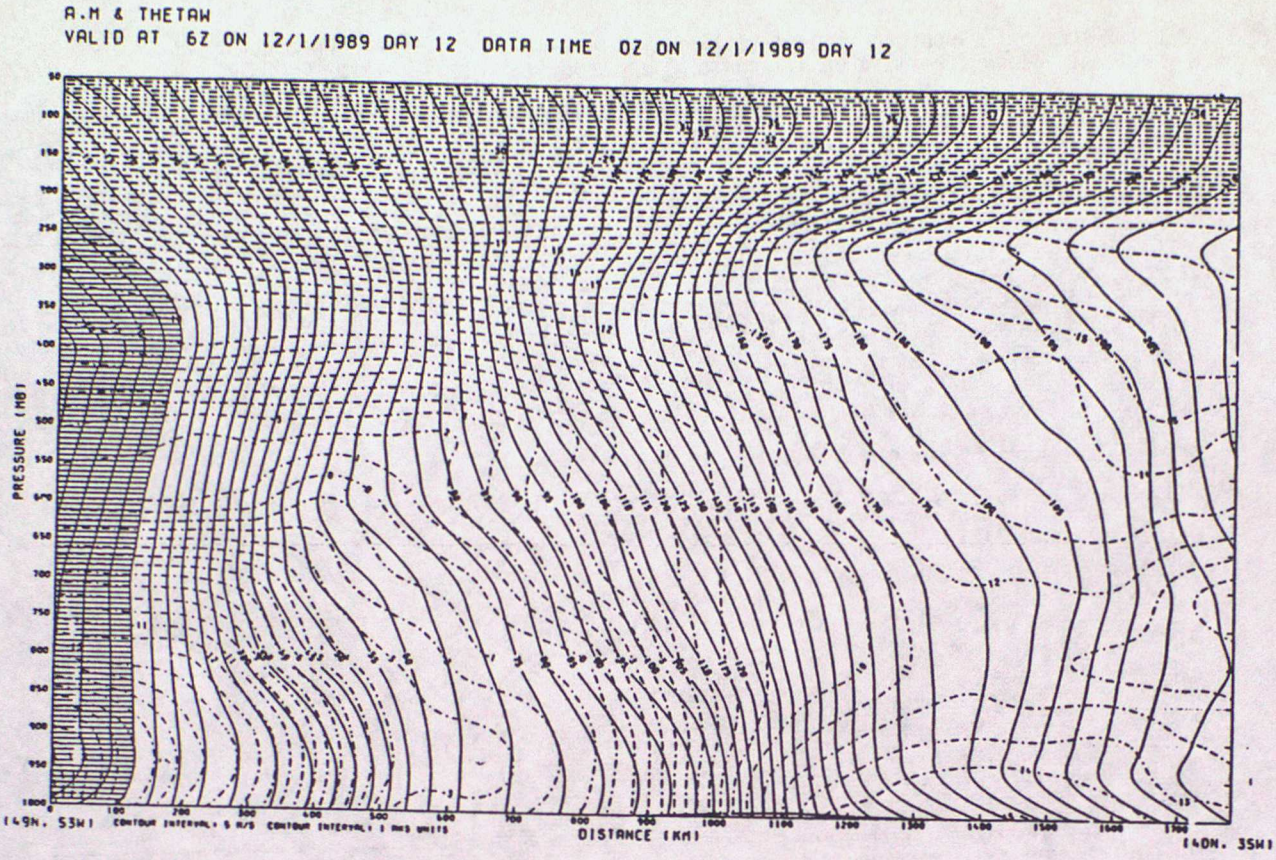

FIG. 18

SCAPE (J/KG X .01) PLOTTED WHERE SCAPE > 100 J/KG

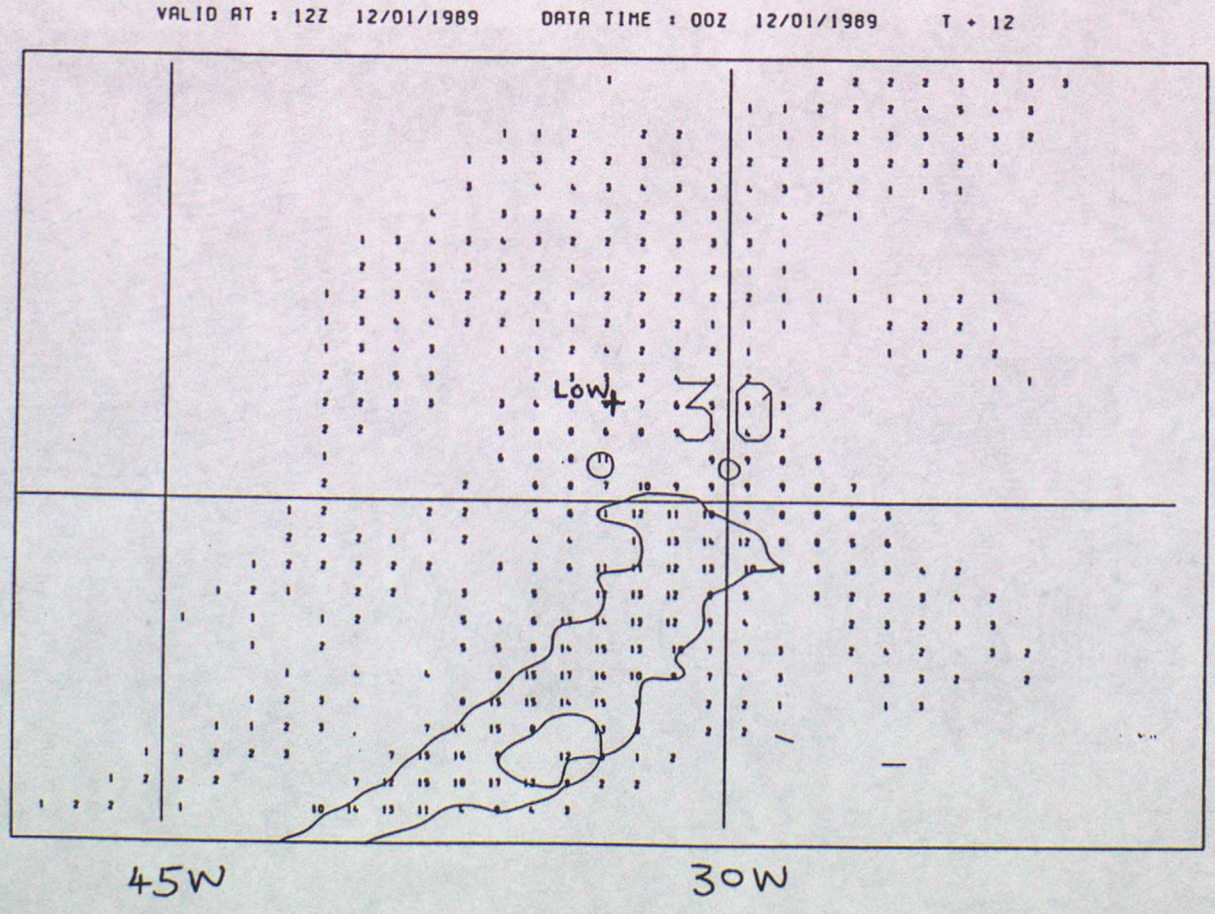

FIG. 19

PMSL
VALID AT 0Z ON 18/1/1988 DAY 18 DATA TIME 12Z ON 17/1/1988 DAY 17
SEA LEVEL

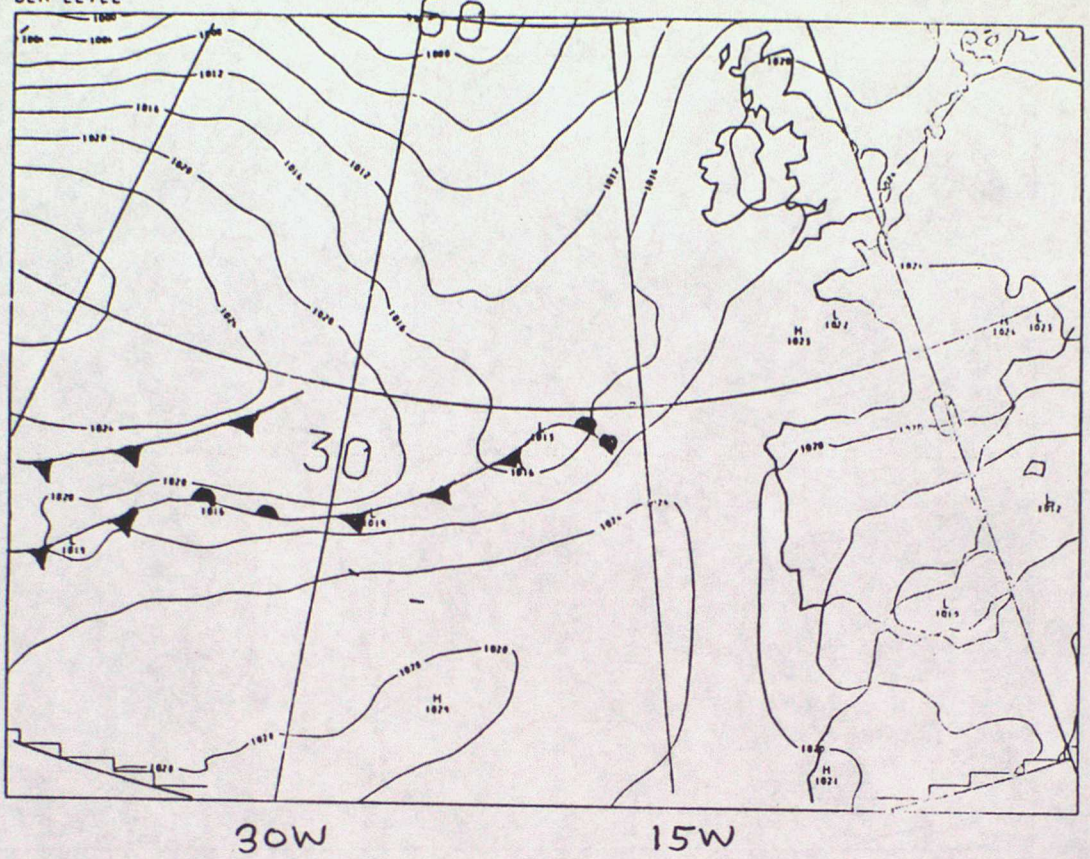

(a)

PV CHART THETA=330.0
900MB POTENTIAL TEMPERATURE
VALID AT 0Z ON 18/1/1988 DAY 18 DATA TIME 12Z ON 17/1/1988 DAY 17
LEVEL: 50 MB

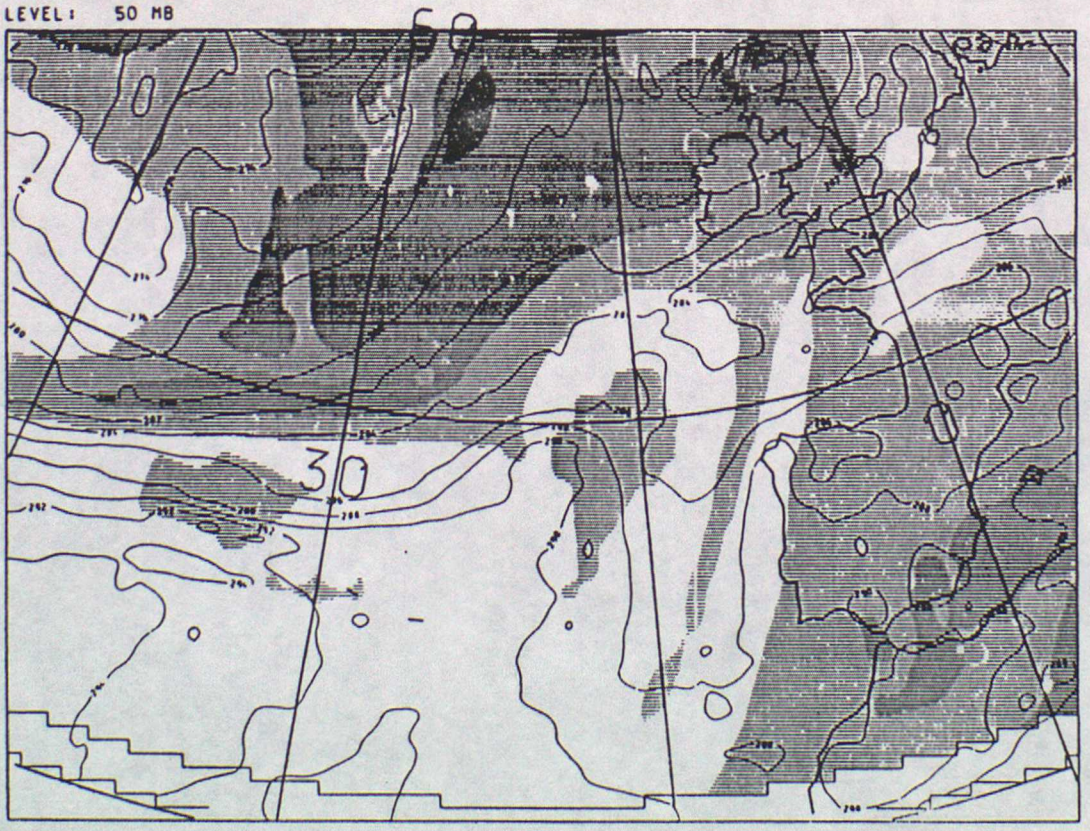

(b)

FIG. 19

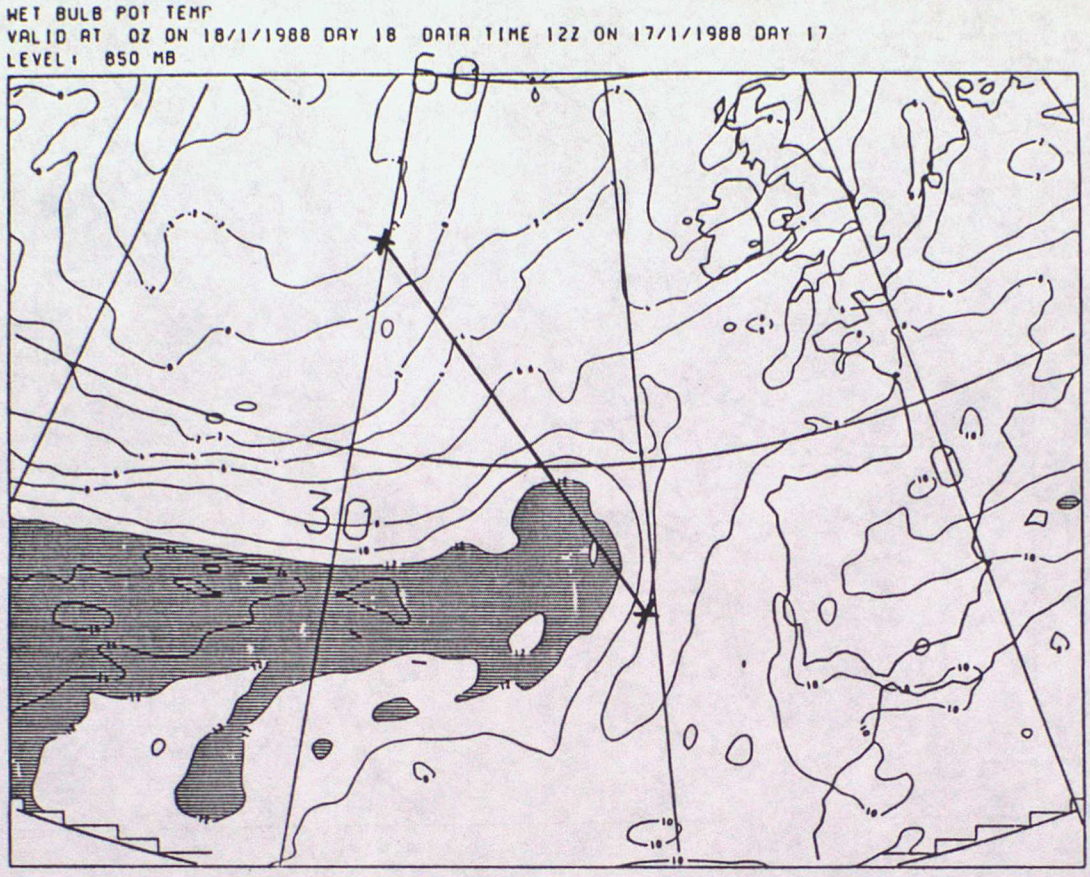
WET BULB POT TEMP
VALID AT 0Z ON 18/1/1988 DAY 18 DATA TIME 12Z ON 17/1/1988 DAY 17
LEVEL: 850 MB
60
30

(c)


VERTICAL VELOCITY
VALID AT 0Z ON 18/1/1988 DAY 18 DATA TIME 12Z ON 17/1/1988 DAY 17
LEVEL: 700 MB
60
30

(d)

FIG. 20

PMSL
VALID AT 0Z ON 19/1/1988 DAY 19 DATA TIME 12Z ON 17/1/1988 DAY 17
SEA LEVEL

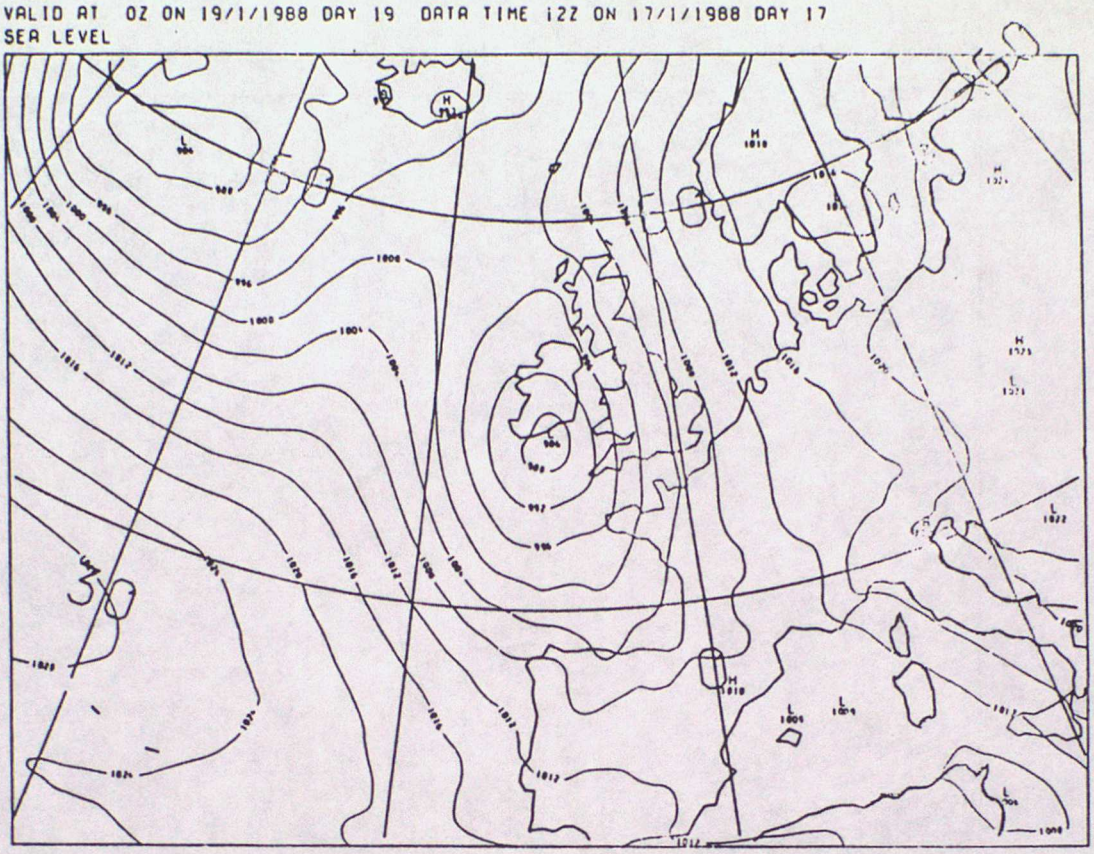

(a)

45N

PV CHART THETA=330.0
900MB POTENTIAL TEMPERATURE
VALID AT 0Z ON 19/1/1988 DAY 19 DATA TIME 12Z ON 17/1/1988 DAY 17
LEVEL: 50 MB

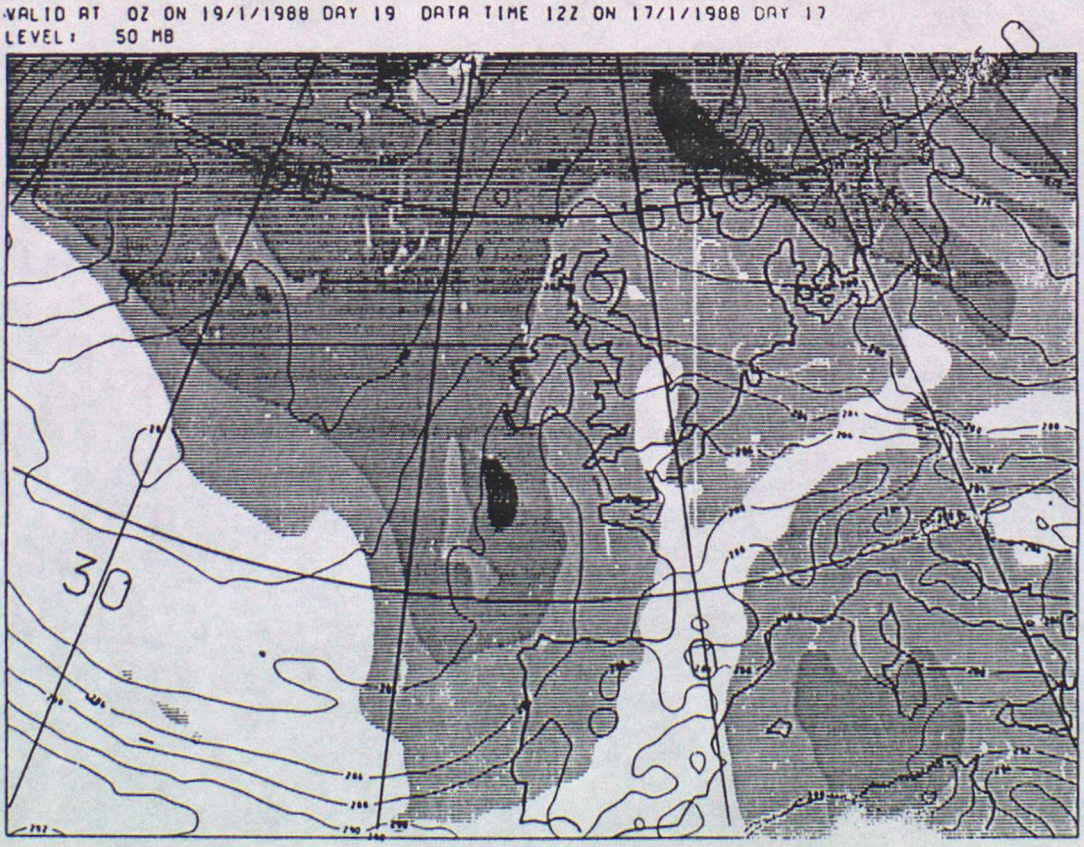

(b)

FIG. 20

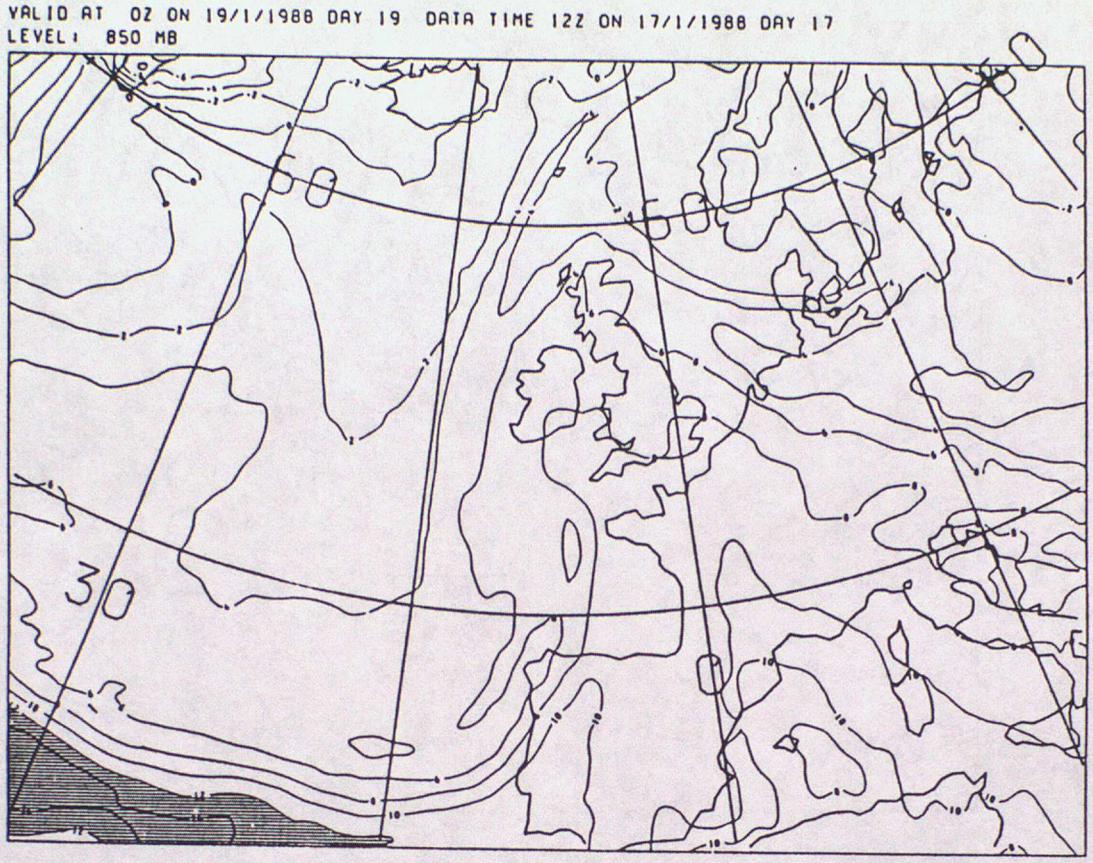
WET BULB POT TEMP
VALID AT 0Z ON 19/1/1988 DAY 19 DATA TIME 12Z ON 17/1/1988 DAY 17
LEVEL: 850 MB
60
30

(c)

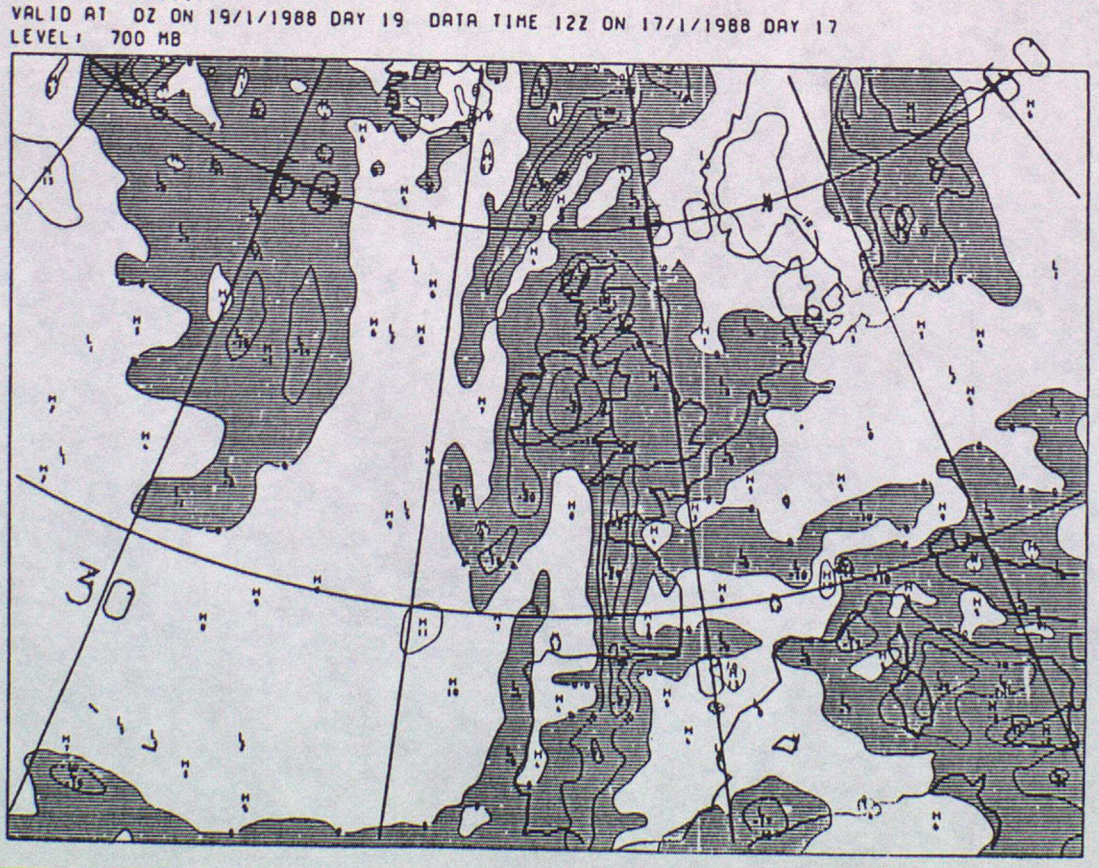
VERTICAL VELOCITY
VALID AT 0Z ON 19/1/1988 DAY 19 DATA TIME 12Z ON 17/1/1988 DAY 17
LEVEL: 700 MB
60
30

(d)

FIG. 21

GC. X-SECTION. V=SOLID CONTOURS -VE SHADED. U&W ARROWS. POT.TEMP=PECKED CONTOURS
VALID AT 0Z ON 18/1/1988 DAY 18 DATA TIME 12Z ON 17/1/1988 DAY 17

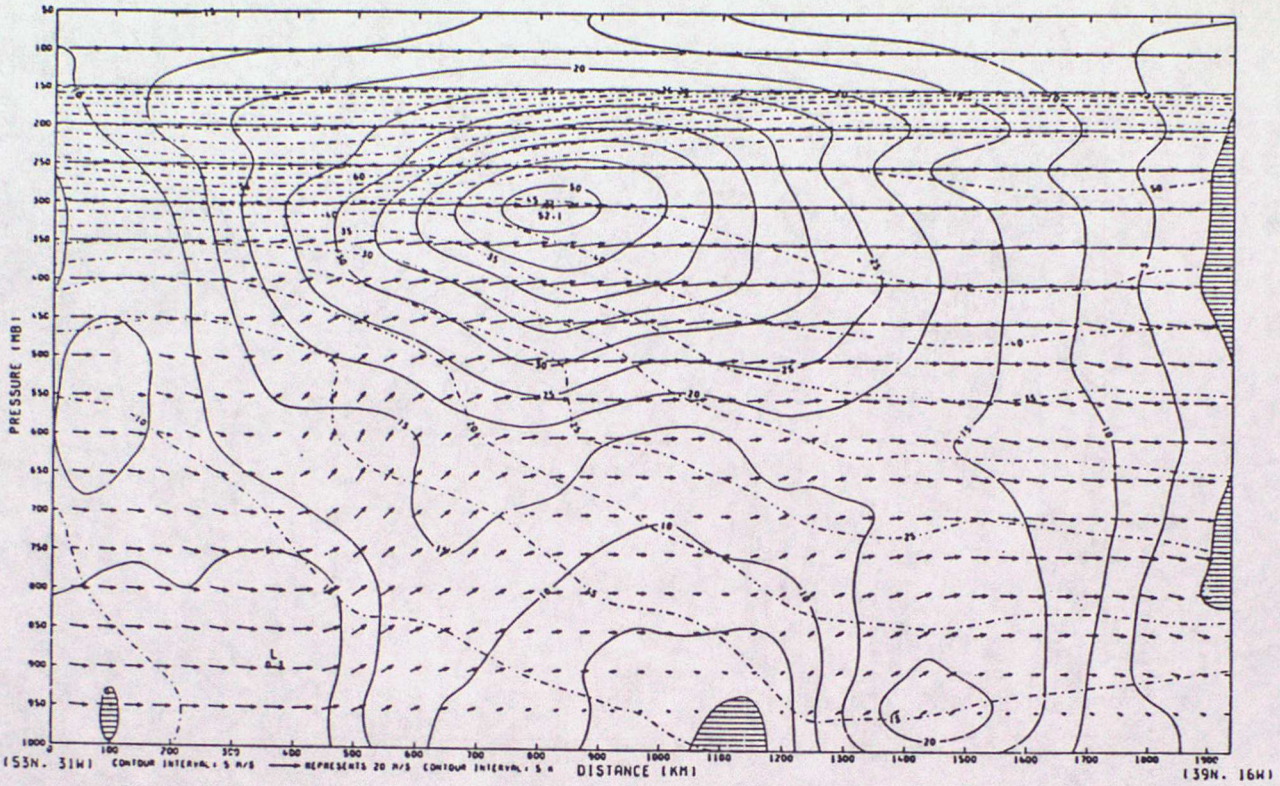

(a)

THETA
VALID AT 0Z ON 18/1/1988 DAY 18 DATA TIME 12Z ON 17/1/1988 DAY 17

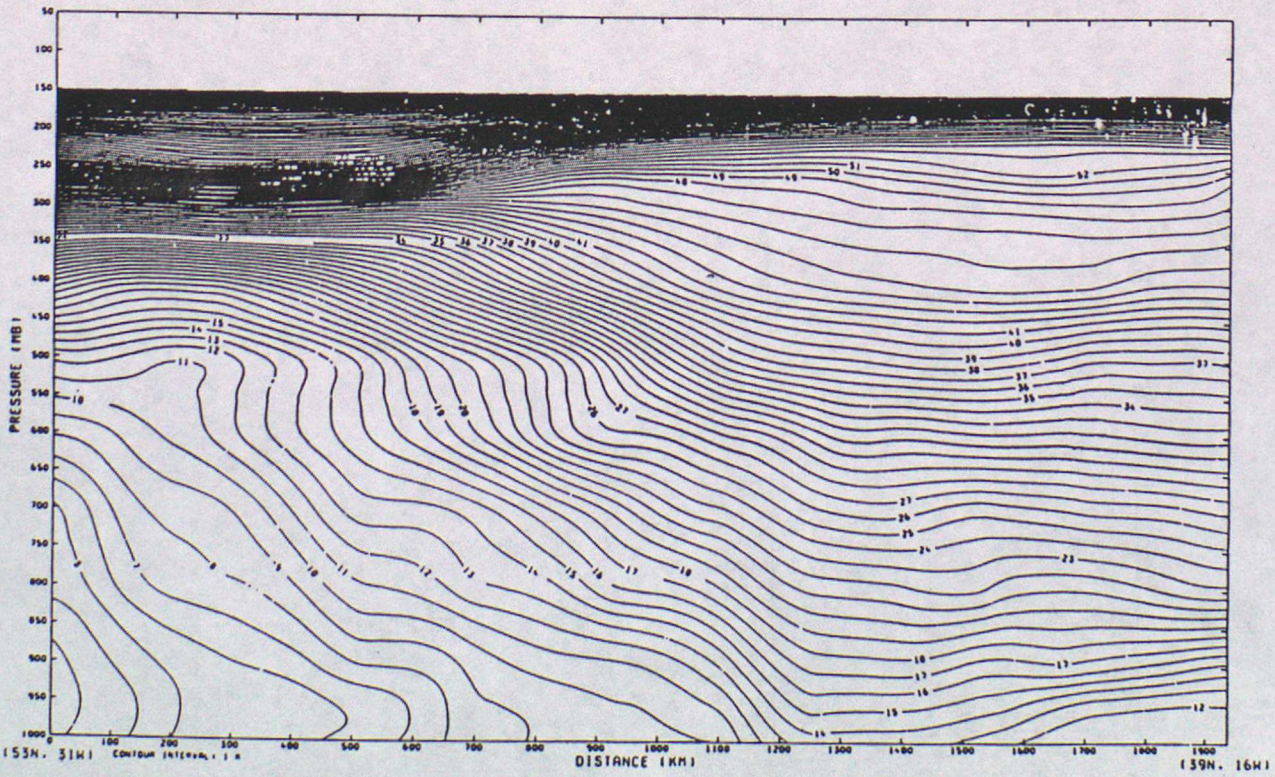

(b)

FIG. 21(c)

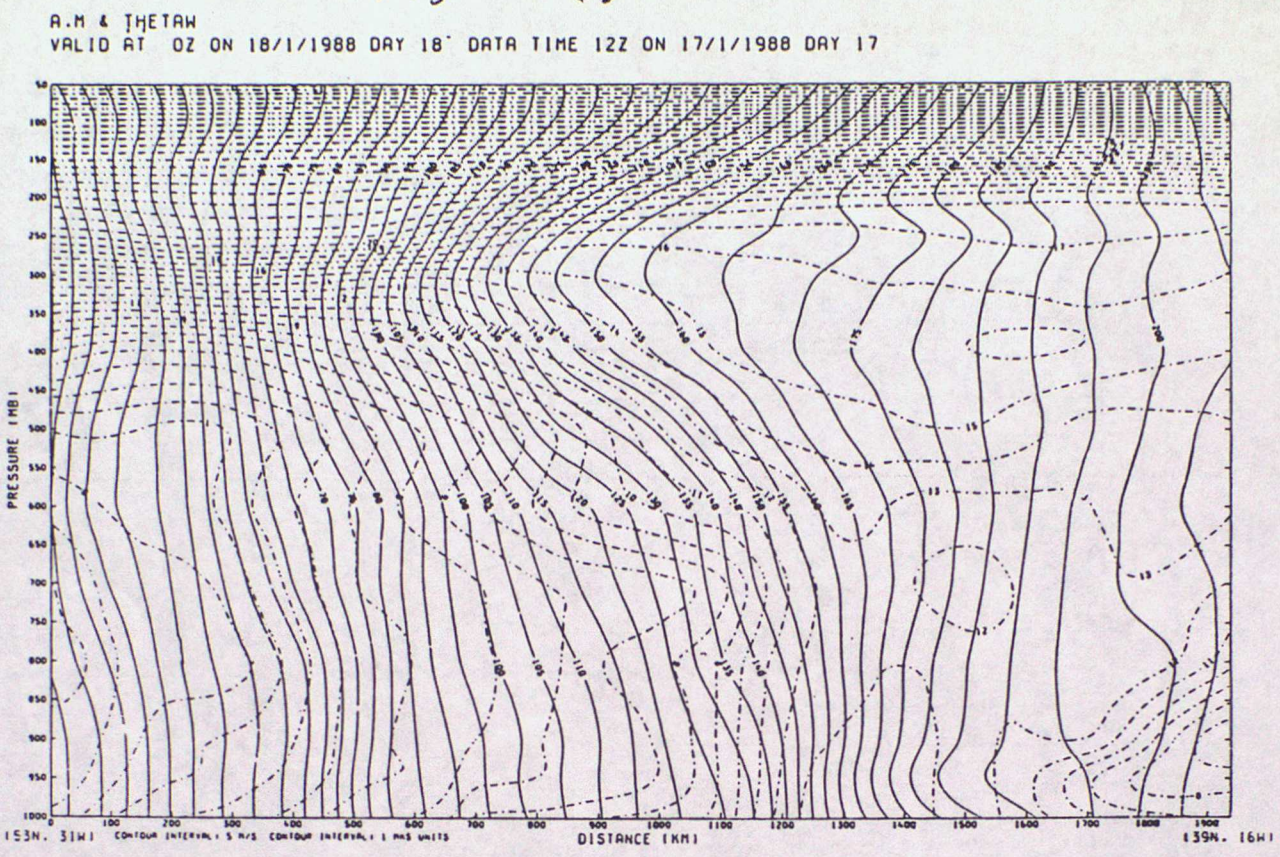

FIG. 22

SCAPE (J/KG X .01) PLOTTED WHERE SCAPE > 100 J/KG

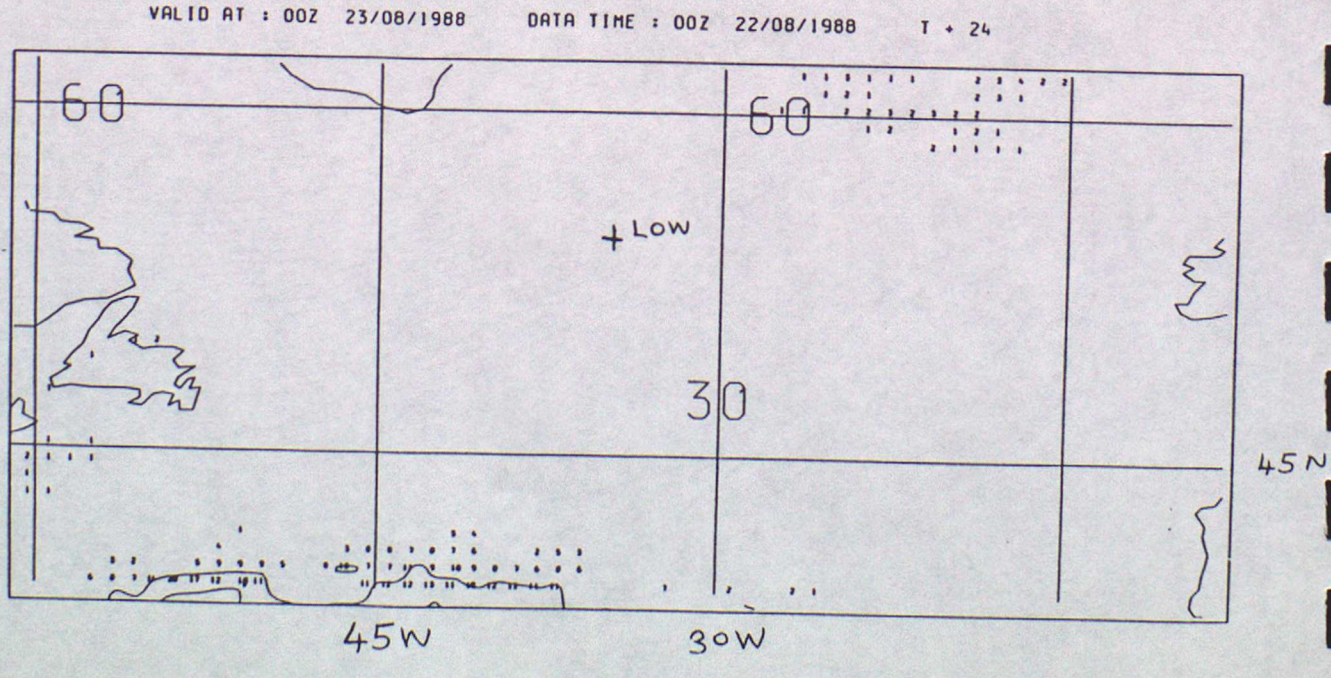

Fig. 23

PMSL
VALID AT 0Z ON 22/8/1988 DAY 235 DATA TIME 0Z ON 22/8/1988 DAY 235
SEA LEVEL

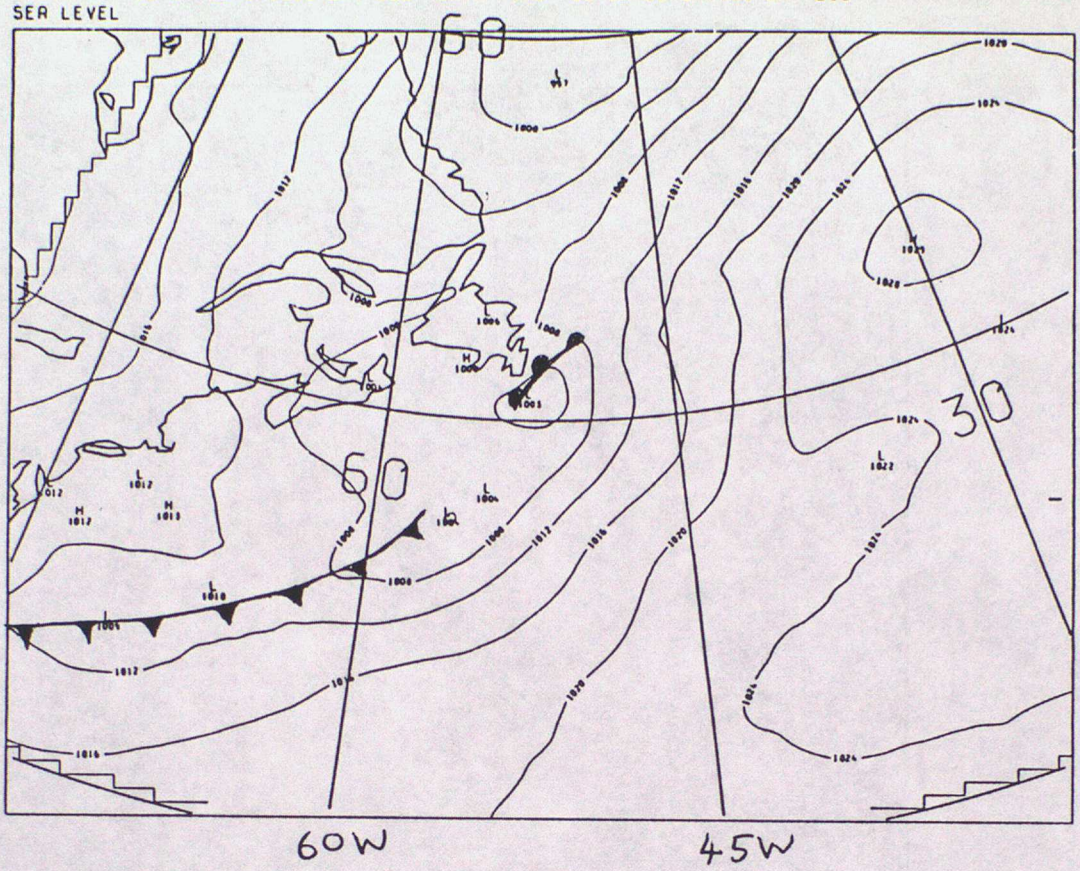

45N

(a)

PV CHART THETA=330.0
900MB POTENTIAL TEMPERATURE
VALID AT 0Z ON 22/8/1988 DAY 235 DATA TIME 0Z ON 22/8/1988 DAY 235
LEVEL: 50 MB

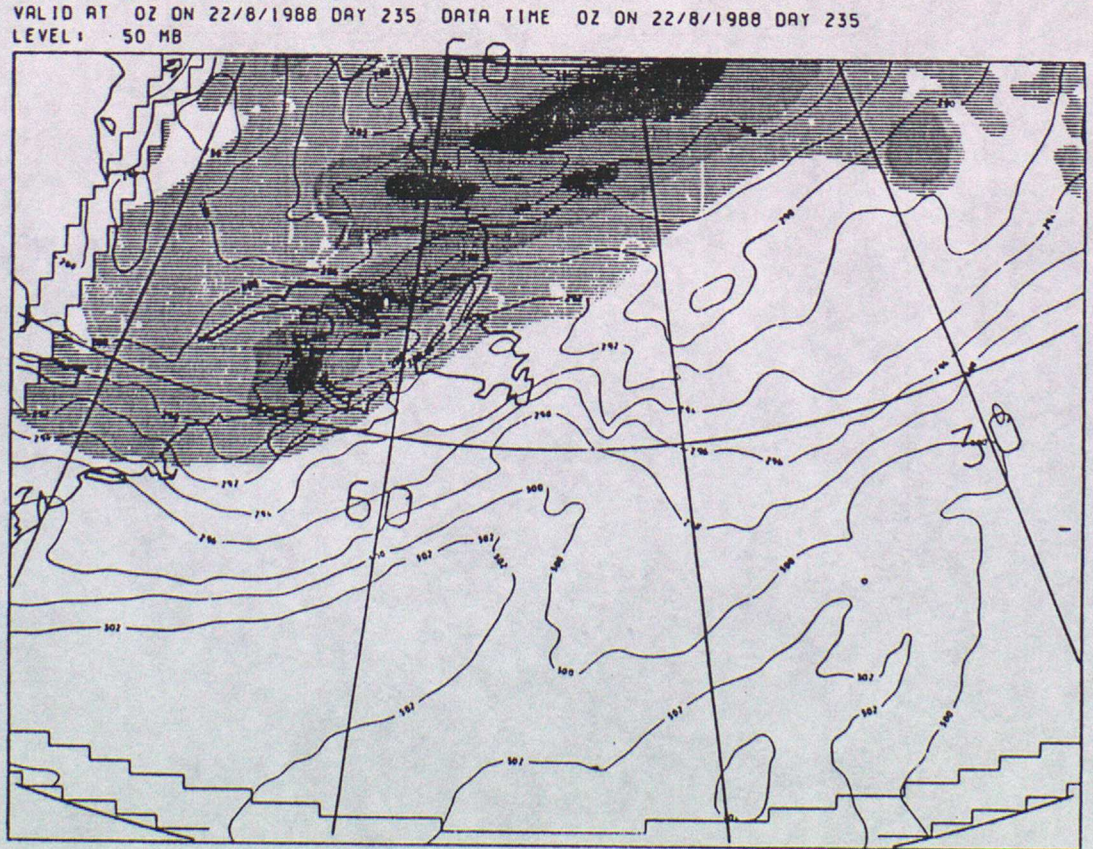

(b)

FIG. 23

WET BULB POT TEMP
VALID AT 0Z ON 22/8/1988 DAY 235 DATA TIME 0Z ON 22/8/1988 DAY 235
LEVEL: 850 MB

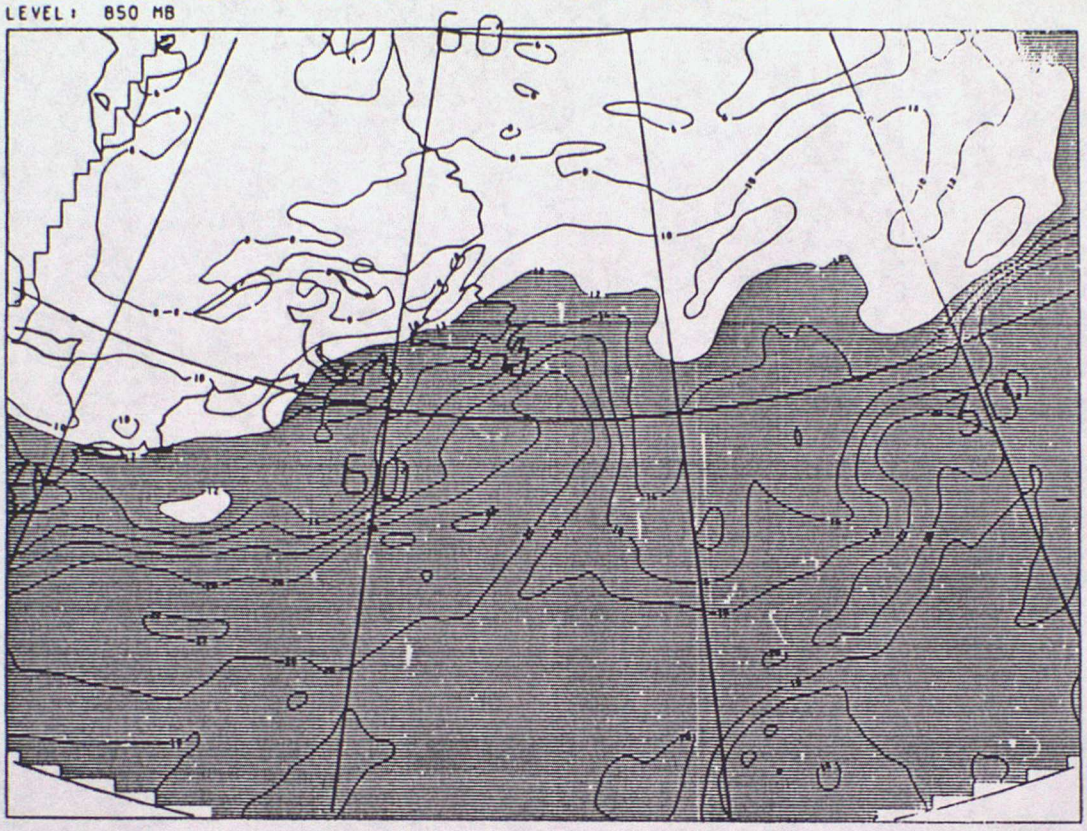

(c)

VERTICAL VELOCITY
VALID AT 0Z ON 22/8/1988 DAY 235 DATA TIME 0Z ON 22/8/1988 DAY 235
LEVEL: 700 MB

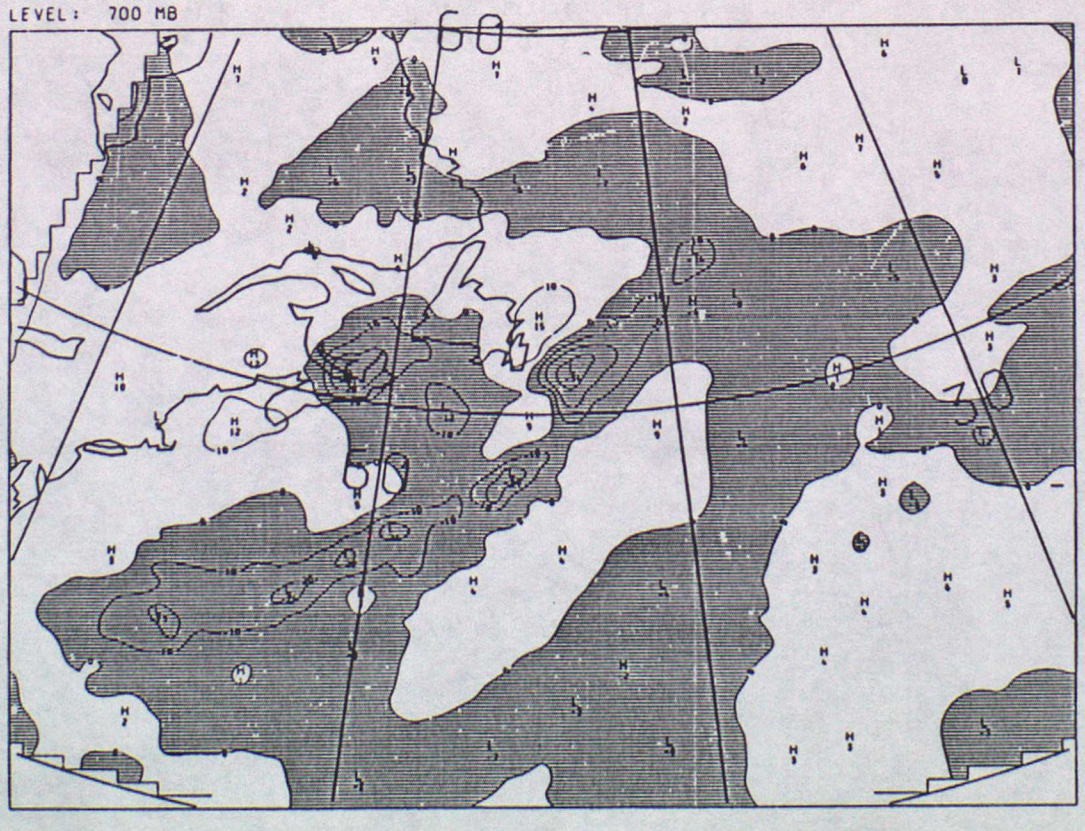

(d)

FIG. 24

PMSL
VALID AT 0Z ON 23/8/1988 DAY 236 DATA TIME 0Z ON 22/8/1988 DAY 235
SEA LEVEL

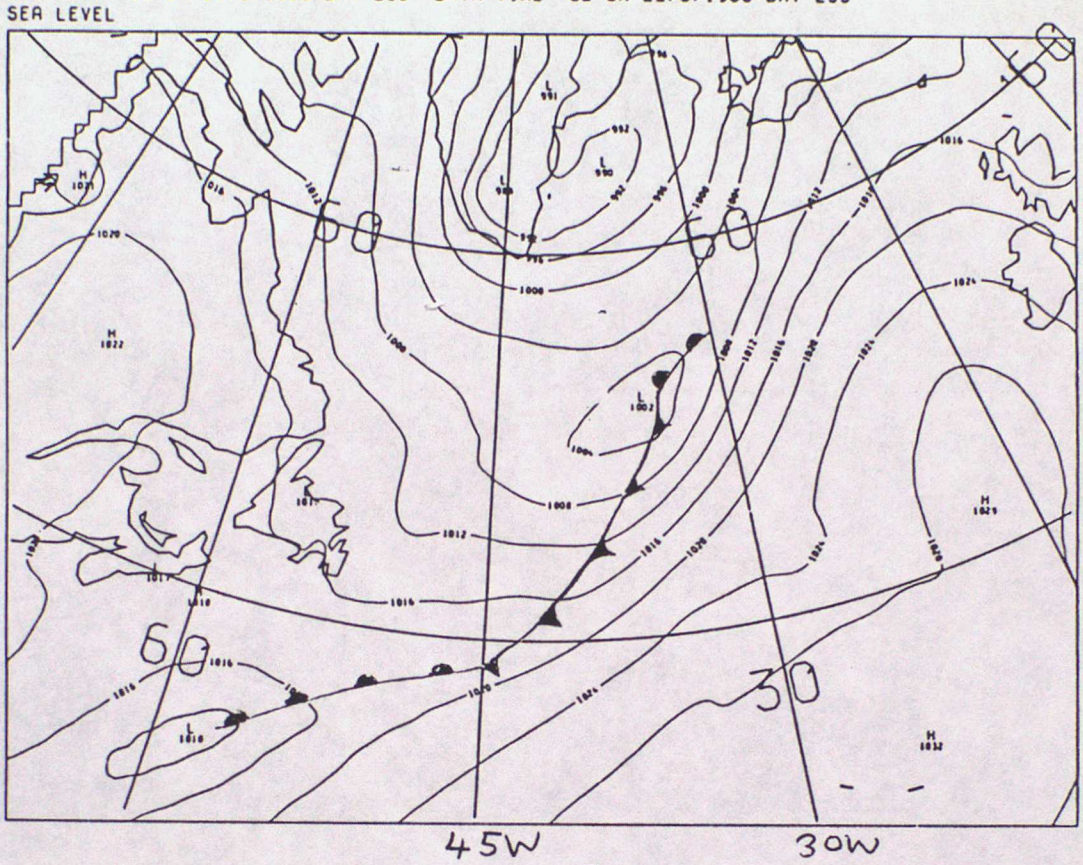

(a)

PV CHART THETA=330.0
900MB POTENTIAL TEMPERATURE
VALID AT 0Z ON 23/8/1988 DAY 236 DATA TIME 0Z ON 22/8/1988 DAY 235
LEVEL: 50 MB

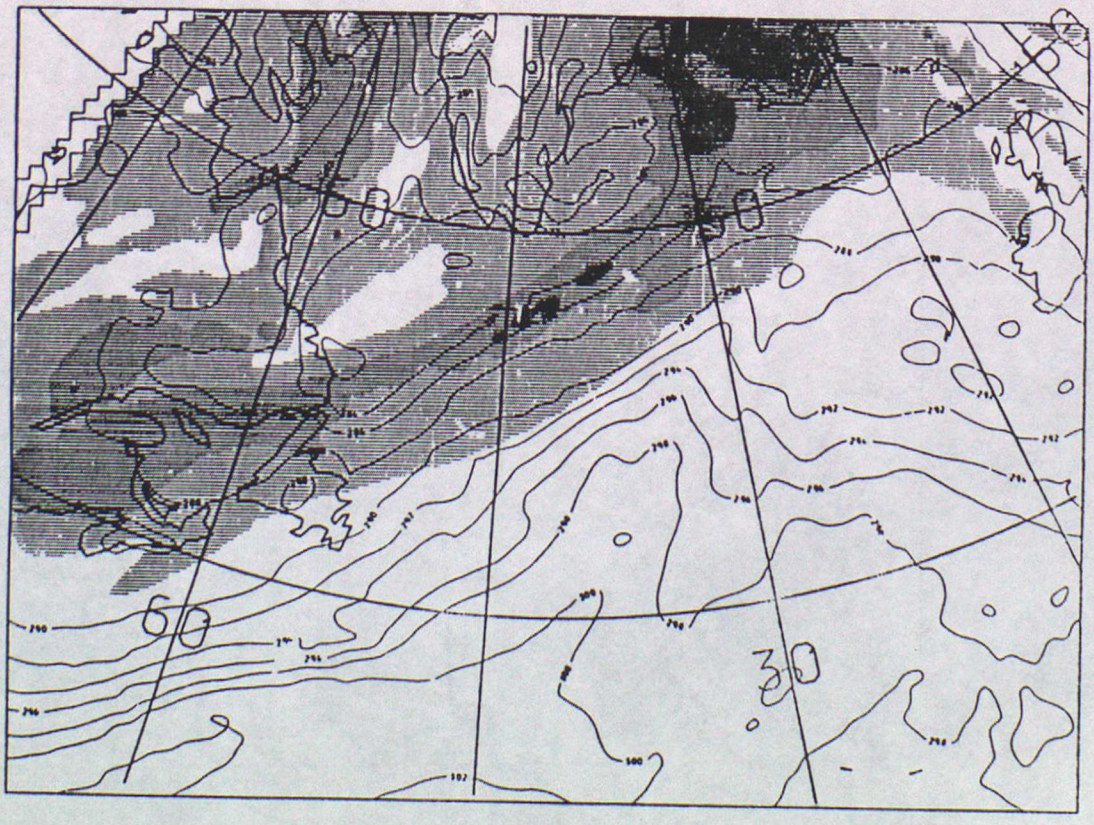

(b)

FIG. 24

WET BULB POT TEMP
VALID AT 0Z ON 23/8/1988 DAY 236 DATA TIME 0Z ON 22/8/1988 DAY 235
LEVEL: 850 MB

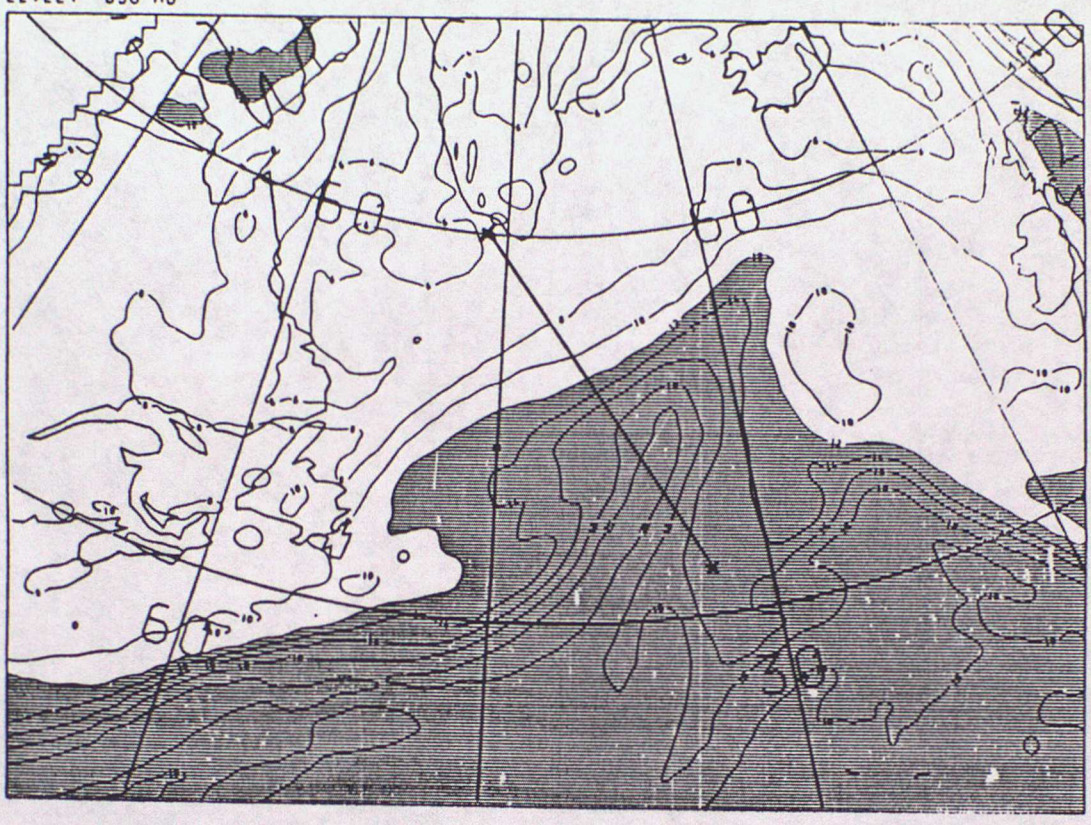

(c)

VERTICAL VELOCITY
VALID AT 0Z ON 23/8/1988 DAY 236 DATA TIME 0Z ON 22/8/1988 DAY 235
LEVEL: 700 MB

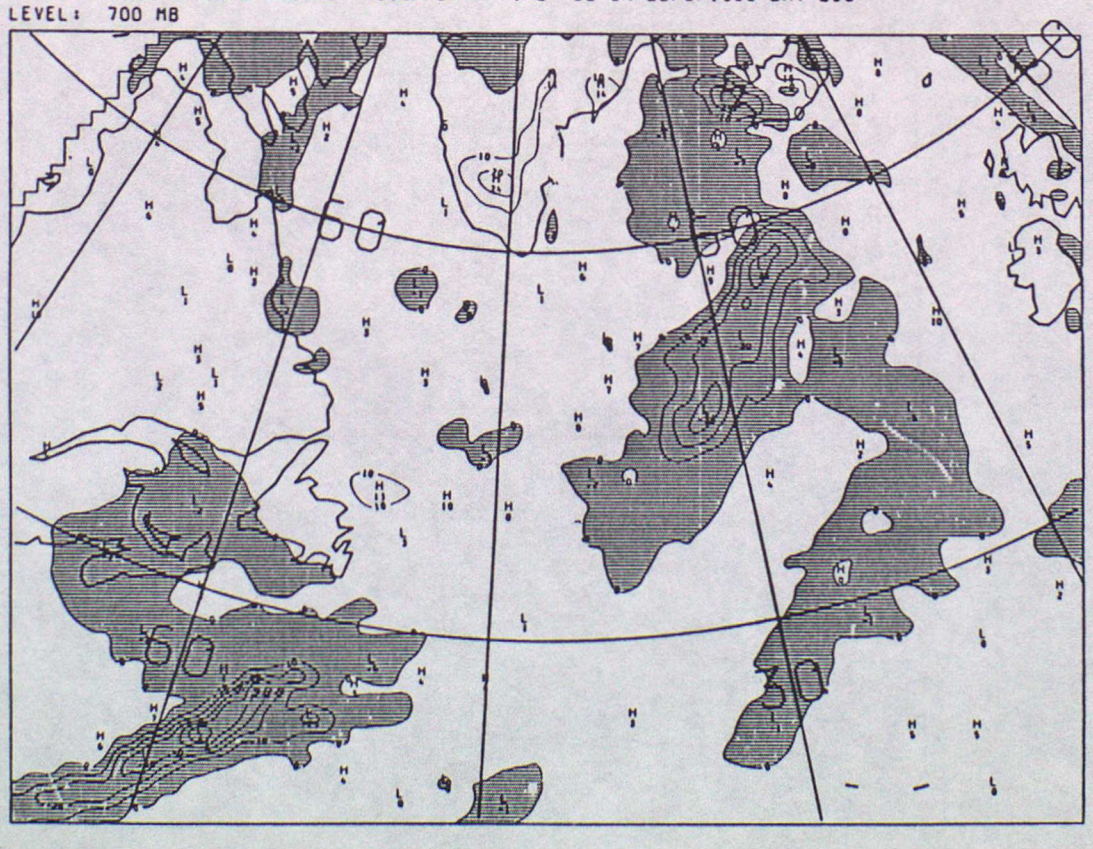

(d)

FIG. 25

GC. X-SECTION. V=SOLID CONTOURS -VE SHADED. U&W ARROWS. POT.TEMP=PECKED CONTOURS
VALID AT 0Z ON 23/8/1988 DAY 236 DATA TIME 0Z ON 22/8/1988 DAY 235

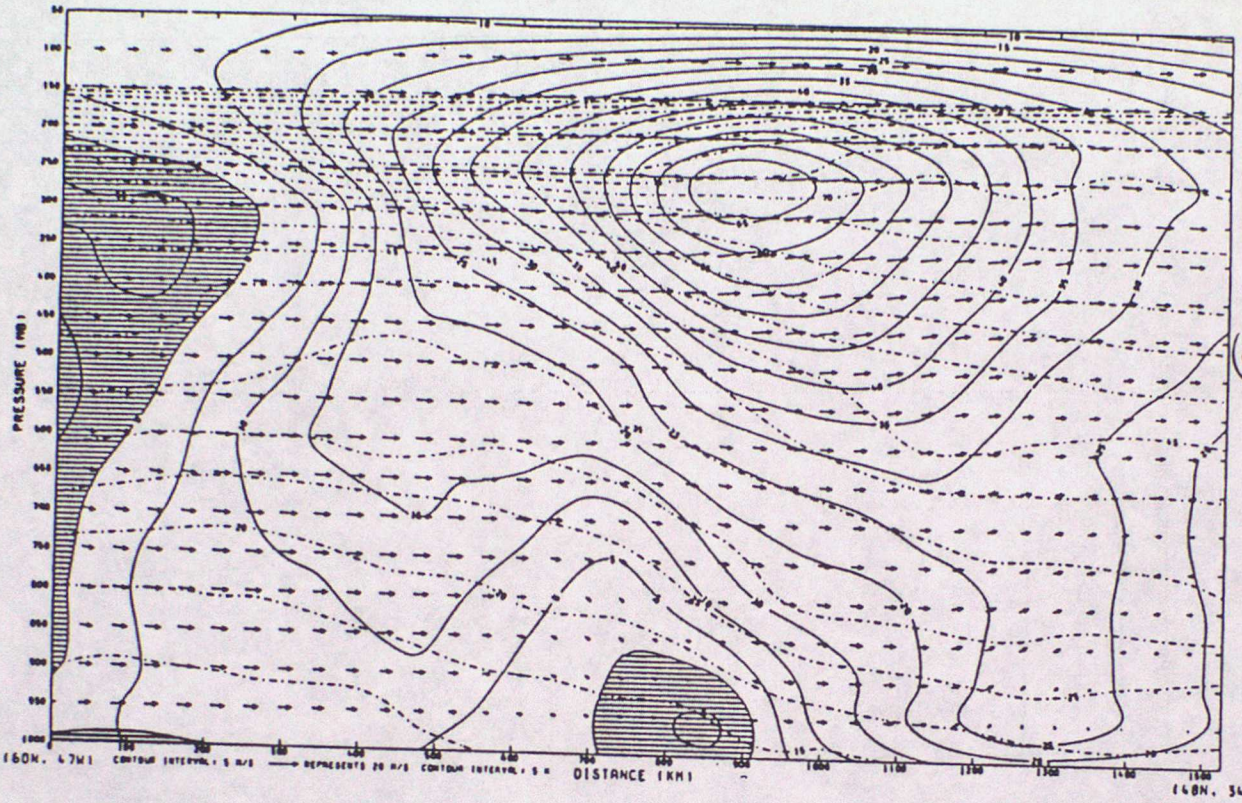

(a)

THETA
VALID AT 0Z ON 23/8/1988 DAY 236 DATA TIME 0Z ON 22/8/1988 DAY 235

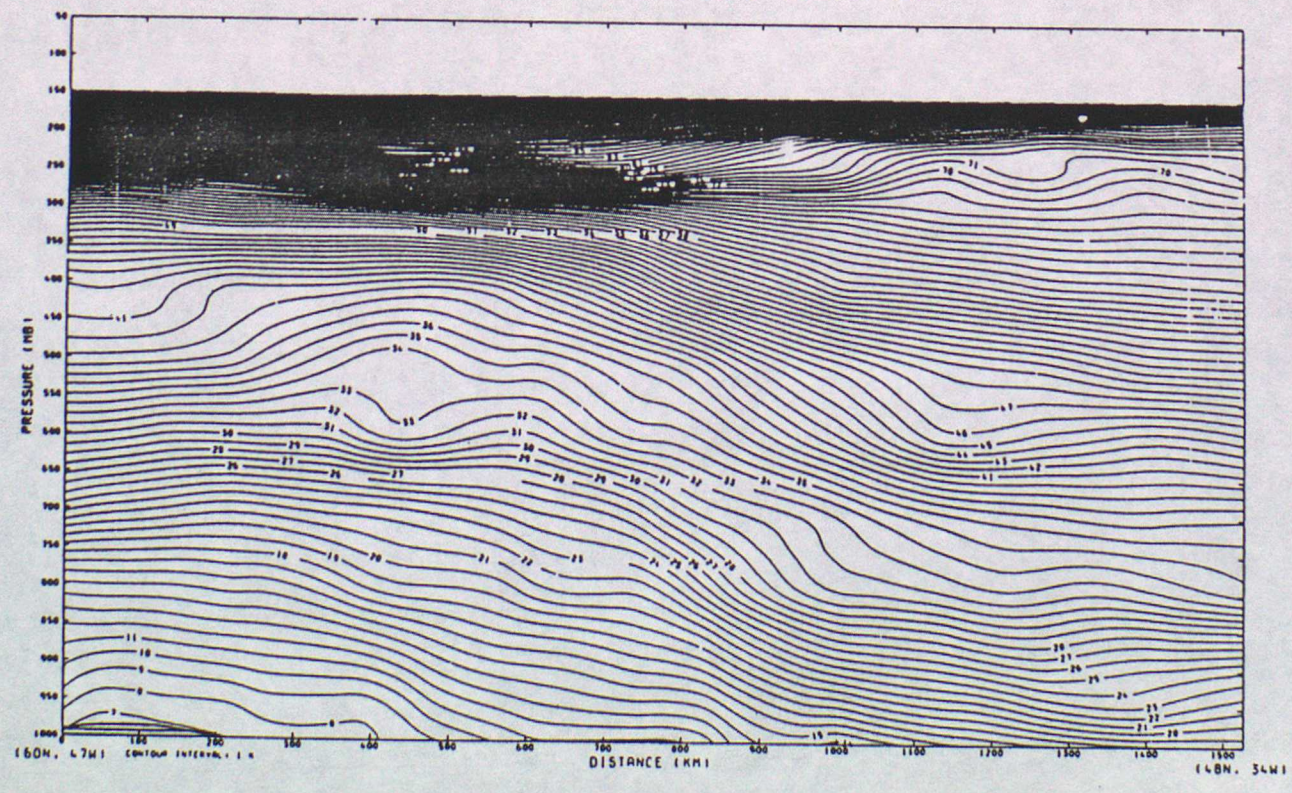

(b)

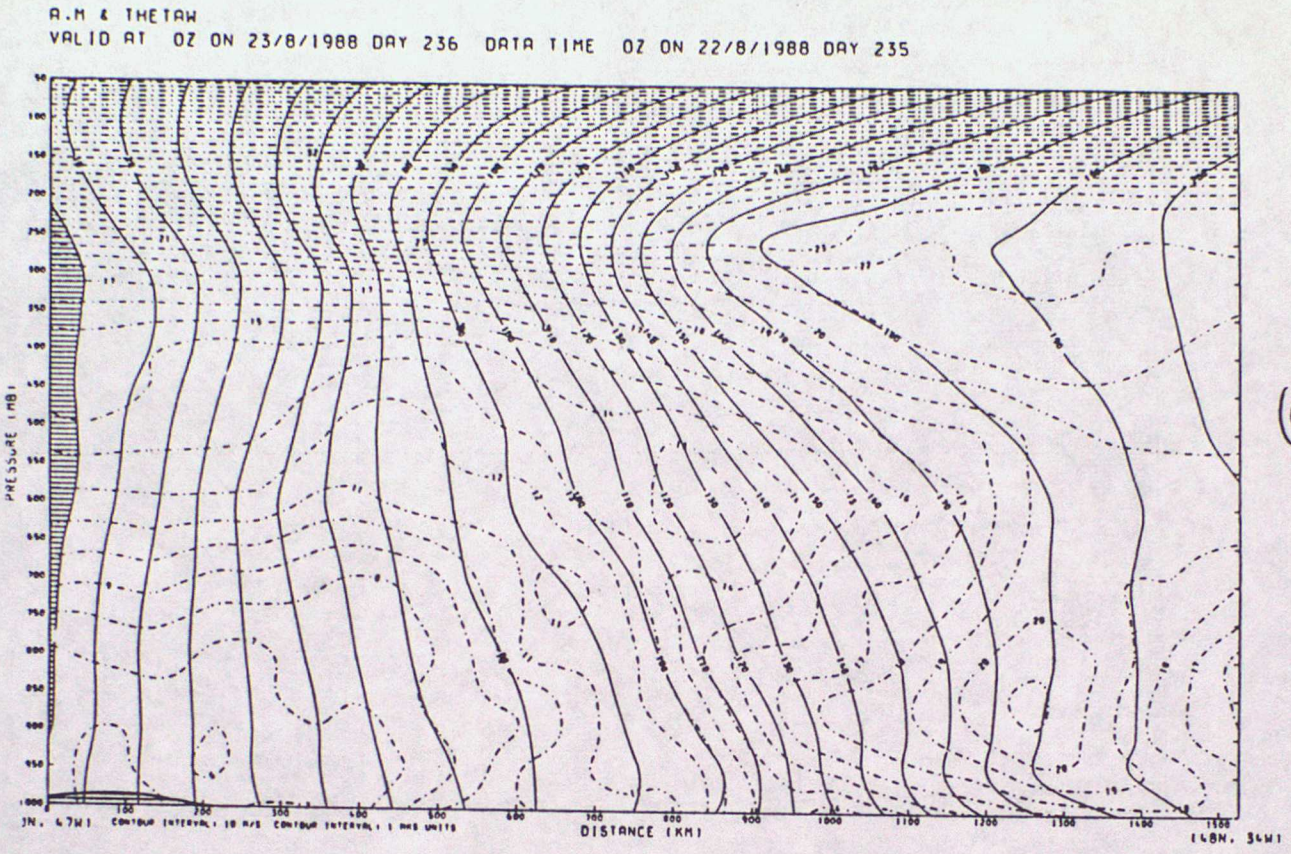

(c)

Fig. 26

SCAPE (J/KG X .01) PLOTTED WHERE SCAPE > 100 J/KG

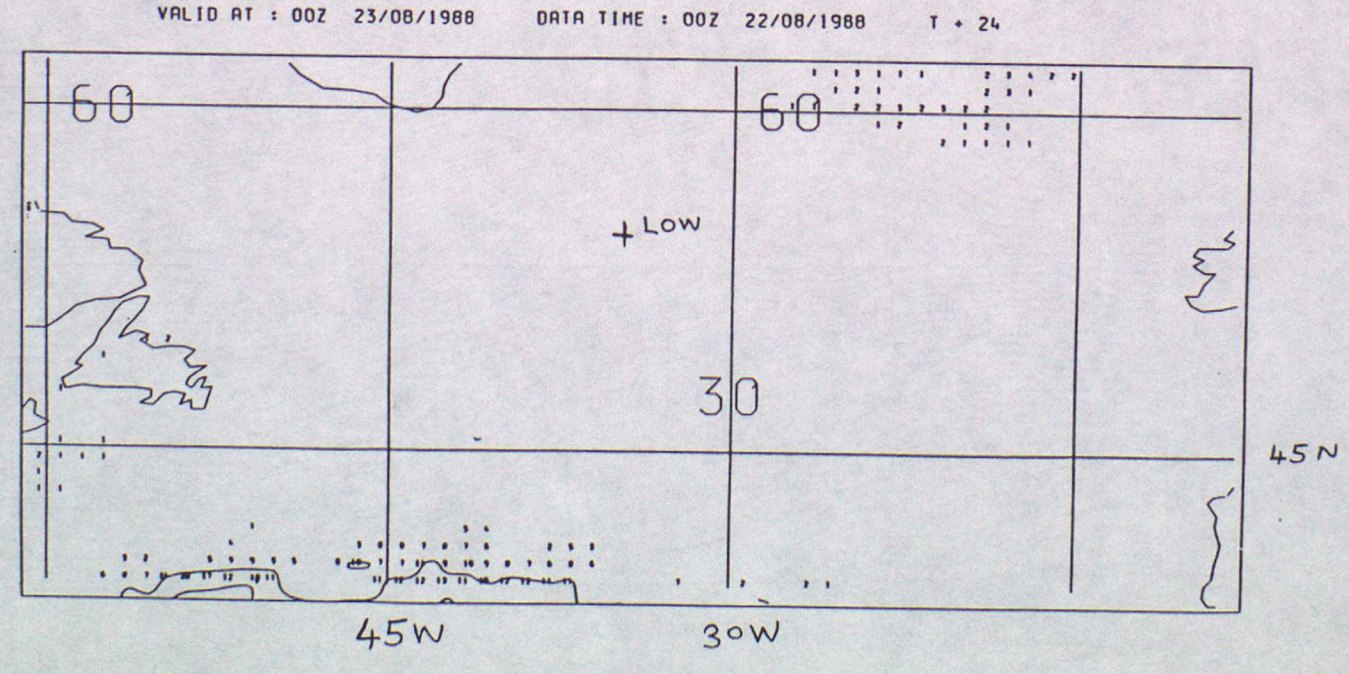

FIG. 27

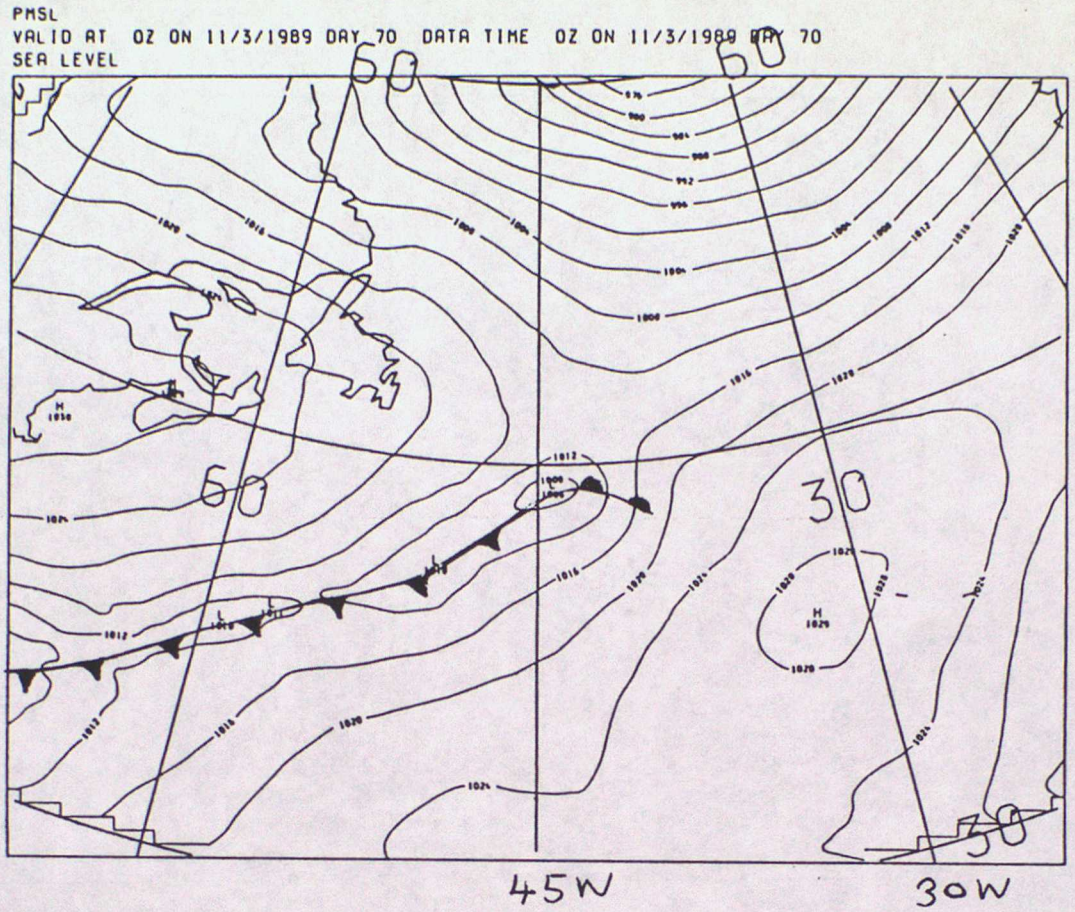
PMSL
VALID AT 0Z ON 11/3/1989 DAY 70 DATA TIME 0Z ON 11/3/1989 DAY 70
SEA LEVEL
60
60
60
30
30
45N
45W
30W

(a)

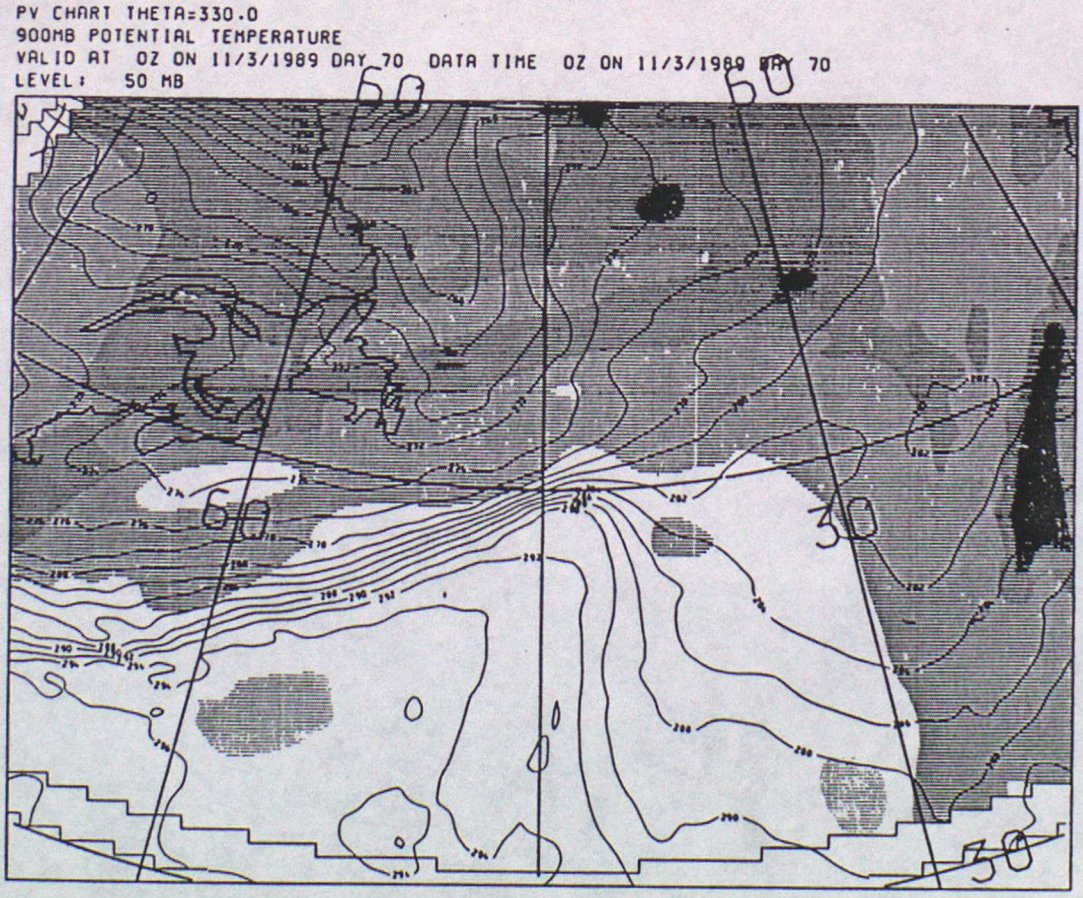
PV CHART THETA=330.0
900MB POTENTIAL TEMPERATURE
VALID AT 0Z ON 11/3/1989 DAY 70 DATA TIME 0Z ON 11/3/1989 DAY 70
LEVEL: 50 MB
60
60
60
30
30

(b)

FIG. 27

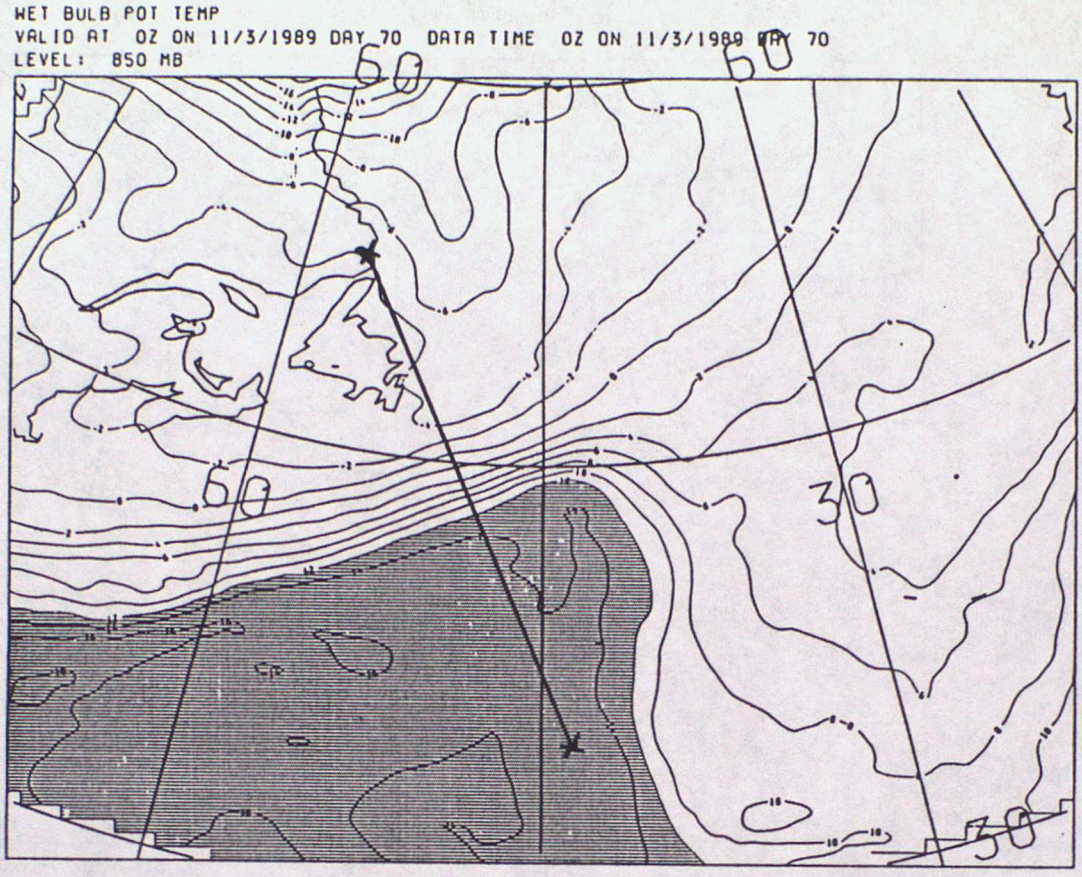
WET BULB POT TEMP
VALID AT 0Z ON 11/3/1989 DAY 70 DATA TIME 0Z ON 11/3/1989 DAY 70
LEVEL: 850 MB
60
60
60
30
30

(c)

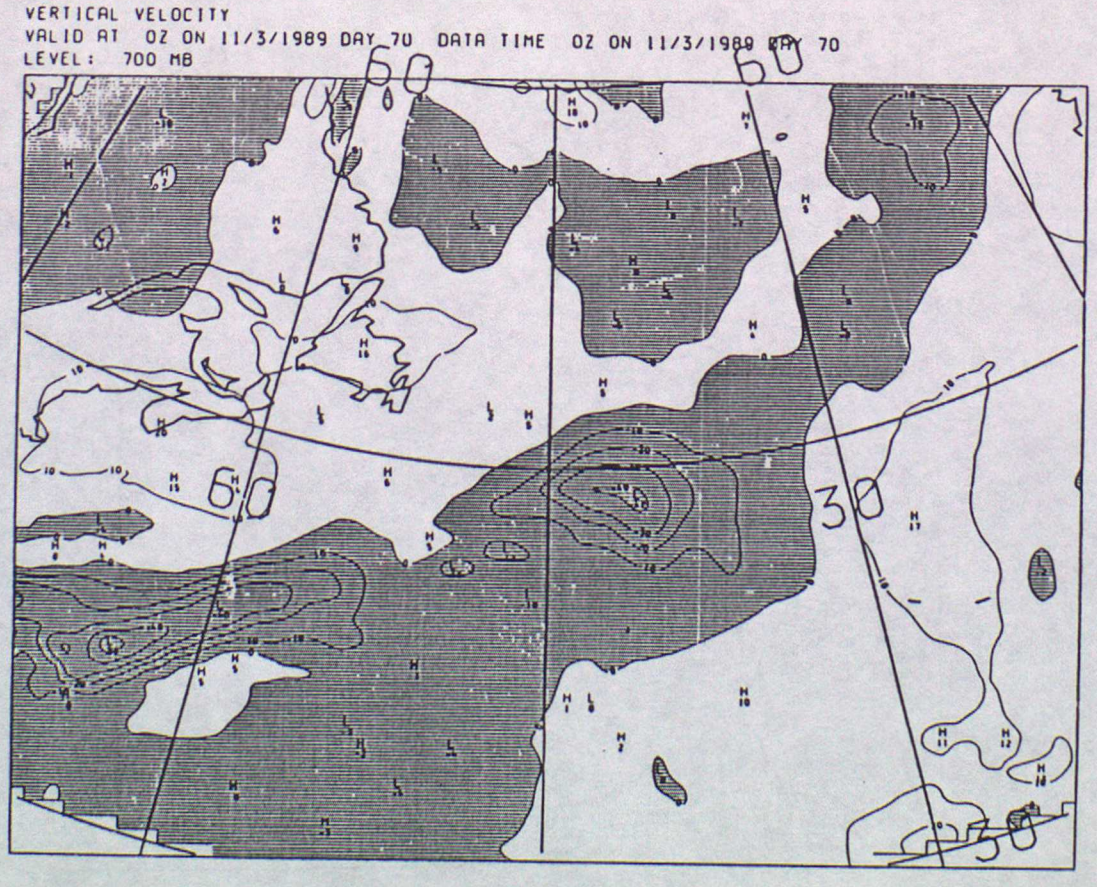
VERTICAL VELOCITY
VALID AT 0Z ON 11/3/1989 DAY 70 DATA TIME 0Z ON 11/3/1989 DAY 70
LEVEL: 700 MB
60
60
60
30
30

(d)

FIG. 28

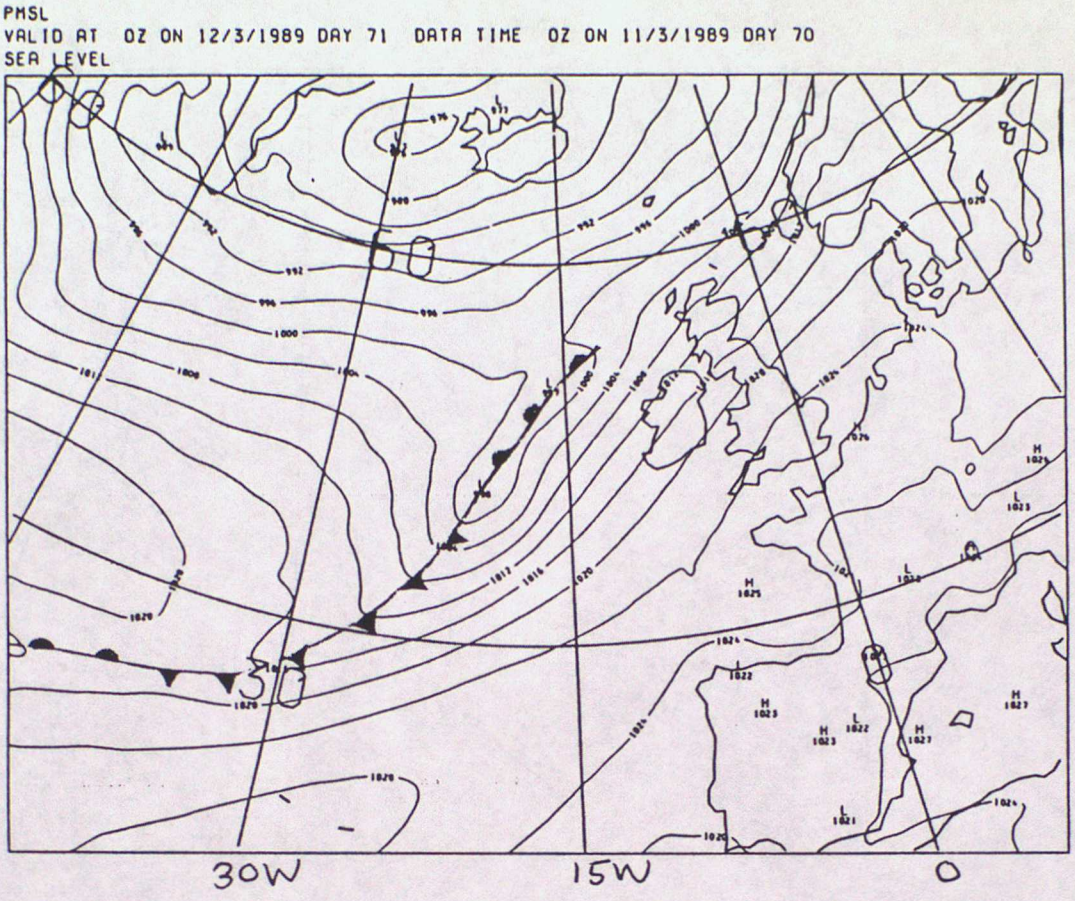
PMSL
VALID AT 0Z ON 12/3/1989 DAY 71 DATA TIME 0Z ON 11/3/1989 DAY 70
SEA LEVEL
30W
15W
0
45N

(a)

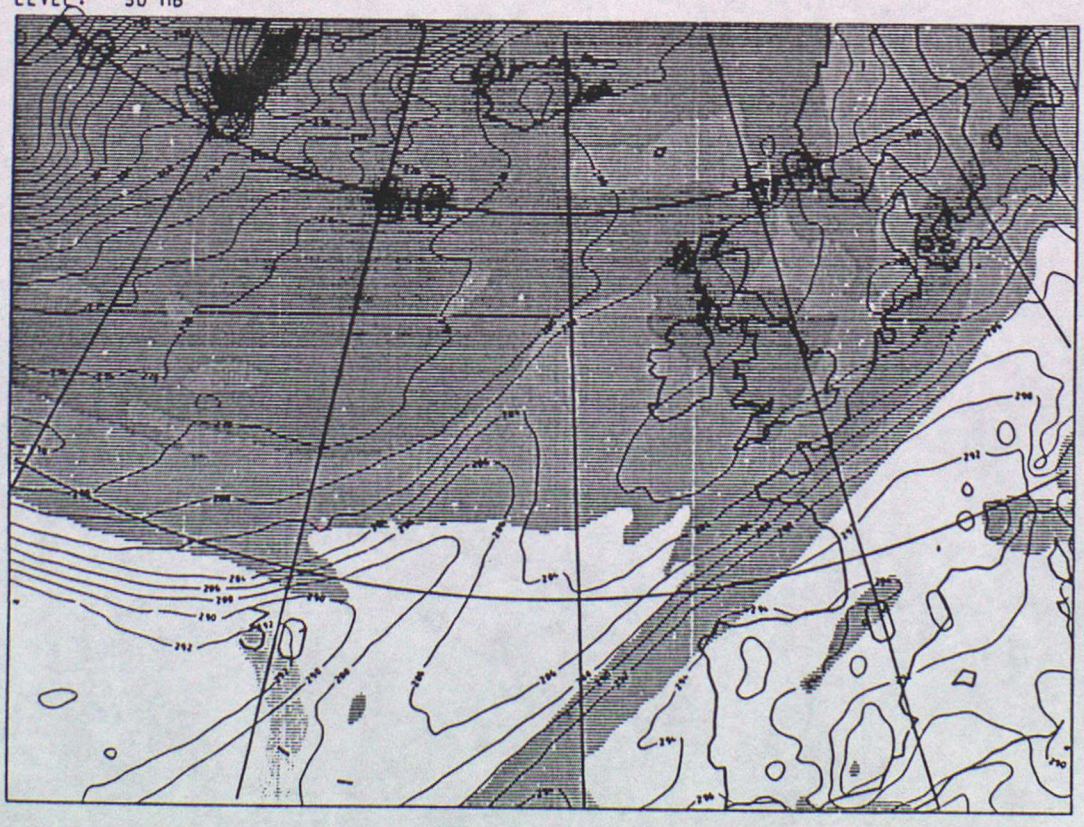
PV CHART THETA=330.0
900MB POTENTIAL TEMPERATURE
VALID AT 0Z ON 12/3/1989 DAY 71 DATA TIME 0Z ON 11/3/1989 DAY 70
LEVEL: 50 MB

(b)

FIG. 28

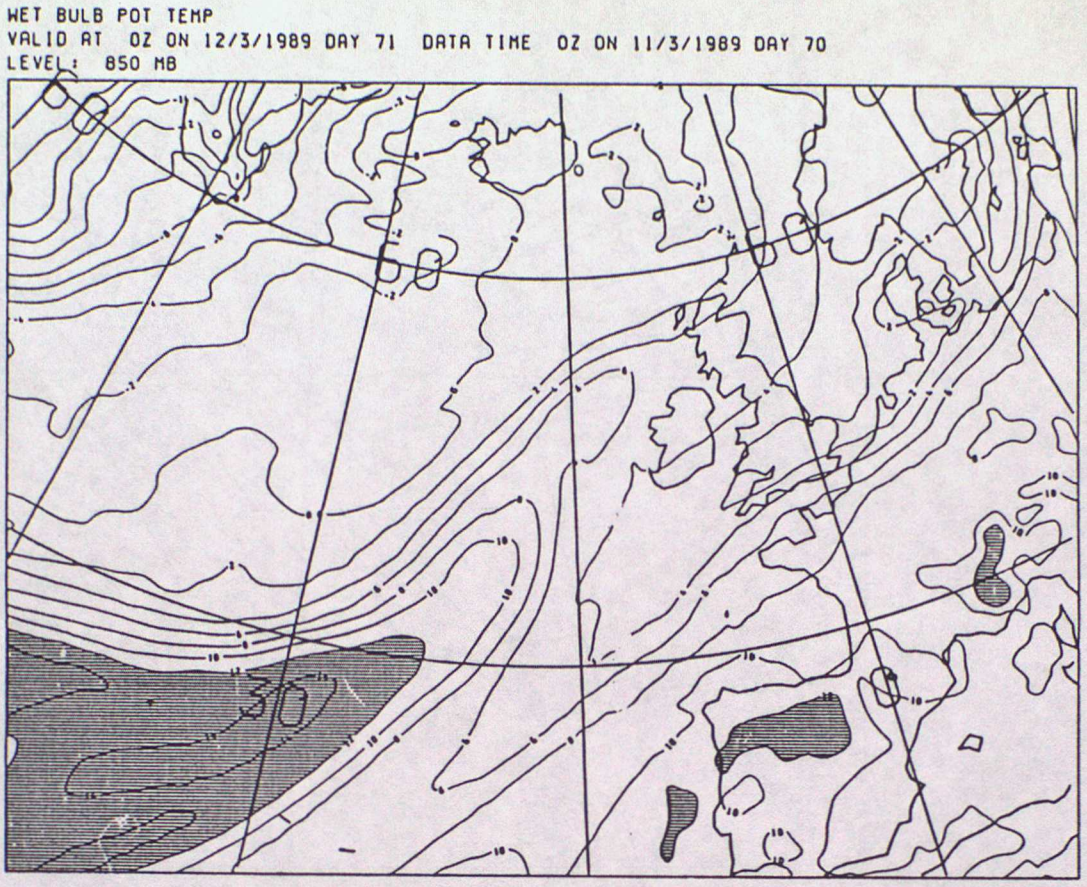
WET BULB POT TEMP
VALID AT 0Z ON 12/3/1989 DAY 71 DATA TIME 0Z ON 11/3/1989 DAY 70
LEVEL: 850 MB

(c)

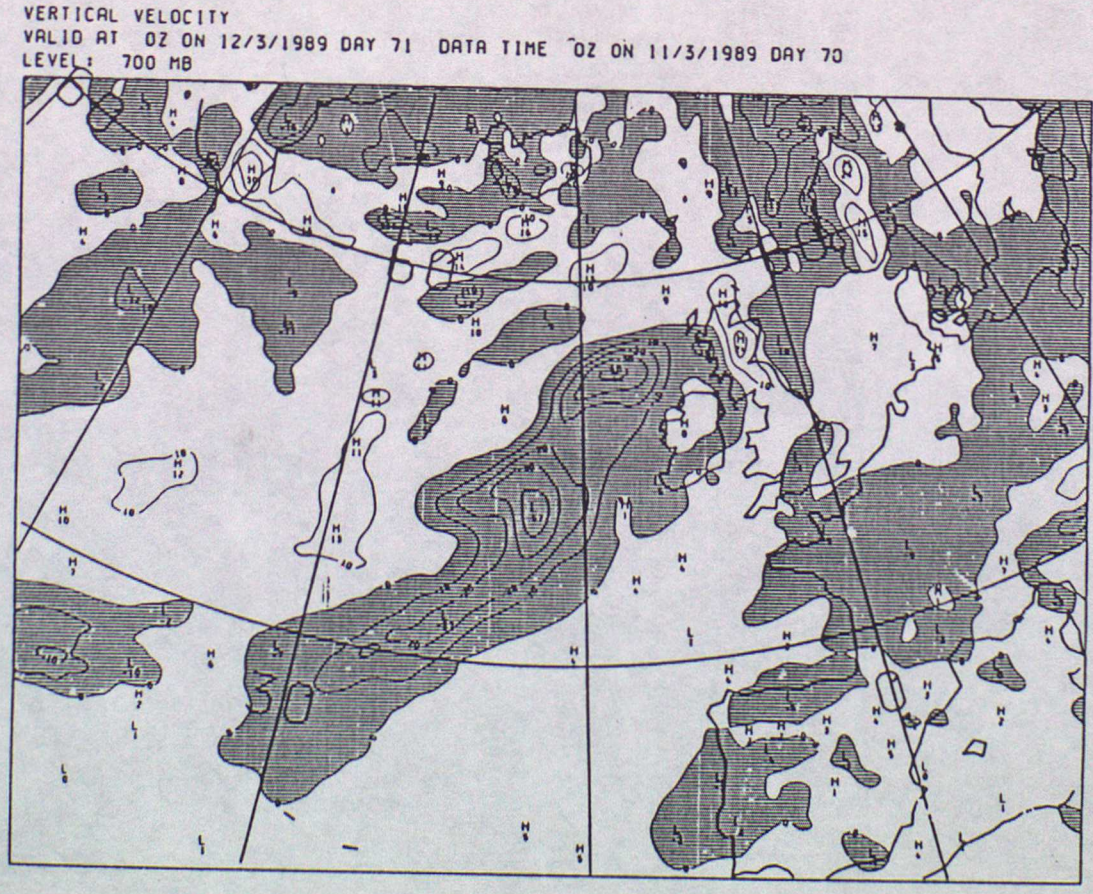
VERTICAL VELOCITY
VALID AT 0Z ON 12/3/1989 DAY 71 DATA TIME 0Z ON 11/3/1989 DAY 70
LEVEL: 700 MB

(d)

FIG. 29

GC. X-SECTION. V=SOLID CONTOURS -VE SHADED. U&W ARROWS. POT.TEMP=PECKED CONTOURS
VALID AT 0Z ON 11/3/1989 DAY 70 DATA TIME 0Z ON 11/3/1989 DAY 70

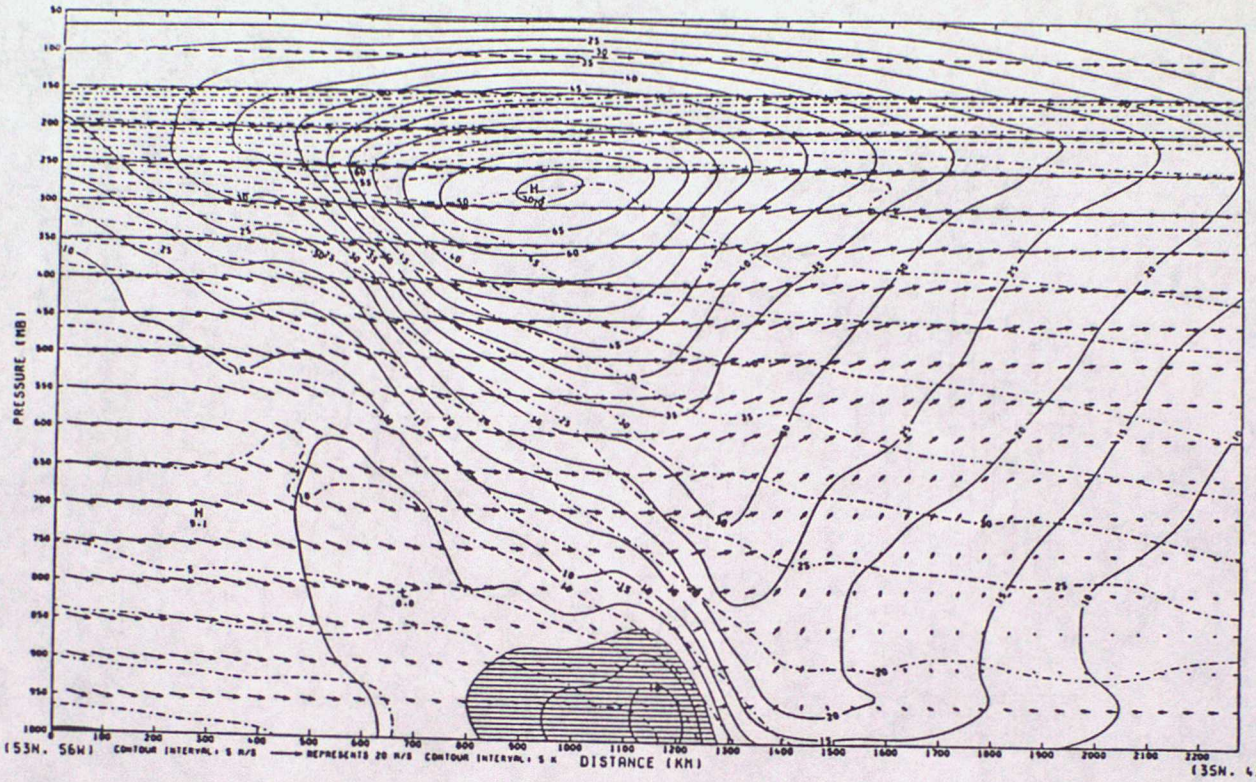

(a)

THETA
VALID AT 0Z ON 11/3/1989 DAY 70 DATA TIME 0Z ON 11/3/1989 DAY 70

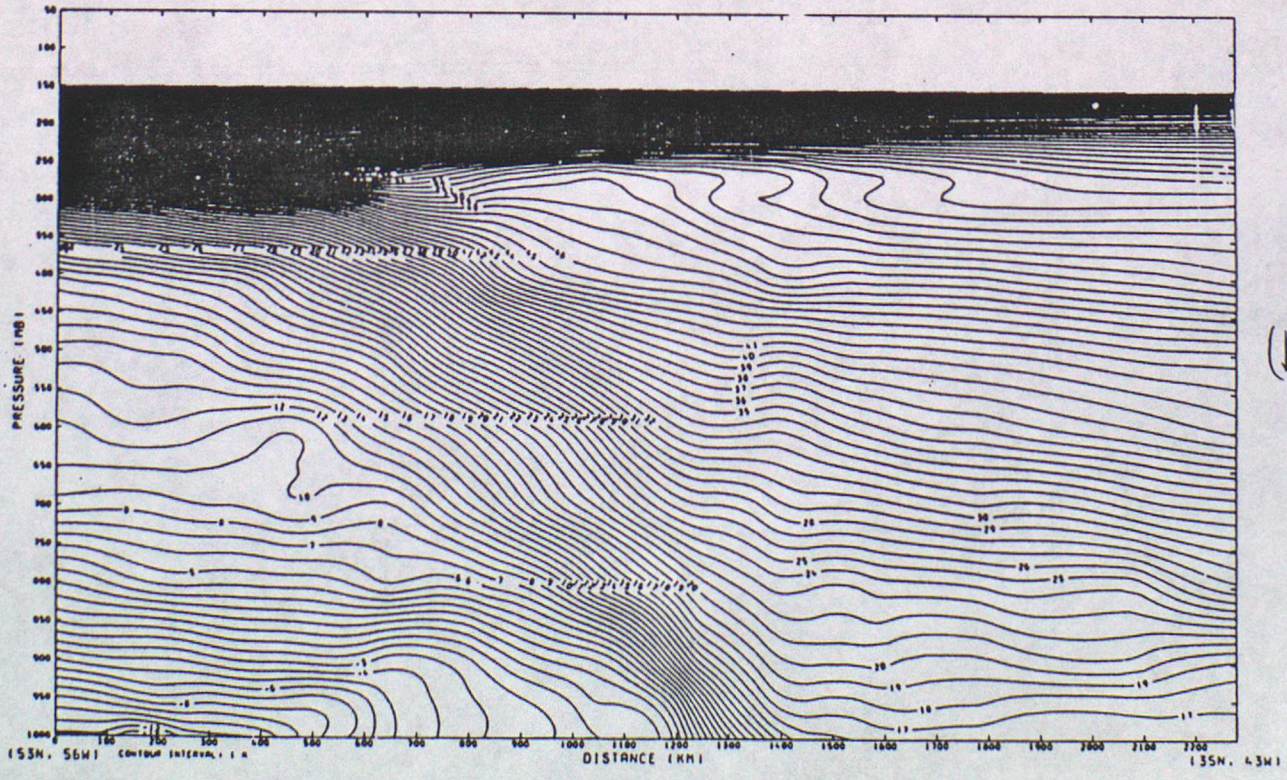

(b)

FIG. 29(c)

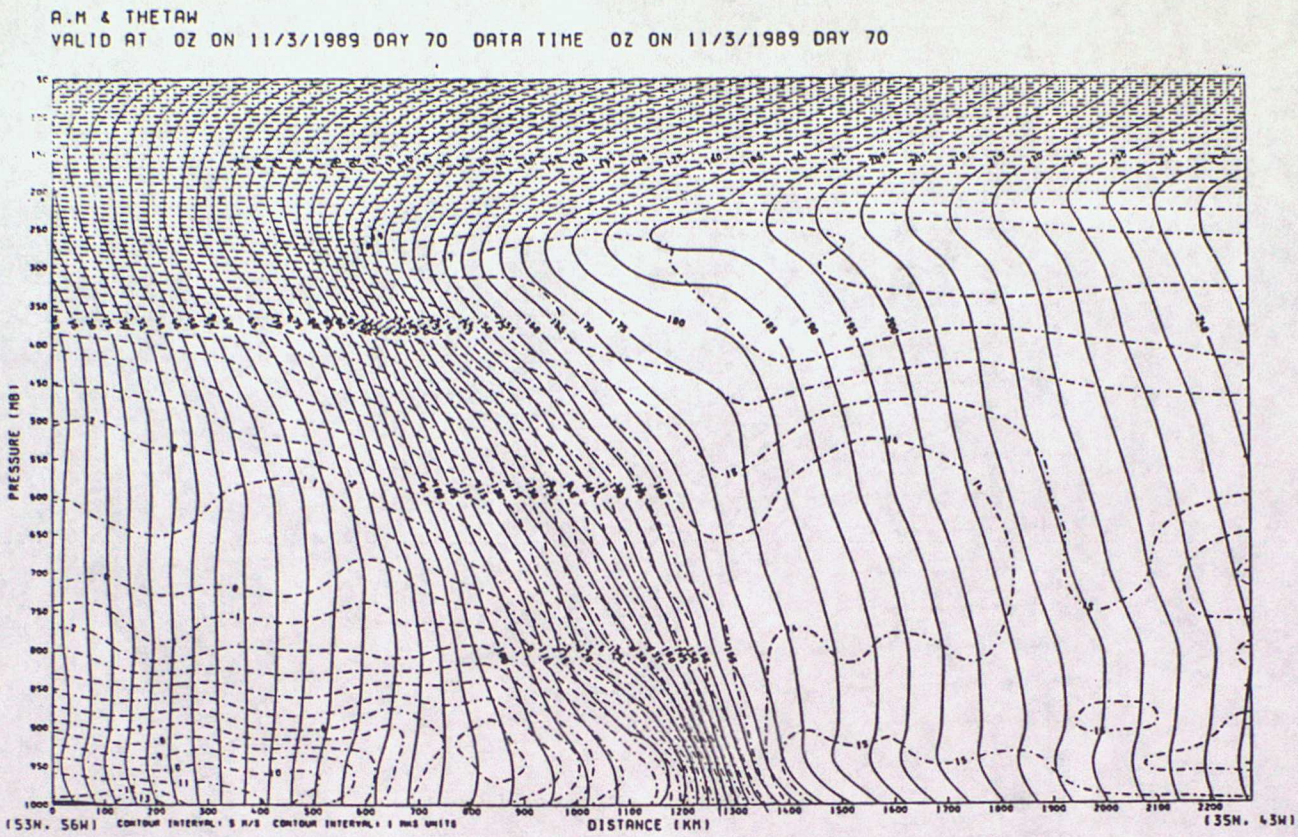

FIG. 30

SCAPE (J/KG X .01) PLOTTED WHERE SCAPE > 100 J/KG

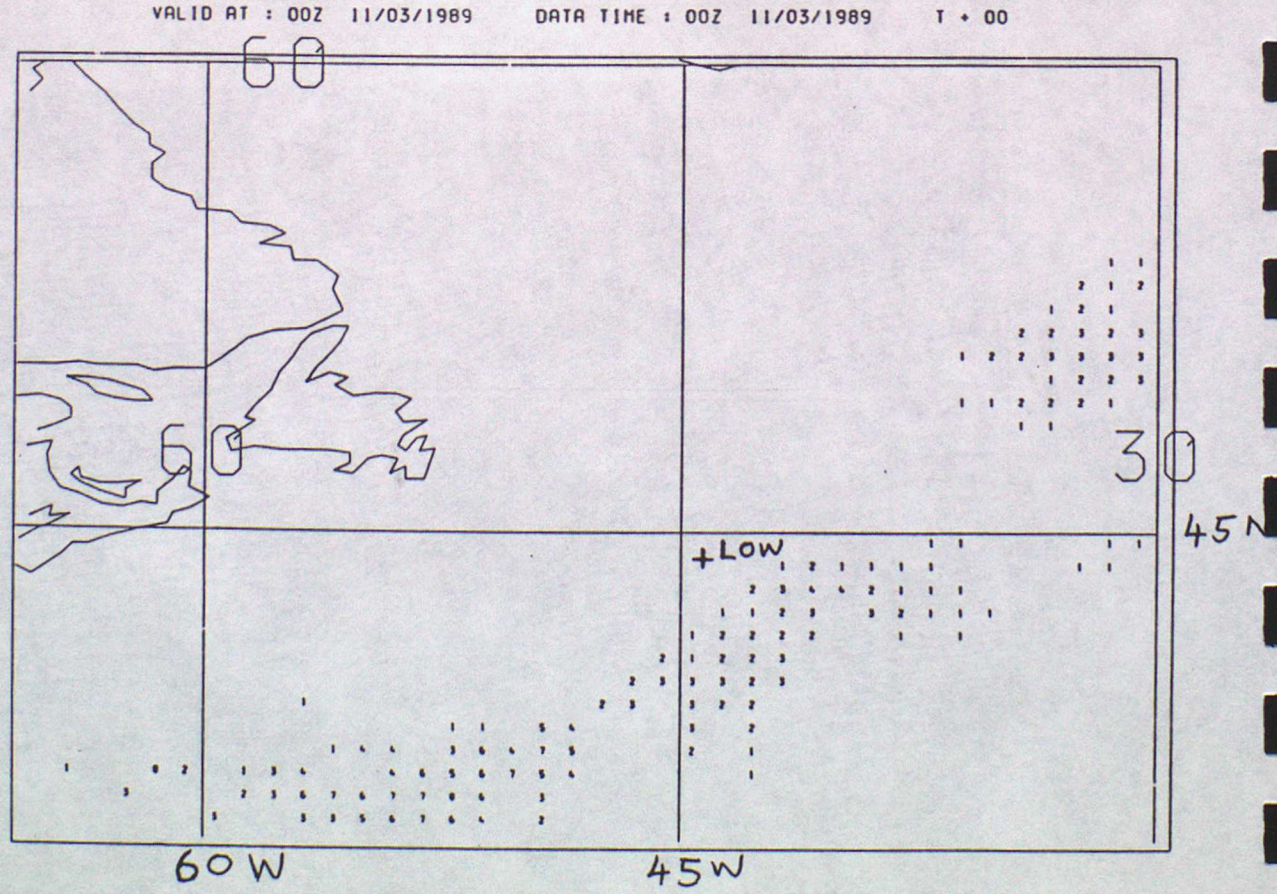

Fig. 31

PMSL
VALID AT 0Z ON 3/12/1988 DAY 338 DATA TIME 12Z ON 2/12/1988 DAY 337
SEA LEVEL

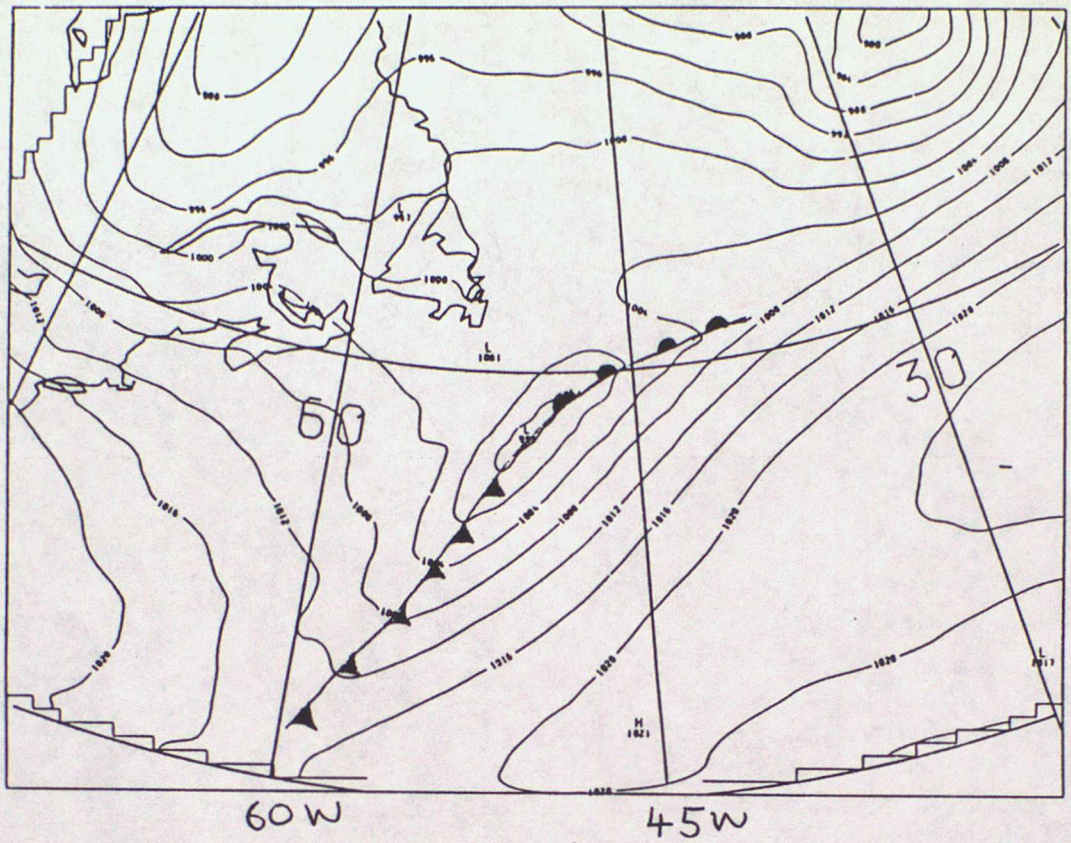

(a)

PV CHART THETA=330.0
900MB POTENTIAL TEMPERATURE
VALID AT 0Z ON 3/12/1988 DAY 338 DATA TIME 12Z ON 2/12/1988 DAY 337
LEVEL: 50 MB

(b)

FIG. 31

WET BULB POT TEMP
VALID AT 0Z ON 3/12/1988 DAY 338 DATA TIME 12Z ON 2/12/1988 DAY 337
LEVEL: 850 MB

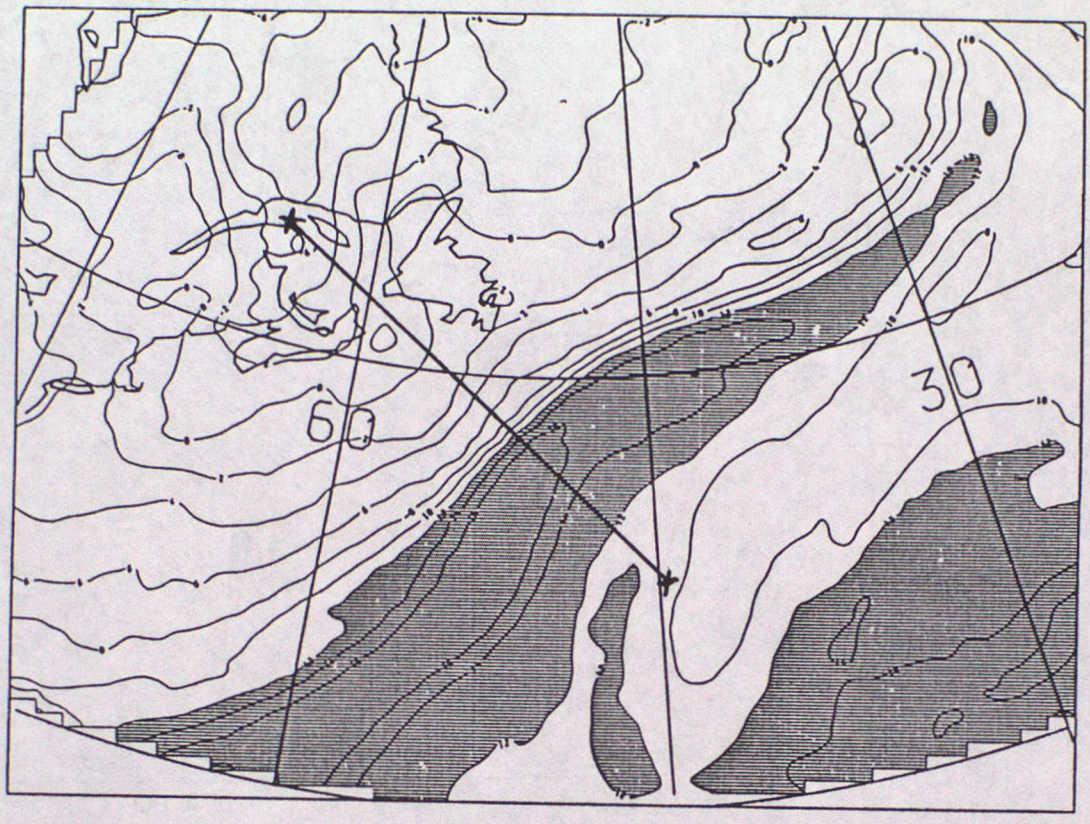

(c)

VERTICAL VELOCITY
VALID AT 0Z ON 3/12/1988 DAY 338 DATA TIME 12Z ON 2/12/1988 DAY 337
LEVEL: 700 MB

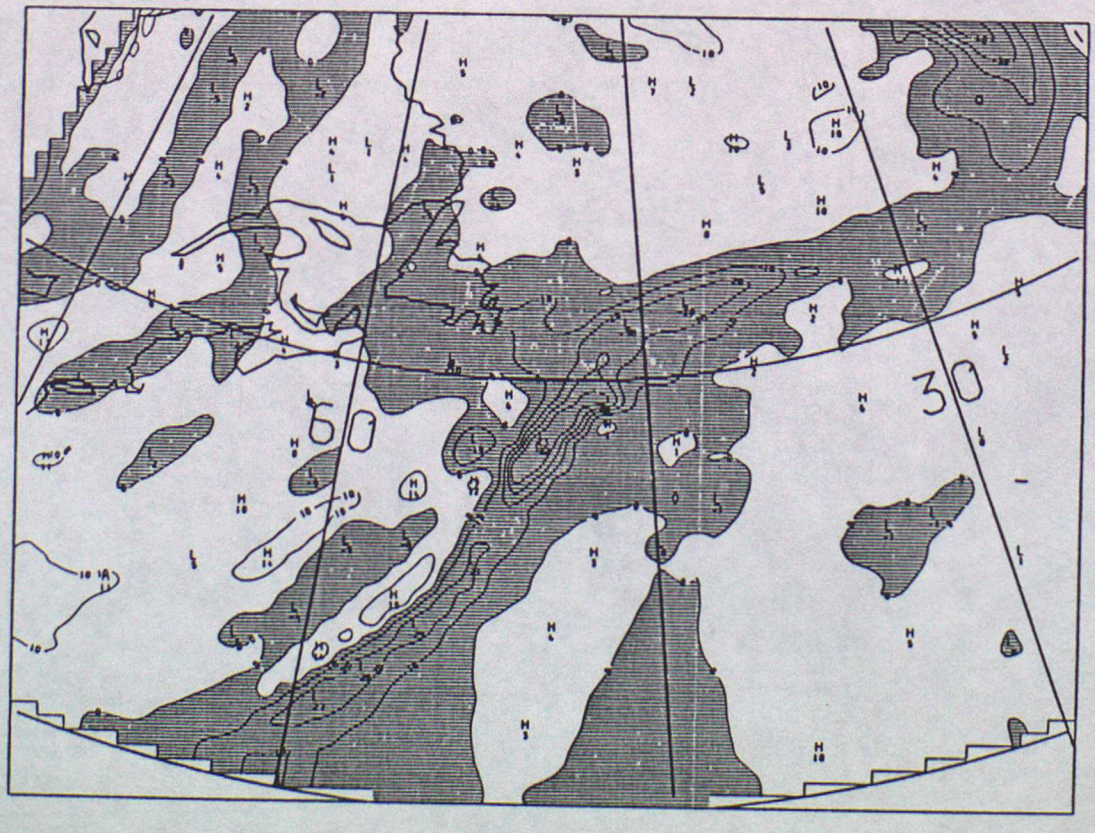

(d)

Fig. 32

PMSL
VALID AT 0Z ON 4/12/1988 DAY 339 DATA TIME 12Z ON 2/12/1988 DAY 337
SEA LEVEL

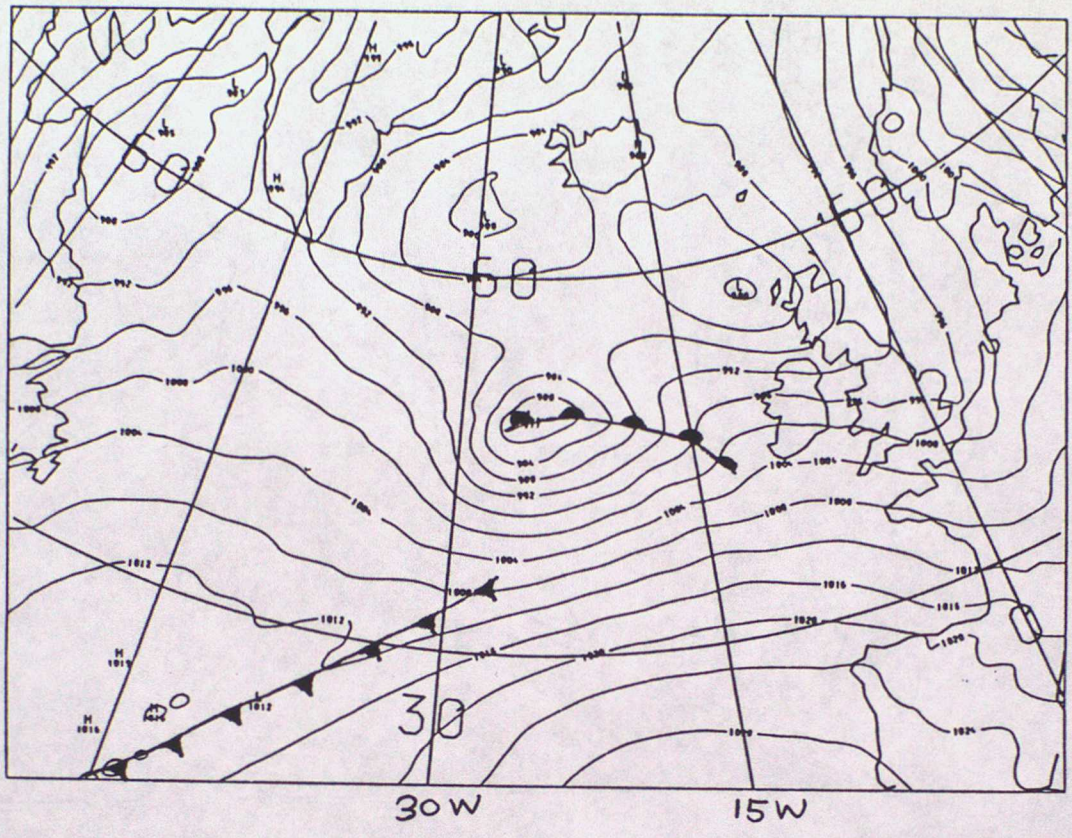

(a)

PV CHART THETA=330.0
900MB POTENTIAL TEMPERATURE
VALID AT 0Z ON 4/12/1988 DAY 339 DATA TIME 12Z ON 2/12/1988 DAY 337
LEVEL: 50 MB

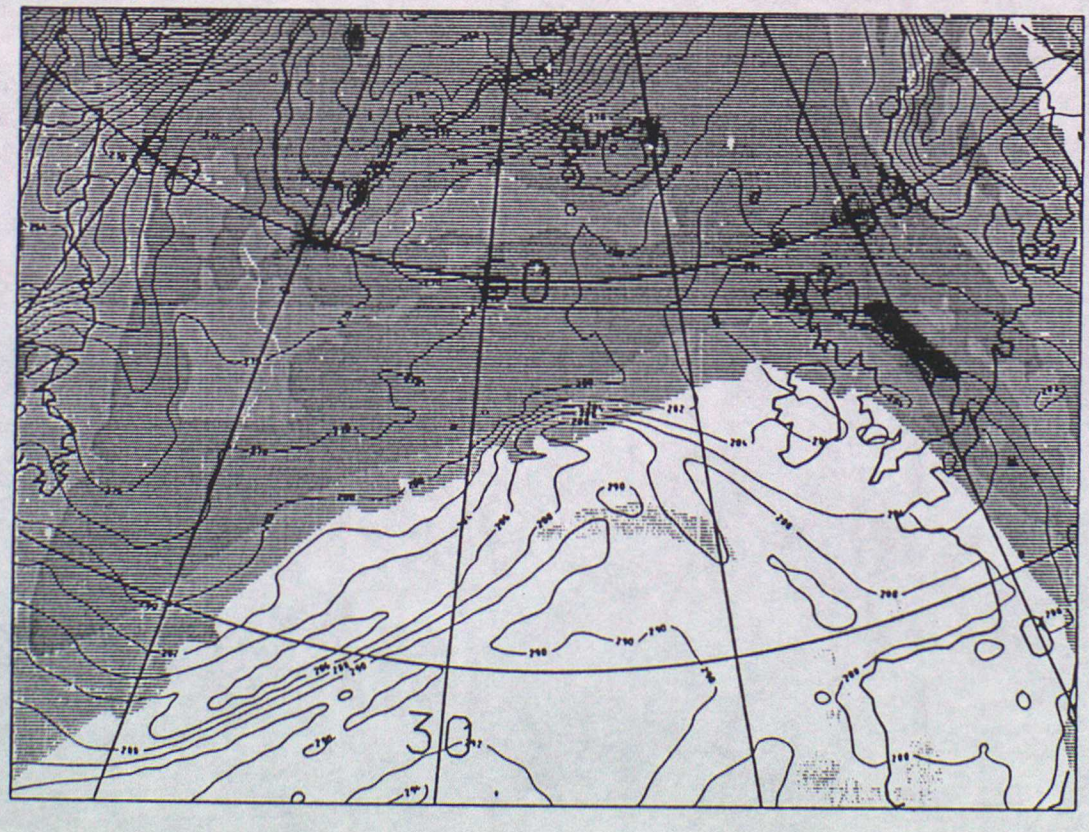

(b)

FIG. 32

WET BULB POT TEMP
VALID AT 0Z ON 4/12/1988 DAY 339 DATA TIME 12Z ON 2/12/1988 DAY 337
LEVEL: 850 MB

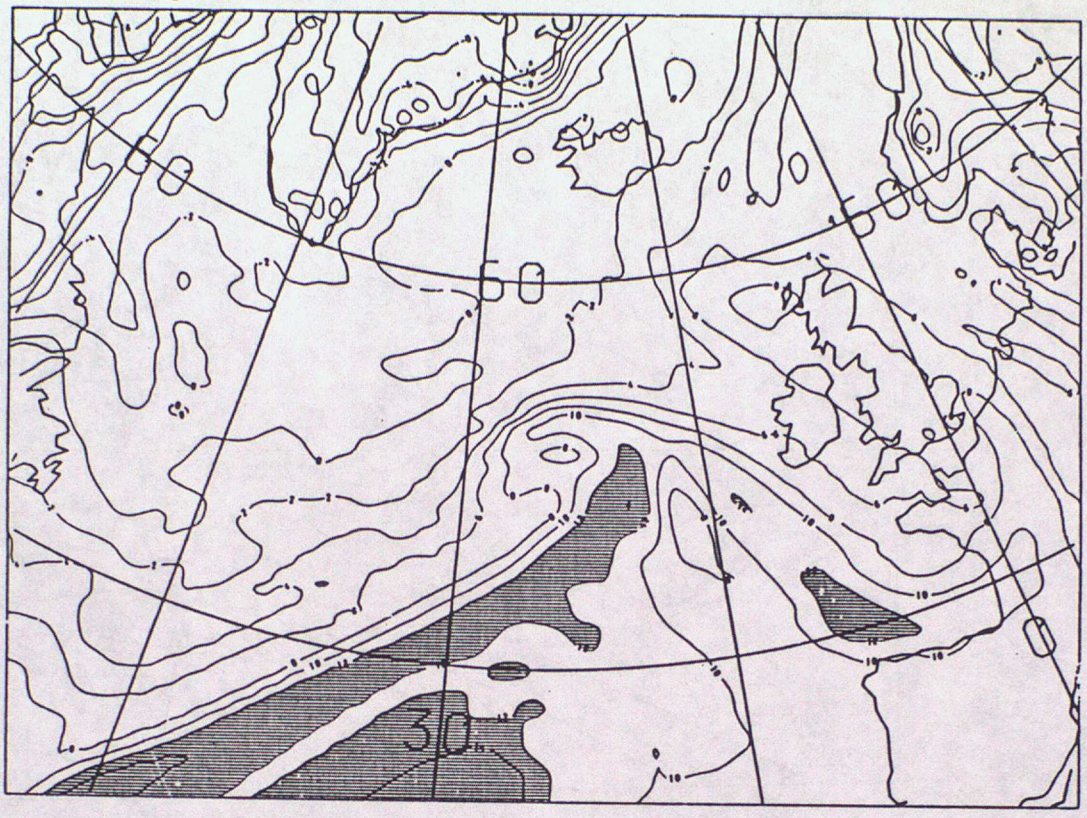

(c)

VERTICAL VELOCITY
VALID AT 0Z ON 4/12/1988 DAY 339 DATA TIME 12Z ON 2/12/1988 DAY 337
LEVEL: 700 MB

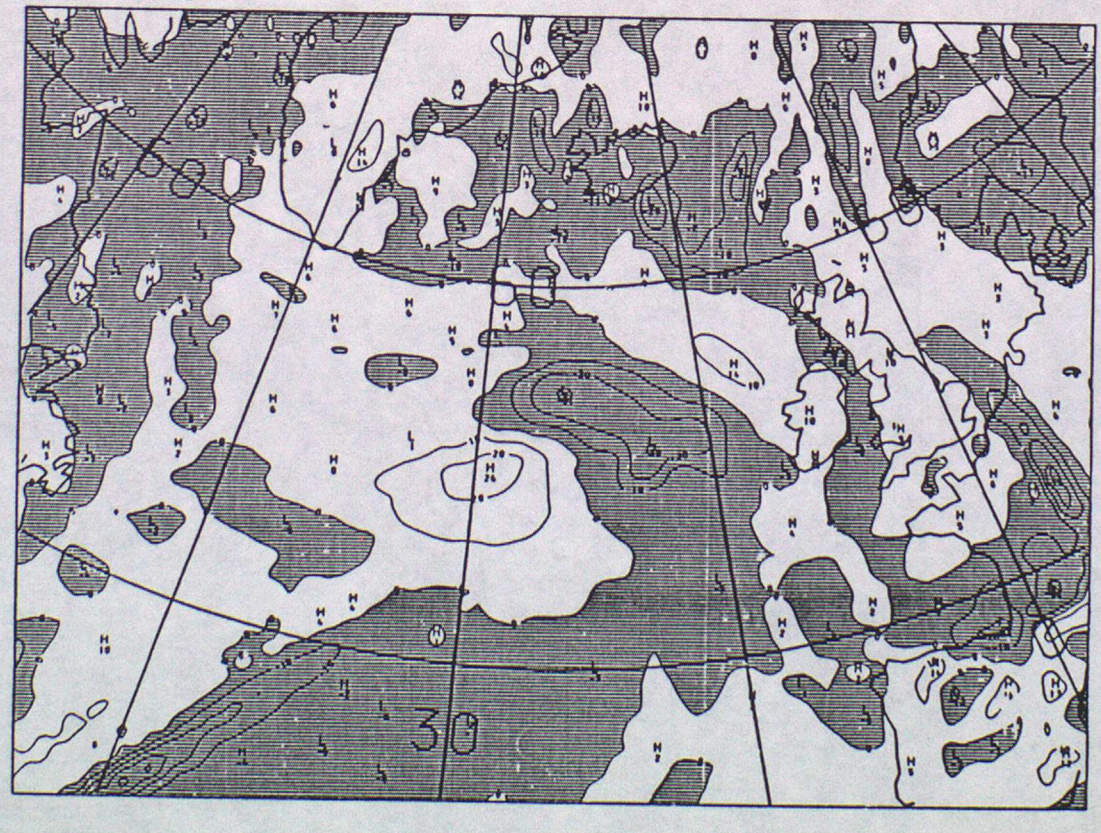

(d)

FIG. 33

GC. X-SECTION. V=SOLID CONTOURS -VE SHADED. U&W ARROWS. POT.TEMP=PECKED CONTOURS
VALID AT 0Z ON 3/12/1988 DAY 338 DATA TIME 12Z ON 2/12/1988 DAY 337

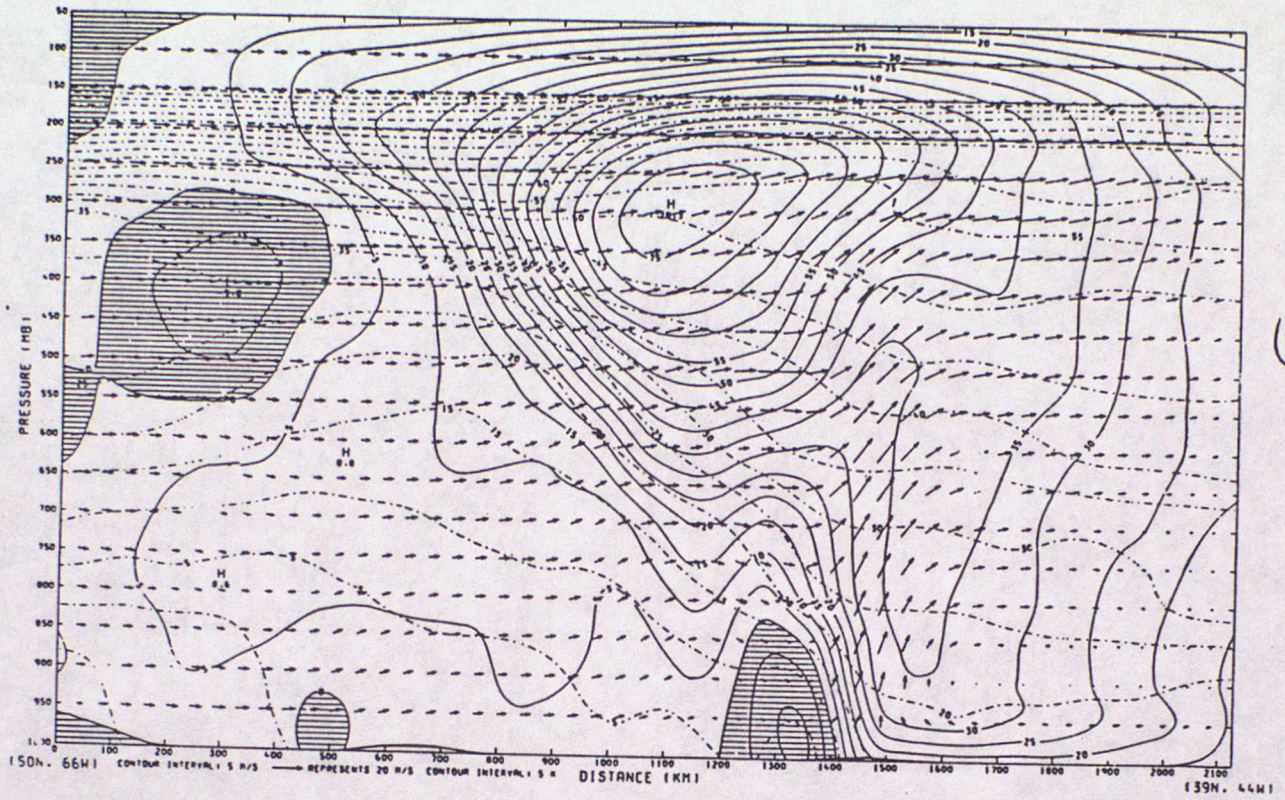

(a)

THETA
VALID AT 0Z ON 3/12/1988 DAY 338 DATA TIME 12Z ON 2/12/1988 DAY 337

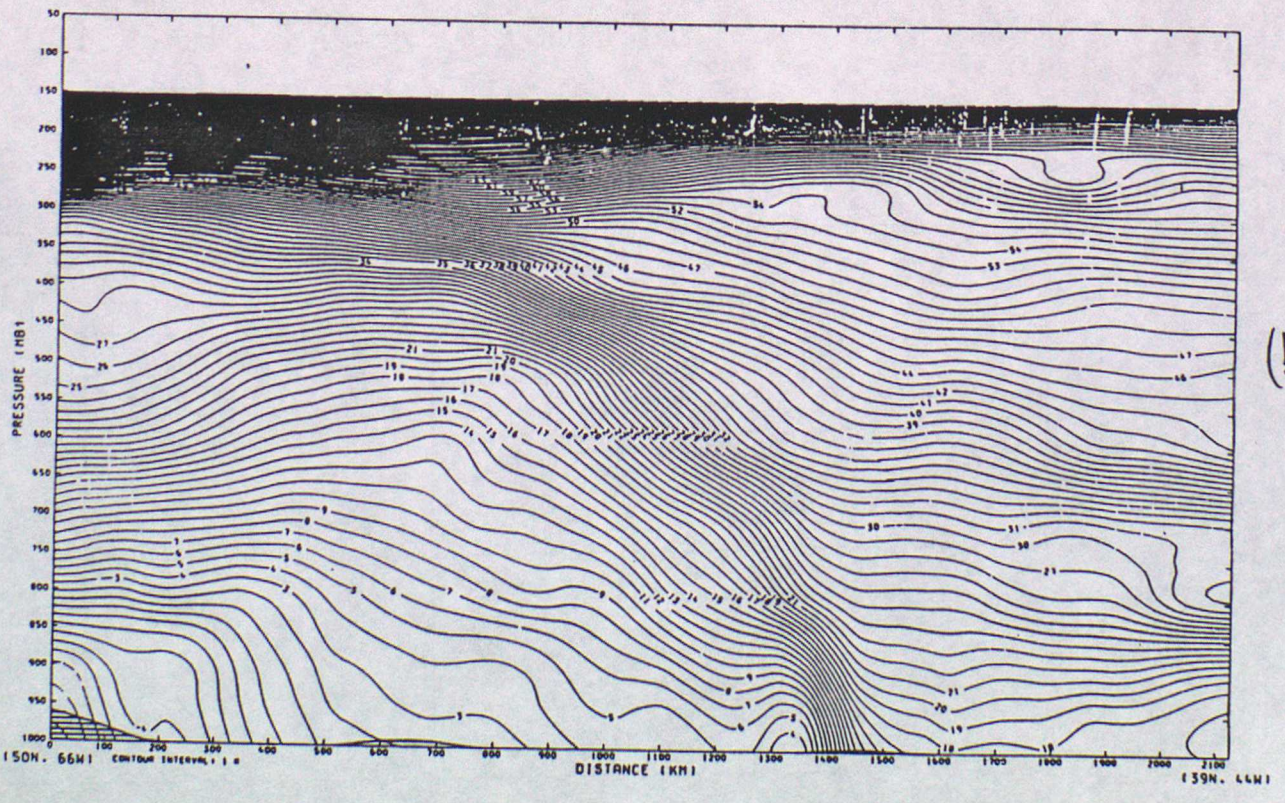

(b)

FIG. 33 (c)

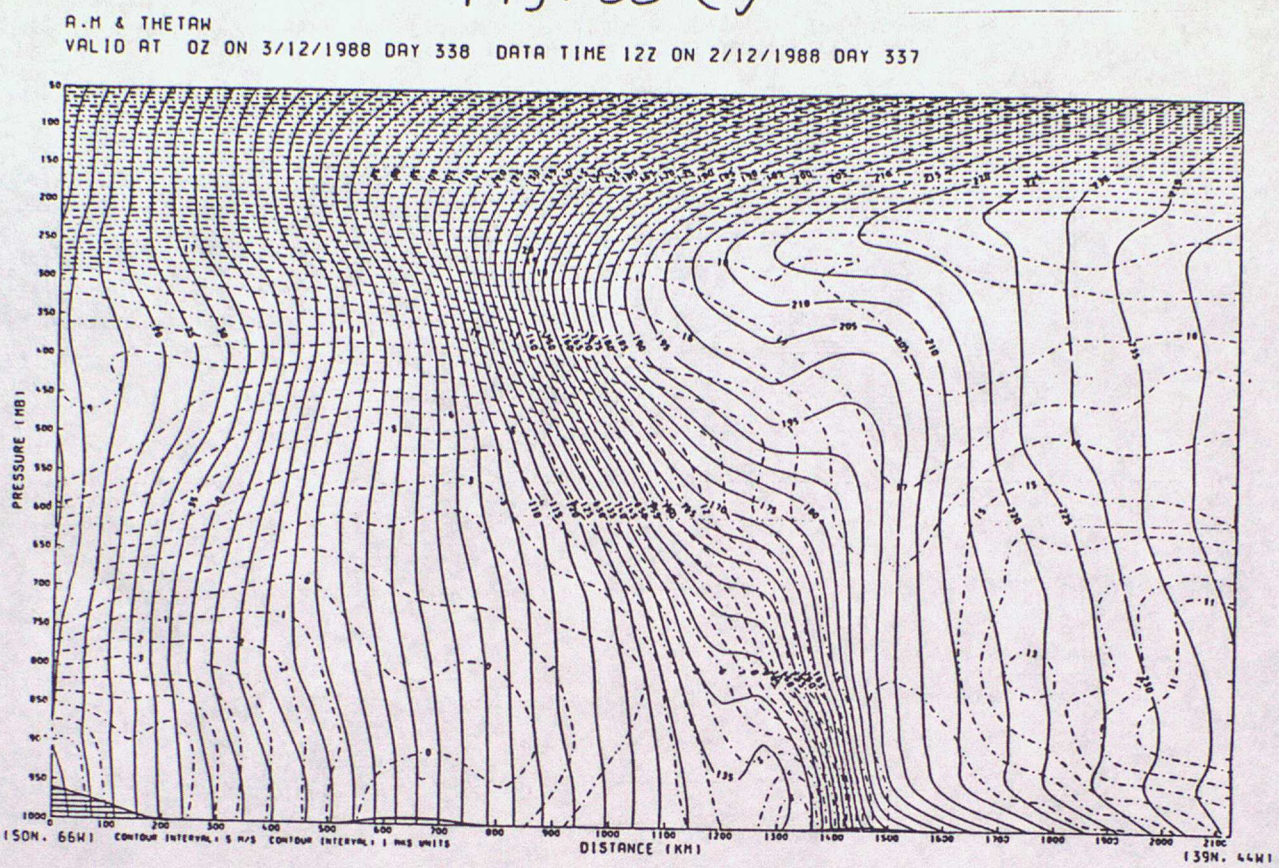

FIG. 34

SCAPE (J/KG X .01) PLOTTED WHERE SCAPE > 100 J/KG

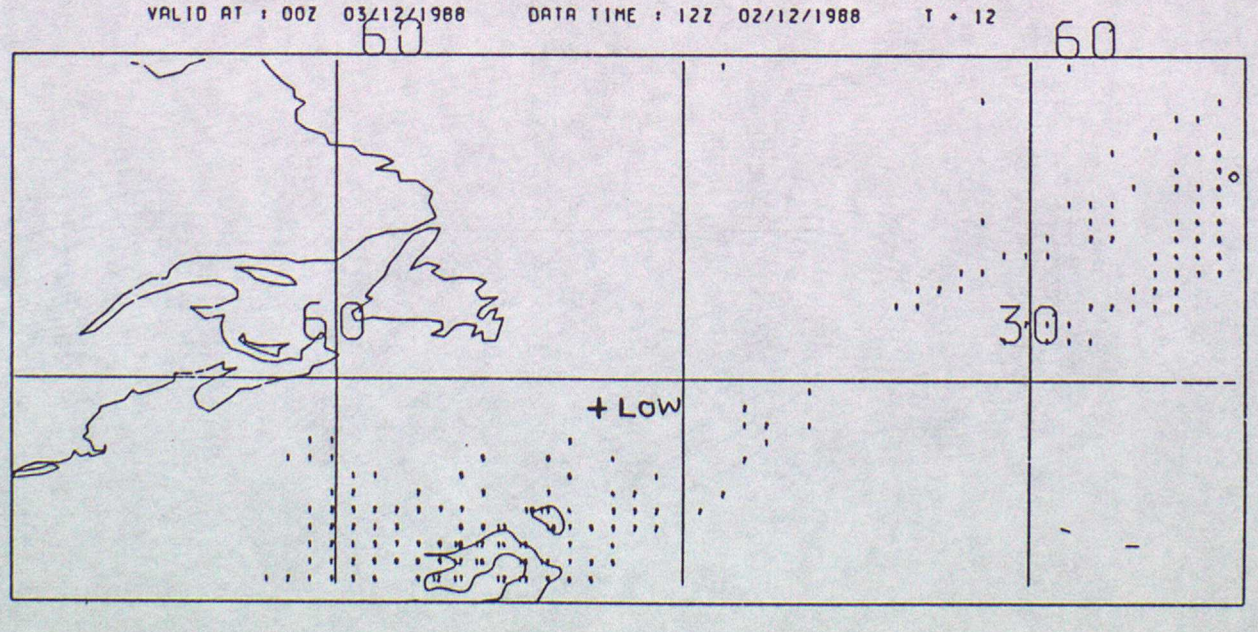

EXPLOSIVE DEEPENER

(a)

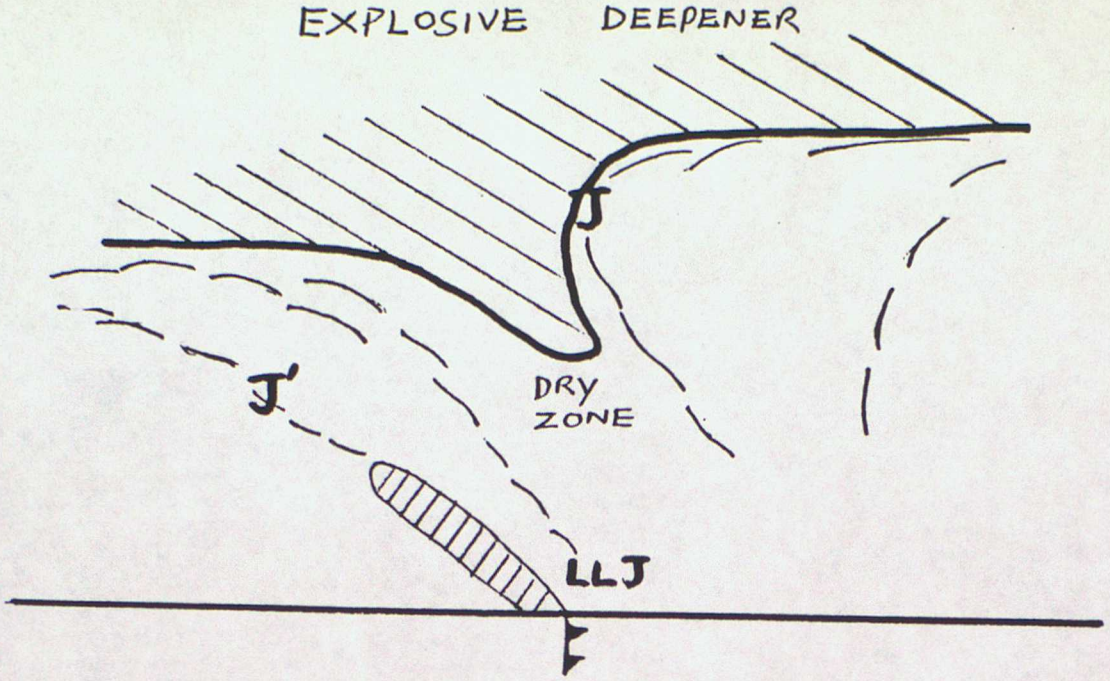

FIG. 35

NON-EXPLOSIVE DEEPENER

(b)

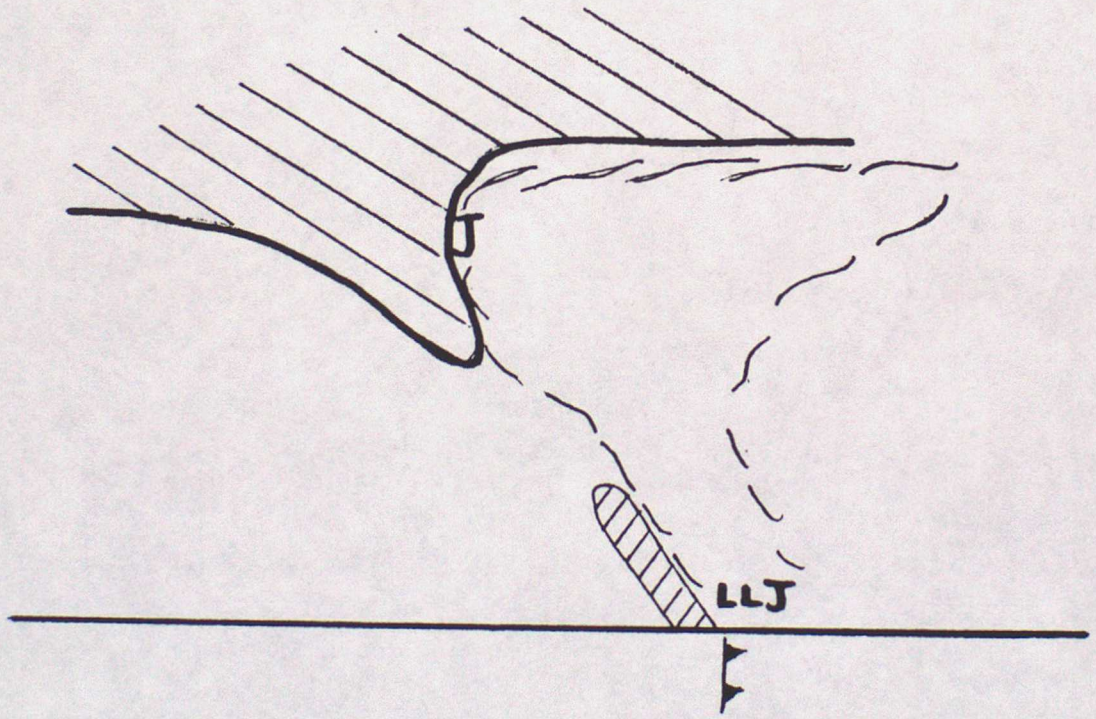

J PRIMARY JETSTREAM AXIS

J' SECONDARY JET

LLJ LOW-LEVEL JET

STRATOSPHERIC AIR

LOWER TROPOSPHERIC FRONTAL ZONE

CLOUD EDGE

SURFACE FRONT